University of Sussex

The Impact of Active Galactic Nuclei and Cooling Mechanisms on the Intra-cluster Properties in the L-Galaxies Semi-analytical Model

Benoit FOURNIER

Supervisor : Peter A. THOMAS

Submitted for the degree of Doctor of Philosophy

University of Sussex

September 2018

Declaration

I hereby declare that this thesis has not been and will not be submitted in whole or in part to another University for the award of any other degree.

Signature:

Benoit Fournier

UNIVERSITY OF SUSSEX

Benoit Fournier, Doctor of Philosophy

The Impact of Active Galactic Nuclei and Cooling Mechanisms on the Intra-cluster Properties in the L-Galaxies Semi-analytical Model

Summary

The intra-cluster medium (ICM) plays a key role in galaxy formation. The cooling of hot gas and its recycling due to feedback are key parameters in understanding the regulation of star formation. Semi-analytical models (SAMs) are quick simulations that allow us to test our understanding of galaxy formation processes. Most of them produce results agreeing fairly well with various galaxy observations, however they fail in reproducing the ICM properties.

In this work we focus on the active galactic nuclei (AGN) feedback and cooling mechanisms affecting the ICM, by developing new physically motivated methods that give a more accurate ICM description in the L-Galaxies SAM. We start by correcting the baryon content of each halos in the simulation. Due to halo mass fluctuations, halos ended up with an over density of baryons. This problem was resolved by introducing an extra phase for the baryons to keep track of the gas that would be considered leaving the halo (during contractions) or inflating (halo growth).

Although this solution solved the baryon problems, it did not answer the question of the excess of hot gas stored inside the virial radius. We investigated different feedback mechanisms, from SNR to black holes and found that ejecting the gas with powerful AGN jets is compulsory to reduce the hot gas content of the halos. In order to reduce the gas content, a new model of AGN feedback was implemented and tuned to reproduce the observational gas fractions available in the literature. The AGN can not only now reheat cold and cooling gas, but also eject it via powerful jets. In addition to this feedback, four new black hole accretion models were compared, based on different gas reservoir. The most accurate agreement with observations for most AGN and galaxy properties came from a model where the AGN was fed by accretion of cold clouds from the ISM of the host galaxy.

Finally we investigate the effect of our improved feedback on the ICM itself. In addition to the new AGN feedback, we developed a more physical cooling mechanism based on

Bremsstrahlung radiation and a Beta profile of the gas. This change enabled us to give X-ray predictions for our model to compare with observational data, including the most recent XMM results. We found that the change in cooling only slightly affects the results (gas fractions, metallicities), as expected. However the X-ray luminosities of our groups and clusters of galaxies are now in agreement with observations, mainly due to the gas content reduction done by the new feedback mechanism.
This new version of L-Galaxies manages to reproduce both galaxies and ICM properties in fairly good agreement with observational data.

Preface

This research work aims at improving the intra-halo description in the L-Galaxies model by studying the complete recycling mechanism of the halo's hot atmosphere. This topic is particularly fundamental because it is a main mechanism in galaxy formation and star formation regulation. In order to investigate the gas behaviour, the L-Galaxies model was used as it provides reliable answers to galaxy properties, with limited amount of computational time needed.

This thesis work is divided into three main chapters.

The extra-halo phase has been developed in order to remove the excess of baryons. This problem was discovered randomly during a side project involving the comparison of several semi-analytical models.

The new cooling description is based on an original idea from P. A. Thomas. Implementing these new observational features lead to the collaboration with X-rays astronomers and credits are due to Sunayana Barghava for providing the outstanding work presented in Appendix D.

The need for a new feedback prescription arose from the fact that the baryon content inside the halos was still too high besides our previous improvements. AGN feedback had to be changed in order to remove gas and reproduce a similar behaviour to the one implemented in hydrodynamical simulations.

All the work has been done under the supervision of P. A. Thomas, with useful advices from other collaborators.

All simulations have been made using the L-Galaxies code presented in (Henriques et al., 2015).

Acknowledgements

I would like to start by thanking my supervisor Peter Thomas. It has been a long and amazing journey to achieve this work on the ICM, full of interesting discoveries and difficult problems to resolve. I will never be grateful enough for all the support, the patience and the trust you put in my work. I learnt a lot working with you and will always highly value the opportunity I had. In addition, I would like to thank my two main collaborators, Bruno Henriques and Rob Yates, who have been giving me continuous feedback and help throughout this work. Thank you to Joop Schaye and his group at Leiden University for welcoming me for several months in 2016. I would also like to thank Seb Oliver, DiscNet and the Brighton and Hove City Council for the work placement opportunity during this PhD. Additionally, a special thank you to Kathy Romer and Ian McCarthy for having been great viva examiners and reviewing my thesis work. Finally, thanks to the University of Sussex and the Science and Technology Facilities Council (STFC) to have provided the means to make this work possible.

I owe a special thanks to my family, for having supported me throughout my studies and during this long journey far from home even though they never really understood anything I was working on, leading to entertaining discussions during family dinner each time I got home.

When I left for Brighton, I left a lot of friends behind in France. Special thanks go to Baptiste Trillat, Boris Kauff, Jérémy Dampne and Thomas Freitas. Even if I wasn't back often, you made me feel comfortable back home, as if nothing had changed. You're the greatest friends someone could ever hope to have. Special thanks to Jill Chevalier, aka Jillyfish, for her constant support and daily updates on life. I hope the gnocchis are ready for when I come back!

These four years in Brighton have been the most exciting years of my life. During this time, I met extraordinary and interesting people and developed strong friendships with most. I would start by thanking my big bro', housemate since the start, Dániel Molnár. We've been through a lot together and I am glad to have you as one of my closest friend.

Equally important are two persons that helped me survive through my PhD and they deserve a special thank you. Scott Clay, for having been the best "colleague" even though we couldn't understand each other during the first three months. I will always remember the nights out we had and all the random shared stories; David Sullivan, for never saying no to a tea break, and the discussions, games and beers we had together. You've both become valuable friends and I am glad we will be on tour again soon enough, in Cardiff, Leeds, or somewhere else.

I would also like to thank all my housemates from THOA : Ridwan Barbhuiyan, Alexander Eggemeier, and Heena Jagatia. You've been the best housemates someone could have, so thank you for all the good moments, laughs and games we had in this house! I'll miss not hearing a "mate" echoing in the background. Additional thanks go to my other housemates : Satoko Nakamura, Jacob Thorne and Panka Bencsik. Moreover, I would like to thank people from the Astronomy Center, which became more friends than just colleagues : Hannah Ross, for the endless teas and discussions and also the nights in Revenge; Lucía Fonseca de la Bella, for your constant happiness and laugh in Spanish; Steven Duivenvoorden for always being up for a beer; Zé Vieira for the endless arguments. Special thanks to Ciaran Fairhurst, Christopher Lovell and Jessica May Hislop for all the laugh and good moments we had in the office. It has been a real pleasure to share an office and so many stories with you. Thank you also to Dimitrios Irodotou (for continuing the hard work with L-Galaxies), Pippa Cole, Azizah Hosein, Michaela Lawrence, Carlos Vergara, Rose Coogan, Antonio Vasquez and Alba Carrillo for all the good moments, parties and chats we had! Additional thanks go to my komrad Sunayana Barghava for the endless chats about triggering subjects without getting bored (and also sometimes about science).

I would also like to give a mention to other people in the department for their kindness and helpful chats.

In addition, I would also like to thank the Pavese family. You've been a support through my studies and part of this PhD, and I am grateful for that. Thank you also to Maria Drozdovskaya, for making me visit the Netherland and so many countries (and towers...) but also to have been part of this journey with me. You're a great person and I am proud of your success.

At last, but not least, a special thanks to Alix de Yelst for supporting me at the very end.

L'Astronomie est utile, parce qu'elle
nous élève au-dessus de nous-mêmes;
elle est utile, parce qu'elle est grande;
elle est utile, parce qu'elle est belle.

Henri Poincaré

La Valeur de la Science (1905)

Contents

List of Tables

List of Figures

Chapter 1

Introduction

With the buildup of large datasets of observational data at different wavelengths and redshifts (with the large coverage of telescopes available) it is possible to get reliable statistics of galaxy populations and their evolution through cosmic time. From the oldest galaxies known at this present day at z = 10 (e.g. Oesch et al., 2012) down to our local universe, observers have been gathering observational datasets to trace the characteristics of galaxies on a large selection of properties : active/passive abundance of galaxies, mass functions, metallicity of the galactic gas, luminosities, and so on.
However if observational data are important to set expectations on the realistic properties of galaxy, it lacks a proper understanding of the physical phenomena involved. Thus simulations are used to probe and understand better the astrophysical processes playing a role in the evolution of galaxy. They strive to reproduce the widest range of properties to then compare to real observations.

In this introduction we summarise the key concepts that will be involved in this thesis work.

1.1 Concepts of cosmology

1.1.1 Modern cosmology

In order to understand the evolution of our Universe and describe its content, a basic understanding of Einstein's General Relativity theory (1915) and the cosmological principle is necessary. This principle states that the Universe is both isotropic and homogeneous. This implies that the Universe is uniform in space at any given time and in all directions from any given place. A first confirmation of this postulate has been made by Hubble

(Hubble and Humason, 1931) with his famous Hubble's Law :

$$H^2(t) = \left(\frac{\dot{a}(t)}{a(t)}\right)^2 \tag{1.1}$$

where $H(t)$ is the Hubble parameter, $a(t)$ is the scale factor, describing the expansion of the Universe at a given time t. Because of this expansion, the wavelength of photons is undergoing a Doppler shift known as cosmological redshift z. It is defined as :

$$z = \frac{1}{a(t)} - 1 \tag{1.2}$$

The metric for a homogeneous and isotropic Universe is defined by the Friedmann-Lematre-Robertson-Walker (FLRW) metric. When evaluating the Einstein equations with this metric, it leads to an analytical solution called the Friedmann equation :

$$H^2(t) = \frac{8\pi G}{3}\rho - \frac{kc^2}{a^2(t)} + \frac{\Lambda c^2}{3} \tag{1.3}$$

Where G is the gravitational constant, ρ the energy density, k the geometrical curvature of the Universe and Λ is the cosmological constant. This equation, while being the simplest solution of the Einstein equations, describes how the size of the Universe depends on its curvature and content.

If we assume a Friedmann Universe (flat and without cosmological constant), we obtain the critical density of the Universe, ρ_c :

$$\rho_{c,0} = \frac{3H_0^2}{8\pi G} \tag{1.4}$$

Where $H_0 = H(t = 0) = 100h$ km s^{-1} Mpc^{-1} and h is the dimensionless Hubble parameter.

We can then define the density parameter as :

$$\Omega = \frac{\rho}{\rho_c} \tag{1.5}$$

As observational evidence suggests that the total energy density is comprised of matter, radiation and dark energy (cosmological constant), we can rewrite Equation 1.3 in terms of density parameters evaluated at the present day :

$$\Omega_0 = \Omega_{m,0} + \Omega_{r,0} + \Omega_{k,0} + \Omega_{\Lambda,0} = 1 \tag{1.6}$$

Where the index details the content (matter, radiation, curvature and dark energy) and $\Omega_{m,0} = \Omega_{b,0} + \Omega_{DM,0}$ is the sum of baryonic and dark matter (DM) components.

In order to constrain the cosmological parameters, observers have been using different methods, one of which is investigating the power spectrum of the Cosmic Microwave Background (CMB), as we can see for example from the Planck satellite's results (Planck Collaboration et al., 2014). Studying the baryonic acoustic oscillations from the recombination era that happened 380000 years after the Big Bang is giving hints at the Universe properties. Indeed, the number and amplitude of these oscillations correspond to particular solutions to GR equations.
However, all these parameters can be more or less entangled and this method is generally coupled to others in order to improve the accuracy on these fundamental parameters (cluster studies, etc).

1.1.2 Dark matter and halo formation

According to observations, the amount of baryonic matter is not enough to explain the behaviour of massive astronomical objects (lensing, galaxy rotation curves, etc). As seen in the previous section, the total amount of matter in the Universe is shared between a baryonic component (visible) and a DM component. The mysterious component is assumed to correspond to 82% of the total amount of matter in the Universe. These particles are not emitting any light and are considered to be weakly interacting through gravitational interactions. Even though the nature of these particles remains unknown, different candidates exist, depending on their possible properties (e.g. WIMP, neutrinos...).
During the last decades, two theories have been developed, assuming different speed (and energy) for the candidate particles : Hot Dark Matter (HDM) and Cold Dark Matter (CDM) models. However, the HDM has been dismissed due to conflicts with cosmological observations. Indeed, it is commonly accepted nowadays that the matter distribution we observe today grew from small initial fluctuations. As a consequence, high speed particles such as neutrinos would have been moving so fast that these small fluctuations wouldn't be able to clump together in order to create larger structures.

Thus, the most used cosmological framework is the so-called ΛCDM model and will be used for the rest of this thesis.

It is important to note that CDM alone is not enough to explain the rapid growth of structure in the early Universe for example. A Mixed DM (MDM) model consisting of warm and cold DM particles is generally investigated rather than HDM alone nowadays.

As explained before, small scales fluctuations are believed to be the initial source of the structures we see today. Small perturbations grow linearly until they reach a critical density. Then they stop their expansion and collapse to form gravitationally bound dark matter halos. These small halos are then expected to grow into the massive structures we observe today, through merger events.

Halos are often assumed to be spherical and their density profile is generally assumed to be a Navarro-Frenk-White (NFW) profile (Navarro et al., 1996). The mass of a halo is generally taken to be the mass enclosed inside a radius where the overdensity Δ is hundreds of times greater than the critical density of the Universe ρ_c :

$$M_\Delta \approx \Delta \rho_c r_{\Delta c}^3 \tag{1.7}$$

This last equation implies that the properties of a halo are time dependent.

The value of $200\rho_c$ is often taken as a reference in simulations as it encloses 99% of the mass, while observers generally use an overdensity of 500 or less, due to observational limitations. However, the halo can extend beyond this overdensity radius. One can argue that a radius to truly define the boundaries of a halo is the splashback radius ($r_{SP} \approx 2.5 r_{200c}$) as it corresponds to a sharp density drop at the outskirts of a halo. Yet this radius is not constant and can be impacted by the environment. In massive objects, the splashback radius is indeed reduced due to subhalos experiencing dynamical friction. This phenomenon is due to an effective drag force induced on a massive object because of its gravitational interaction with nearby matter (Binney and Tremaine, 2008), and is particularly present in galaxy clusters.

It is important to note that the virial radius (radius within which the virial theorem applies) is often close to r_{200c} and no differences between the two will be made for the rest of this thesis.

1.2 Galaxy formation

1.2.1 Galaxy formation and the hierarchical model

In the CDM paradigm, galaxy formation is happening through different steps following the gravitational collapse of dark matter particles into halos (White and Rees, 1978). Following this dramatic event, baryonic matter (gas) will be accreted due to gravitational forces. It is then shock heated due to the compression of the gas while infalling into the newly created potential well. Once the gas is virialised and in thermostatic equilibrium, it will cool towards the center via cooling flows. If the halo is too small, the shocks will

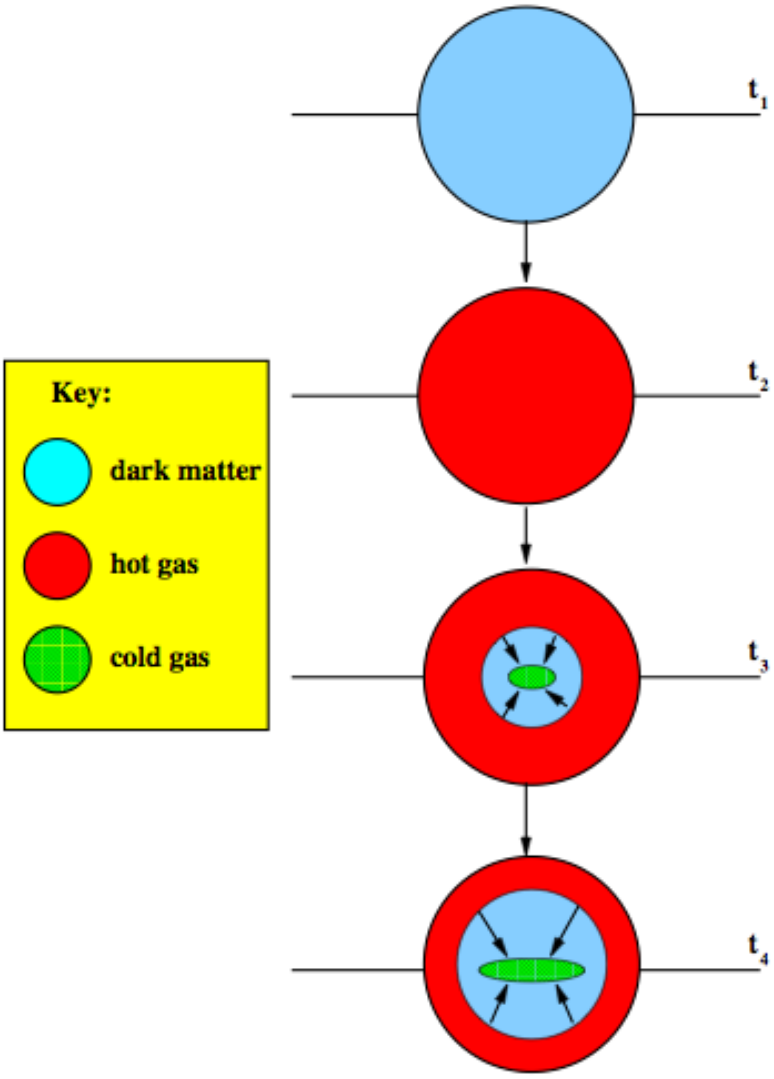

Figure 1.1: Schematic of galaxy formation from Baugh (2006).

happen close to the center. The gas will not have time to reach the equilibrium and will flow towards the center at free-fall velocity. This vision is simplistic and modern views on the matter suggest that the gas is funneled via thin streams, a process called "Cold Accretion" (e.g. Kereš et al., 2005; van de Voort et al., 2011). However, even if more accurate, this accretion process is difficult to reproduce in semi-analytical models for example due to a lack of resolution and missing local information.

Then cold gas phase creates a disk which is rotationally supported and which will be the location of star formation for the new galaxy. This formation mechanism is illustrated in Figure 1.1. Different feedback mechanisms from the galaxy will then regulate the cooling flows through heating processes of the surrounding gas. .

However, if this scenario works for the formation (and evolution) of an isolated galaxy, it is insufficient to explain the observations of massive galaxies and actual mergers. The hierarchical model of galaxy formation states that larger structures are formed by the cumulative mergers of smaller ones through time. Moreover, even if this model if often referring to the galaxy growth, it gives a sensible explanation for the existence of groups and clusters of galaxies. Indeed, as galaxies are compact structures, they are not disrupted by the merging of two halo structures. Thus it leads to galaxy clustering inside the same host halo.

1.2.2 Groups and clusters of galaxies

Clusters of galaxies are the most massive structures known in the observable universe, with halo masses varying from $\approx 10^{14} M_{\odot}$ up to $\geq 10^{15} M_{\odot}$. They are formed through a hierarchical process, as explained before. They are composed of a dark matter halo ($\approx 85\%$ of the mass), a hot diffuse atmosphere ($\approx$10-12%) and up to hundreds of active or passive galaxies. Groups of galaxies, on the other hand, are smaller structures ($10^{13} - 10^{14} M_{\odot}$) and contain a lower hot gas content than clusters ($\approx 5\%$), while hosting tens (up to a hundred) of galaxies. The definite limitation between these two classifications is, however, not clearly established. Groups and clusters of galaxies are extremely interesting objects to study and to test galaxy formation theories as they are the location of various physical processes :

• Radiative cooling of the hot atmosphere through X-ray emissions (temperature, entropy, density profiles).

• Galaxy clustering and statistical properties.

• Gravitational interactions between galaxies and environmental processes such as ram-pressure stripping or tidal forces.

The last 20 years have seen the fast development of X-ray astronomy through the joint launch of the Chandra and XMM-Newton telescopes, leading to improvements in the accuracy of cluster observations in addition to the creation of large surveys. In addition to these physical phenomena, massive clusters are sufficiently large to achieve a baryon fraction leaning towards the cosmic mean value. Hence they reveal themselves to be useful cosmological probes. With the increase of the number of cluster sources in recent surveys (e.g. Lloyd-Davies et al., 2011a; Mehrtens et al., 2012) to improve the statistical analysis, clusters have been proven reliable candidates in the estimation of cosmological parameters

(e.g. Hu et al., 2014).

Another observational effect of clusters is the Sunyaev-Zel'dovich effect. It corresponds to the distortion of the radiation emitted by the CMB due to inverse Compton scattering effect by the highly ionised plasma. This effect is also a key element to constrain the cosmological parameters (Barbosa et al., 1996).

1.3 The Intra-Halo Medium

The intra-halo medium (hereafter IHM), also called intra-cluster medium (ICM), is the name given to the hot gas atmosphere surrounding galaxies inside a halo. This diffuse atmosphere is the main baryonic component of clusters (10-12% of the total amount of matter), but is present in lower quantities ($\leq$ 5%) for groups of galaxies. The gas particle extend up to the outskirt of the halo and its average density is low (around 10^{-3} particles.cm^{-3}) with an increase towards the center. The temperature of this gas is on the range of 10^4 - 10^8K. The existence of the ICM was proposed for the first time by Limber (1959), however 7 years were necessary before the first proof of its existence was published (Biviano, 2000). Most semi-analytical models and theories adopt an isothermal model in order to describe the gas behaviour. Even if this results in a good approximation, recent observations show a decrease in temperature with increasing radius (e.g. Pratt et al., 2006).

Moreover, this gas is essential in the formation and evolution of galaxies as its cooling will feed the interstellar medium (ISM) of the galaxies and thus enhance star formation.

1.3.1 Gas physics

During its infall inside the halo, the gas is heated by shock waves inducing gas compression (Baugh, 2006) and the velocity of the gas dramatically increases. Collisions of highly energetic particles then lead to significant heating of their surrounding. Further gravitational collapse is avoided by the resulting pressure of this hot baryonic gas and then eventually the hot atmosphere gets virialised. In the case of an isothermal sphere (used by most SAMs), all the gas is considered being at the virial temperature once the equilibrium state is reached. In reality, observations from XMM and Chandra surveys tend to suggest a temperature profile decreasing as we reach towards the outskirt of the halo (e.g. Pratt et al., 2006).

Due to its hot temperature (10^4 - 10^8K), the hot plasma is highly ionised. Hence loss of energy from thermal Bremsstrahlung processes is occurring. In addition, line emission (re-

combination) is also important at temperatures close to the virial temperature of groups (1 keV). The gas, releasing its energy in the form of X-ray radiations, then cools towards the center, thus fuelling star formation. Observers can then deduce ICM properties through cluster luminosities (X-ray) and temperatures, assuming a set of assumptions. In the case of simulations, and especially semi-analytical models, realistically modelling the cooling flow is a challenge.

Entropy profiles from clusters can give extra information about cooling mechanisms. The entropy at the outskirt of the halo can give an insight into the type of accretion for the gas (smooth or lumpy) and thus provides information about the gas density or the presence of preheating mechanisms. In addition, by looking at the radial entropy profiles of the hot atmosphere, the presence of a cool core can be revealed. The creation of this core was due to the heating of the gas through feedback mechanisms, causing an adiabatic expansion of the gas.

The entropy profiles for a pure collisional gas (Einstein-de Sitter-Sedov) can be predicted in our models using the entropy integrals described in Bertschinger (1983) and Bertschinger (1985). The dimensionless entropy integral is defined as follows :

$$P\rho^{-\gamma}M^{\zeta} = P_2\rho_2^{-\gamma}M_2^{\zeta} = cst$$

and

$$\zeta = \frac{2(\gamma+\eta-2)}{2-3\eta}$$

Where P, ρ and M are the pressure, density and mass of the gas, the index 2 refers to the post-shock shocked corresponding parameters of the gas as defined in Bertschinger (1985). γ is the Laplace coefficient (5/3) and $\eta \approx 0.8$.

It is worth noticing that the crucial entropic aspect of the hot gas has not been covered in this thesis work, for several reasons : the implementation of the entropy integrals and the mechanisms taking into account the entropy profiles modifications was challenging in the L-Galaxies SAM and not trivial in order to get realistic results. Hence it was beyond the preliminary goal of this thesis work. Future improvements, however, will try to add this feature.

Similarly, simulations have noticed an overcooling phenomenon happening without a regulation through feedback mechanisms. As seen on Figure 1.2, two mechanisms are generally involved in order to regulate star formation : supernovae (SNae) for low mass galaxies and active galactic nuclei (AGN) for the most massive objects.

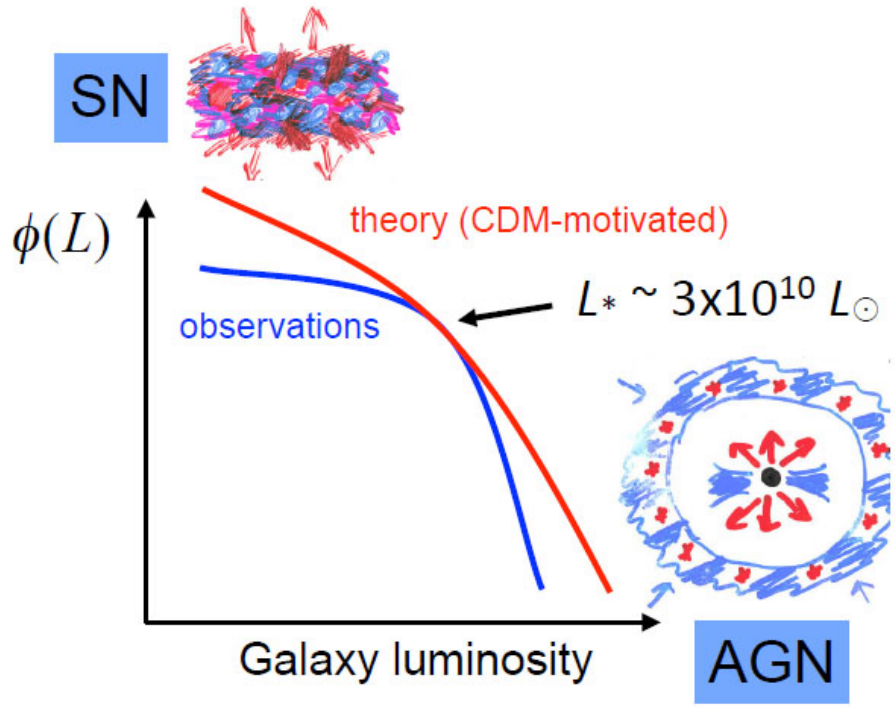

Figure 1.2: Schematic of the impact of different feedback mechanisms on the luminosity function of galaxies Silk and Mamon (2012).

1.3.2 Hydrostatic equilibrium and cluster mass

In a cluster, the virialized gas particles from the hot atmosphere undergo two types of forces : pressure P from gas particles above and under them, and gravity forces due to its weight. If we assume a constant fluid velocity here, the sum of these forces should be equal to zero. This leads to the hydrostatic equilibrium equation. For the mass of a cluster $M(r)$ inside a sphere of radius r, assuming spherical symmetry, we can write it as follows :

$$\mathrm{d}P = -\rho \frac{GM(r)}{r^2} \mathrm{d}r \tag{1.8}$$

Where ρ the density of the gas.

Or, in a more useful form :

$$\frac{1}{\rho}\frac{\mathrm{d}P}{\mathrm{d}r} = -\frac{GM(r)}{r^2} \tag{1.9}$$

The pressure for the gas is given by :

$$P = nk_BT \tag{1.10}$$

Where n and T are the density and temperature of the gas and kB is the Boltzmann constant.

Integrating the Equation 1.9 leads to an estimate for the mass $M_{\rm HE}$:

$$M_{\rm HE}(r) = -\frac{rk_BT}{G\mu m_p}\left(\frac{{\rm dln}\rho}{{\rm dln}r} + \frac{{\rm dln}T}{{\rm dln}r}\right) \tag{1.11}$$

Where this equation can be simplified by assuming isothermality, which cancels the second term of the equation.

1.3.3 Supernovae feedback

Massive and short lived stars, in addition to white dwarfs, end their life in a cataclysmic explosion called supernovae (SNae). Two categories exist : Type I and II, corresponding to the presence of hydrogen in their spectrum or not. These two types also contain sub categories depending on the elements present in their spectrum.

Once reaching a critical mass, these stars undergo gravitational contractions leading to a powerful explosion, releasing 99% of the energy in the form of neutrinos. The metals, created during the lifetime of the stars and their explosion itself, are then released into the surrounding medium. Moreover the winds created by the explosion will reheat the environment near the star (e.g. Martizzi et al., 2016; Fielding et al., 2017; Henriques et al., 2013). They can be powerful enough to create a galactic fountain, where the gas is ejected temporarily from the galaxy into the ICM. This mechanism is key to understanding the enrichment of the ICM.

1.3.4 AGN and their outflows

As seen in the previous section, the feedback of SNae is not sufficient to prevent cooling mechanisms in large structures according to simulations. In order to explain the quenching of massive galaxies, feedback via jets and winds of AGN has been suggested. Observationally, evidences exist of such an impact of AGN outflows on the surrounding gas (e.g. Cicone et al., 2014; Harrison et al., 2018). AGN are supermassive black holes (SMBH) commonly found at the center of galaxies. They are the most efficient mechanism to convert baryonic matter into energy.

According to observations, we can distinguish different types of AGN (for example : Seyfert galaxies, QSO, blazars, ...) depending on their luminosities. However, the unification paradigm (Urry, 2003) states that these AGN types all share a set of fundamental ingredients. The observational differences between these different types are in fact due to the inclination of the jets and the type of accretion disk surrounding the SMBH (thin/thick). An AGN consist of a supermassive black hole, surrounded by an accretion disk and/or a

dusty torque, in addition to a powerful jet. The maximum luminosity a SMBH can emit is called the Eddington Luminosity L_{Edd}, which is the highest luminosity of a source in hydrostatic equilibrium (although, some exceptions can exceed this theoretical accretion limit leading to super-Eddington luminosities).

However, the accretion of gas on a SMBH is a complex theoretical problem to solve and various mechanisms can be involved (e.g. Mayer et al., 2010; Hopkins and Quataert, 2011; Yuan and Narayan, 2014). It is a challenging phenomenon to model in large scale structure simulations, as the resolution is not high enough to resolve the sub-pc scales involved. Most of these simulations (e.g. Schaye et al., 2015) rely on a boosted Bondi-like type of accretion (Bondi, 1952), often limited to the theoretical Eddington limit. This limit can make sense as it is the highest rate achievable while keeping the hydrostatic equilibrium between radiation pressure and gravitational forces. The feedback created by the jets is then used to reheat the gas and eject particles out of the galaxy (e.g. Cicone et al., 2014; Harrison et al., 2018). It is important to note that quenching might not be the only consequence of AGN feedback but they could also be the cause of an enhancement of star formation in companion galaxies, as some study suggests (e.g. Molnár et al., 2017).

To summarise, the ICM is a crucial component in galaxy formation and clusters physics. Its physical properties inform us on the fuelling mechanisms involved in the formation of stars as well as the feedback mechanisms regulating it.

1.4 Thesis outline

The goal of our work in this thesis is to give a more accurate description of the ICM physics and its recycling, as it has been a key component in galaxy formation models. In order to achieve this objective, we focus on the gas content and its cooling mechanism, but also on the AGN feedback impacting the gas in the groups and clusters of galaxy range. To perform the study, we use the L-Galaxies semi-analytical model. In Chapter 2, we present the different types of simulations usually used for large scale studies of galaxy formation and detail the main properties of the L-Galaxies model we are using.

In Chapter 3, we compare the ICM and baryonic content of eight different semi-analytical models from the nIFTy workshop. We discuss the causes of the baryonic excess and propose a physically motivated solution to correct it with the introduction of an external phase in our model.

In Chapter 4, we investigate how the ICM fraction can be lowered with a different type of feedback. We develop a new type of AGN feedback including gas reheating and ejection

by jets and compare the effect of four different types of accretion for our black holes. We then discuss the impact of this new feedback implementation on AGN and galaxy properties. In Chapter 5, we have a closer look at the ICM physics and properties. In order to increase the accuracy of our predictions, we develop a new cooling description for our model by changing the gas density to a β profile. We then include this new cooling method in addition to the previous AGN feedback modifications and discuss their impact on the gas content, its luminosity and metallicity.

Finally, the global conclusion of our work is presented in Chapter 6, in addition to future work suggestions.

Chapter 2

Simulating the large scale structures

If observations are a key component in understanding the evolution of our Universe and the galaxies therein, it fails to give all the information to comprehend the physics involved in the formation of galaxies. In order to gain a better insight into the physical mechanisms, experiments through simulations are necessary. Comparing the predictions of simulations with observations helps us to get a better understanding of the processes involved and to decide which theoretical explanation is more realistic, or need improvements, to reproduce accurately the real world.

In astronomy, we distinguish three types of simulations which are usually used for large scale structures studies : Hydrodynamical simulations, semi-analytical models, and N-body dark matter only simulations.

2.1 Simulations

The choice and type of simulations highly depend on the goal we strive for. Indeed, even if the hardware is getting more and more performant, computing resources remain limited. Hydrodynamical simulations are the method giving the most complete set of properties available to study galaxies and their environment. However they are computationally expensive as they need to follow both DM and baryonic particles to give the most accurate description. DM only simulations can be run for larger boxes as it tracks only one type of particles but miss the crucial information concerning the baryonic physics involved in galaxy formation.

SAMs fill the gap in between these two different pictures. They are computationally cheap

to run and can be built on top of any DM only simulations, allowing us to describe baryonic properties over large cosmological volumes.

2.1.1 Hydrodynamical and semi-analytical simulations

Hydrodynamical simulations are aimed to reproduce most of the galaxy properties in good agreement with observations. Accurate particle tracking also allows them to give local information for properties in addition to global predictions. This difference with SAMs is critical as it enables the comparison of model predictions with observations. However, the limit in resolution in these simulation also forces the simulations to use sub-grid physics similar to SAMs in order to compute some astrophysical phenomena, such as the black hole accretion mechanisms.
Recent hydrodynamical simulations such as EAGLE (Schaye et al., 2015) or Illustris (Vogelsberger et al., 2014) reproduce with good agreement most of the galaxy properties (e.g. galaxy mass functions). Other simulations, such as BAHAMAS (McCarthy et al., 2017) or the zoomed simulation C-EAGLE (Barnes et al., 2017), focus on clusters and their hot atmosphere properties, giving fairly good agreement with clusters and X-ray observations. However, as mentioned previously, these simulations are expensive to run, and need a careful calibration before running on large volume.

SAMs, on the other hand, implement simple, physically-motivated prescriptions for processes that influence the baryons within DM halos. These halos are extracted from the underlying DM only simulation using halo finder and merger tree codes. SAMs generally include a large description of physical phenomena involved in galaxy formation : primordial infall and its ionisation, radiative cooling of the gas, star formation formulas and SNae feedback, metal enrichment, SMBH growth and AGN feedback, mergers, ... A proper in depth review of SAMs and their properties can be found in Baugh (2006). SAMs, compared to the hydrodynamical simulations, can only describe global quantities as there is no particle tracking. Hence they are more limited in the number of observables they can compare to. However, due to the fact that they are cheap to run, more physical phenomena can be included and testing new model ideas is extremely fast. They make an excellent choice for testing new physics or improvements that can then be used in hydrodynamical simulations. In addition, they can be tuned with gain in accuracy, with the help of statistical methods such as MCMC which requires to run the models thousands of

times.

Lot of different SAMs and their variants exist (a comparison of different SAMs is described in the nIFTy project from Knebe et al. (2015)), with some of the more well known ones being certainly L-Galaxies (Springel et al., 2001; De Lucia et al., 2004; Croton et al., 2006; De Lucia and Blaizot, 2007; Guo et al., 2011, 2013; Henriques et al., 2013, 2015) and GALFORM (Cole et al., 2000; Bower et al., 2006; Font et al., 2008; Gonzalez-Perez et al., 2014; Lacey et al., 2016).

However, with the constant improvements in the hardware and the exponential increase of computational power, one can ask the relevance of SAMs for the near future, once running hydrodynamical simulations can be done in shorter timescales.

2.1.2 The Millennium simulations

In this work, we use the Millennium I simulation (Springel, 2005) as the underlying DM only simulation to run our versions of L-Galaxies. The DM only simulation Millennium I was the biggest of its time with a box size of 500^3 Mpc/h (see Figure 2.1 for illustration) and 10 billion DM particles. The simulation runs from $z = 127$ to $z = 0$ and allows SAMs to probe galaxies in the range of $10^{10} - 10^{12} M_\odot$. Due to its large size for the epoch, the simulation is limited by a resolution of $10^9 M_\odot$. In order to probe lower halo masses for a better description, Millennium II is used in addition for the MCMC routines. Millennium II is a re-run of the previous simulation made in 2009 (Boylan-Kolchin et al., 2009) with a box length 5 times smaller. This leads to a better resolution and enables us to investigate galaxies down to $10^7 M_\odot$. The two simulations were run assuming a flat ΛCDM cosmology with parameters coming from a combination of 2dFGRS (Colless et al., 2001) and WMAP1 (Spergel, 2001) results. However, this cosmology has been now scaled to PLANCK data in Henriques et al. (2015).

The Millennium I simulation stored the data in 64 snapshots (rescaled to 58 due to the change in cosmology). However, the raw data from the simulation is not directly usable by SAMs as we need to first identify the structures and substructures of DM halos and their merger history. In order to identify bounded particles, a Friends of Friends (FoF) algorithm is used (Geller and Beers, 1982). This program identifies groups of particles where the DM density is approximately equal to 200 ρ_c. In order to get the subhalos information inside these FoF groups, we use SUBFIND (Springel et al., 2001), which identifies the overdense substructures inside the FoF group and calculates all their virial properties.

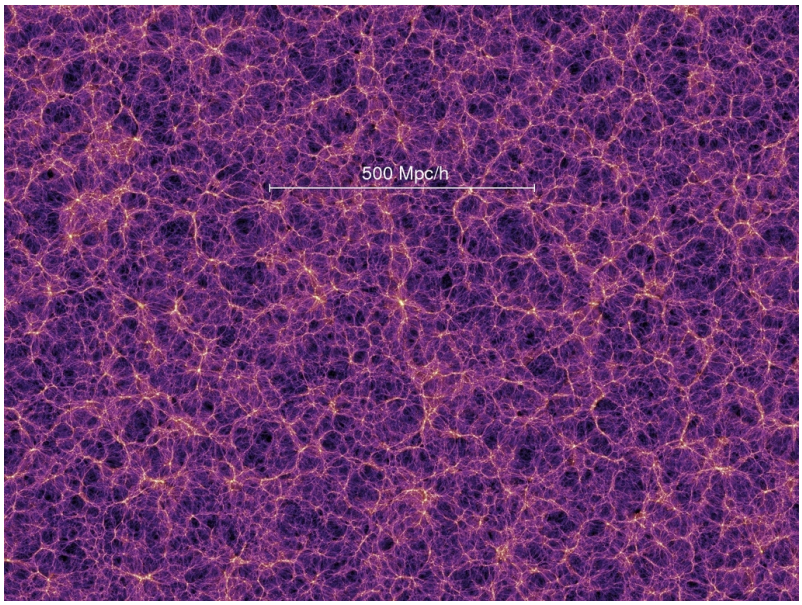

Figure 2.1: Stamps of 15 Mpc/h thick slices from the Millennium simulation at resolution of 500 Mpc/h. Illustration taken from the Millennium Simulation Project website (https://wwwmpa.mpa-garching.mpg.de/galform/virgo/millennium/).

These substructures are crucial as they correspond to halos hosting the galaxies of our SAM.

At last, an algorithm is use to create the merger trees in order to track the history and evolution of halos, and consequently our future galaxies too. It is important to note that each group of halos in a merger tree file is independent from the halos from other merger trees. Hence the SAM can be run on each tree independently, increasing the execution speed of the code.

2.2 The L-Galaxies SAM

The L-Galaxies SAM (also known as the Munich Semi-Analytical Model) is a galaxy formation model model built to describe baryonic physics on top of subhalo trees given by a DM only simulation. It has been improved over the last 20 years through several implementations and modifications of the astrophysical phenomena involved in galaxy formation (Springel et al., 2001; De Lucia et al., 2004; Croton et al., 2006; De Lucia and Blaizot, 2007; Guo et al., 2011, 2013; Henriques et al., 2013, 2015).

The current version of the code (Henriques et al., 2015) reproduces with good agreement the stellar mass function of galaxies and the fraction of active and passive galaxies up to $z = 3$.

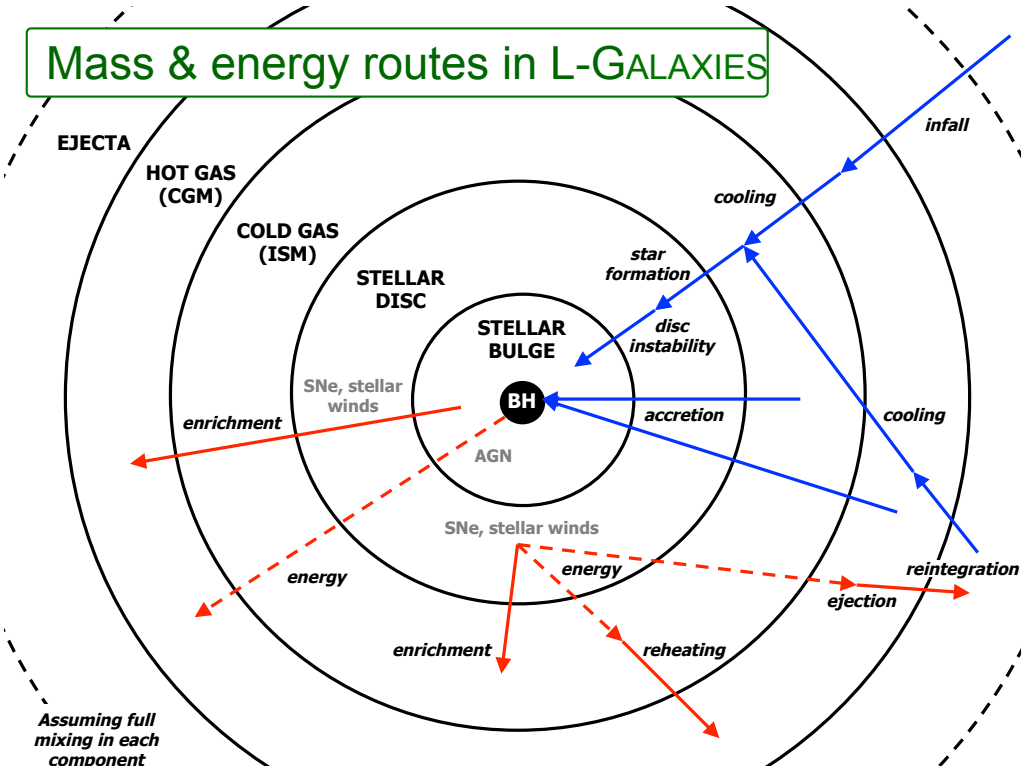

Figure 2.2: Detailed schematic of the different baryonic reservoirs and their interactions in the L-Galaxies model. The dashed lines correspond to a transfer of energy while the solid lines represent a transfer of mass. Schematic created by R. Yates.

In this model, the baryonic content of halos is divided into boxes (also called reservoirs) that interact with each others through physical processes, as shown in Figure 2.2.

In addition, galaxies are labelled by type in order to define their roles. Type 0 galaxies correspond to the central galaxy of the main halo of the FoF group. Type 1 and 2 galaxies correspond to the satellite galaxies of this central one, the only difference being the presence of a dark matter halo surrounding them or not (orphan galaxy).

As most of the physical processes are not completely understood yet or lack the necessary resolution (sub-grid Physics), free parameters can be used to overcome these difficulties. The best fit for their values are obtained through a Markov Chain Monte Carlo (MCMC) process (see Section 2.2.9). The best values obtained for these parameters are given in Table B in Appendix B.

This work is based on the L-galaxies version described in Henriques et al. (2015) [1]. We summarise in this chapter the main physical mechanisms present in the code and relevant to the work performed in this thesis. We then explain in depth our modifications and their motivations for the infall in Chapter 3, for the AGN feedback in Chapter 4 and for the cooling mechanism in Chapter 5.

2.2.1 Infall

The baryonic content of the halo is set to reach the cosmic mean at any given time, following the description from White and Frenk (1991), with the addition of an ionising factor (Okamoto et al., 2008) to reproduce the impact of the photo-heating done by the UV background field.
In this scenario, a halo can only accrete pristine hot gas if its baryonic content doesn't exceed the cosmic mean limit. A more in depth explanation of the infall mechanism is provided in Chapter 3.

2.2.2 Cooling

As previously seen in the introduction, during its infall in the halo, the gas is expected to be shock heated to the virial temperature. Then the gas is cooling towards the galaxy through thermal Bremsstrahlung radiations and line emission. The cooling rate of the gas is based on the cooling radius method introduced by White and Frenk (1991), where only the gas up to a defined cooling radius is able to cool. From this situation, two different cases are expected.
• If the cooling radius is smaller than the virial radius (massive halos and late times), a hot quasi-static atmosphere is formed and the gas inside this radius cools towards the center through what are called cooling flows.
• However, if the cooling radius is greater than the virial radius (in the case of small halos and at early times), the shock happens too close to the center and the gas is unable to form this atmosphere. Thus all the gas inside the halo is able to cool on the galaxy directly at the free fall rate.
A more in depth description of this method and its limits is provided in Chapter 5.

[1] The public version of the code can be found here : http://galformod.mpa-garching.mpg.de/public/LGalaxies/

2.2.3 Bulge formation and growth

Mergers of galaxies are a key mechanism in the bulge formation and growth for galaxies. During a major merger, all the stars (from both galaxies) are moved to the bulge. On the contrary, during a minor merger, only the stars from the smaller galaxy are transferred to the bulge of the new galaxy.

The growth of a bulge is then given by the energy conservation and virial theorem (Guo et al., 2011) :

$$\frac{G\mathrm{M_{newbulge}}^2}{\mathrm{R_{newbulge}}} = \frac{G\mathrm{M_1}^2}{\mathrm{R_1}}\frac{G\mathrm{M_2}^2}{\mathrm{R_2}} + 2\alpha_{inter}\frac{G\mathrm{M_1M_2}}{\mathrm{R_1+R_2}} \tag{2.1}$$

The term on the left of this equation represents the binding energy of the final budge. Similarly, the first two terms on the right are the binding energy for the two merging galaxy while the last term is the binding energy created by the relative orbit of the two progenitors during the merger. α is the binding energy invested in this orbit relative to that in the individual systems. It has been shown that a value of 0.5 gives bulges in good agreement with observations in SDSS data.

Another growing mechanism for the bulge is through disk instabilities. As the disk becomes unstable due to star formation and a change in the angular momentum, stars are driven towards the center and become part of the bulge in order to stabilise the disk structure. This particular point is detailed in Appendix A for more in depth information.

2.2.4 Star Formation

Stars are assumed to be created from the ISM content of the galactic disk. The star formation rate is given by :

$$\dot{\mathrm{M}}_* = \alpha_{SF}\frac{(\mathrm{M_{gas}} - \mathrm{M_{crit}})}{\tau_{dyn,disk}} \tag{2.2}$$

where α_{SF} is an efficiency parameter adjusted through MCMC runs, $\mathrm{M_{gas}}$ is the total amount of cold gas available, $\tau_{dyn} = \frac{\mathrm{R_{disk}}}{\mathrm{V_{200c}}}$ is the dynamical time of the disk. The rotation velocity of the disk is equal to $\mathrm{V_{200c}}$ and independent of radius due to the isothermal mass profile assumed. $\mathrm{M_{crit}}$ is a threshold mass (Kauffmann, 1996) given by :

$$\mathrm{M_{crit}} = \mathrm{M_{crit,0}}\frac{\mathrm{V_{200c}}}{200\mathrm{km.s^{-1}}}\frac{\mathrm{R_{gas}}}{10\mathrm{kpc}} \tag{2.3}$$

where $\mathrm{M_{crit,0}}$ is a free parameter set through MCMC runs, $\mathrm{R_{gas}}$ is the radius of the gas disk and $\mathrm{V_{200c}}$ is the velocity at 200 times the critical density of the DM halo.

Among all the stars formed, some are expected to have an extremely short life spans and a fraction $R_{ret} = 0.43$ is returned directly to the cold gas phase. This value is determined by the Chabrier (2003) initial mass function (IMF). This leads to a net increase in stellar mass of :

$$\delta \mathrm{M}_* = (1 - R_{ret})\dot{\mathrm{M}}_* \Delta t \tag{2.4}$$

In addition to this quiescent star formation process happening at every timestep Δt, a burst event of star formation can happen during mergers of galaxies. To reproduce such an event, we use the collisional starburst model of Somerville (2001) (based on simulations from Mihos and Hernquist (1996)) given by :

$$\delta \mathrm{M}_{*,\mathrm{burst}} = \alpha_{SF,burst} \left(\frac{\mathrm{M}_1}{\mathrm{M}_2} \right)^{\beta_{SF,burst}} (\mathrm{M}_{\mathrm{cold},1} + \mathrm{M}_{\mathrm{cold},2}) \tag{2.5}$$

where $\mathrm{M}_1 < \mathrm{M}_2$ are the total mass of the two galaxies, and $\mathrm{M}_{\mathrm{cold},1}$ and $\mathrm{M}_{\mathrm{cold},2}$ their cold gas mass. $\alpha_{SF,burst}$ and $\beta_{SF,burst}$ are two free parameters tuned via the MCMC process.

Moreover, it is important to note that this SAM reproduces the observed Kennicutt-Schmidt star formation law.

2.2.5 Supernovae feedback and reincorporation

Star formation produces a large range of stellar masses. The most massive stars have a short life spans and end their life as SNae. This explosion releases a dramatic amount of energy into the immediate surrounding medium. Hence this cataclysmic event can have different effects : enriching the ISM in metals, reheating the surrounding cold gas, or even ejecting the gas through powerful winds. In addition, it is also a key mechanism in galaxy evolution to stop the gas cooling from the hot atmosphere and to control the star formation (Larson, 1974; White and Rees, 1978; Dekel and Silk, 1986).
The total energy released through the SNae is given by the following formula :

$$\mathrm{E}_{\mathrm{SN}} = \epsilon_{halo} \frac{1}{2} \Delta \mathrm{M}_* {\mathrm{V}_{\mathrm{SN}}}^2 \tag{2.6}$$

where ϵ_{halo} is efficiency ejection depending on the halo velocity and $\mathrm{V}_{\mathrm{SN}} = 640\mathrm{km/s}$ is the supernovae wind speed, which was set through MCMC runs.

The amount of energy required to reheat the gas from the ISM is given by a similar formula, assuming a disk efficiency parameter ϵ_{disk} and $\mathrm{V}_{200\mathrm{c}}$ instead of V_{SN}. The change in velocity dependence for the formula is obvious as the gas is assumed be reheated to the virial temperature.

Then the amount of gas ejected is given by the leftover energy after reheating the gas :

$$\Delta M_{ej} = \frac{\Delta E_{SN} - \Delta E_{SN,reheat}}{\frac{1}{2}{V_{200c}}^2} \tag{2.7}$$

However, the SAM assumes that the gas ejected through this violent wind will not stay outside the halo indefinitely. As seen in Henriques et al. (2013), the regulation of star formation in low mass galaxies requires both strong SNae winds and long reincorporation times. In this prescription, as long as the gas stays in the ejected phase, it is not allowed to cool. The reincorporation formula, as described in Henriques et al. (2013), is :

$$\dot{M}_{reinc} = \gamma M_{ej} \frac{10^{10} M_{\odot}}{M_{200c}} \tag{2.8}$$

where γ is a free parameter which value is set through the MCMC runs.

The goal of this formula is not to properly describe the complex reincorporation mechanism of the gas but rather to model global behaviour. In small halos, the gas can be easily ejected and is poorly retained by the potential well. However, as soon as the halo gets more massive, SNae winds are not powerful enough anymore to properly eject the gas far from the the virial radius. This newly reheated gas in not allowed to cool while remaining inside the halo.

2.2.6 Chemical enrichment

When stars die, they release the metals they produce throughout their lifetime into the ISM. Then these heavier elements are enriching the ICM through the SNae winds mechanism we saw in the previous section. In this model we consider that every solar mass of stars is producing a certain amount of metals, defined by the yield parameter y. This free parameter is tuned using the MCMC method, although the metallicity of the ISM is not used in our case as a constraint. This method gives a rough estimate of the total metallicity present in the gas component.

More accurate descriptions of the metallicity, with tracking of individual elements, has been developed in Yates et al. (2013); De Lucia et al. (2014); Yates et al. (2017). However the version of the code used for this thesis work does not include any of this recent improvements.

2.2.7 SMBH accretion and AGN feedback

In this version of the code, two different modes of accretion and feedback exist for the SMBH : quasar and radio modes.

• In the quasar mode, the SMBH grows by accreting cold gas during merger events. In this regime, the feedback is assumed to be exclusively radiative and only contributes towards the AGN luminosity. Although being a discrete event in time, the quasar mode is the main contributor to the black hole growth in this SAM.

• In the radio mode, the SMBH accretes passively gas from the hot atmosphere at every timestep. The feedback produced by this accretion is considered being mechanical only and help reheating the gas currently cooling. Therefore it provides a quenching of star formation in groups and clusters of galaxy. This mechanism is necessary to prevent the overcooling problem happening in large structures.

A more in depth description of this method and its problems is provided in Chapter 4.

2.2.8 Tidal and ram-pressure stripping

The hot gas atmosphere surrounding a galaxy can also be removed through other phenomena. When a smaller halo infalls in a larger structure, the DM, and by similarity its hot gas, will be suffering mass loss through tidal forces. By applying the King tidal stripping equation to an isothermal sphere, we obtain the following formula :

$$\frac{M_{HG}(R_{tidal})}{M_{HG,infall}} = \frac{M_{200c}}{M_{200c,infall}} \tag{2.9}$$

where $M_{HG,infall}$ and $M_{200c,infall}$ correspond to the mass of hot gas and dark matter before the infall, and M_{HG} and M_{200c} correspond to the current mass of these components. Then, the tidal radius is given by the relation :

$$R_{tidal} = \frac{M_{200c}}{M_{200c,infall}} R_{200c,infall} \tag{2.10}$$

where $R_{200c,infall}$ is the virial radius before the infall.

In addition to this stripping, ram-pressure effects are also impacting the hot atmosphere at the same time. Through these effects, the hot atmosphere bounded to a satellite galaxy is transferred to the central galaxy. This leads to a quenching of star formation for the satellite, as the cooling stops. However, it is important to note that this instantaneous stripping is an oversimplification of the observed phenomenon (McCarthy et al., 2008).

2.2.9 Model parameters and MCMC tuning

A problem encountered by semi-analytical models is the accumulation of free parameters to describe the various astrophysical processes. Thus a proper calibration is compulsory. In order to get the best adjustments for these parameters, MCMC techniques are used to constrain them against a large selection of observational data for key galaxy properties, at different redshifts. For L-Galaxies, we adopt the Metropolis-Hastings algorithm to evaluate the probabilities of our samples. However, with a large multidimensional parameter space, a full MCMC run would take too long to perform on full Millennium (I and II) simulations. The MCMC is instead only run on a representative subsample of merger trees taken from these two simulations.

It is important to keep in mind that SAMs do not use the goodness of fit of a unique best parameter set to decide whether one model is favoured by the observational data more than another one. It instead uses marginal likelihood, which enables us to chose the best model according to statistical evidence.

As described in details in Henriques et al. (2015), the models can be tuned using a large range of observational data as constraints. However, the data we use to constrain our model depend heavily on the properties we will investigate. In Henriques et al. (2015), the model was constrained using the Stellar Mass Function (SMF) and red fractions fo galaxies at different redshifts and black hole - bulge mass relation observations. In this work, as we focus on the ICM, we will constrain only : - the SMF using datasets from Li and White (2009) and Baldry et al. (2012) for $z = 0$ and from Domínguez Sánchez et al. (2011), Ilbert et al. (2013), Muzzin et al. (2013) and Tomczak et al. (2014) for $z = 2$. - the gas fractions of groups and clusters at $z = 0$, using observations presented in Vikhlinin et al. (2006), Anderson et al. (2007) and Sun et al. (2009). This was necessary in order to force the model to adjust the gas fractions and also to check if the results would be consistent with the previous best set of parameters.

It is important to note that the black hole - bulge mass relation from McConnell and Ma (2013) is not used here as a constraint because of problems detected with the bulge of our galaxies.

Chapter 3

The baryonic excess of halos

3.1 Introduction

In semi-analytical models (SAMs), unlike hydrodynamical simulations, it is impossible to know the gas distribution outside of the halo or the Friends of Friends (FoF) group. It is thus a challenge to calculate accurately the amount of gas allowed to infall onto the halo. In order to solve this problem, in most SAMs, the total amount of baryons allowed inside the halo is set to the cosmic mean value $\frac{\Omega_b}{\Omega_M}$. If the sum of all baryonic content is lower than this limit, pristine hot gas will inflow until it is reached. Otherwise, the accretion doesn't take place. According to this simple criterion, one could think that the distribution of the baryon fraction inside the halo will be flat and equal to the cosmic mean value. However, in practice it appears more complicated, as we will see through the following example from the nIFTy project.

3.1.1 The nIFTy project

SAMs are quick and powerful tools used to put in practice the theories about galaxy formation and to give us results to compare to observations. However, even in same family of SAMs, different flavours of the same model can emerge, depending on the different physical recipes and assumptions used to describe the various range of astrophysical phenomena. As a consequence, their results can agree to various degree with the large sets of observational data available.

In order to give a fair comparison for all these existing SAMs, the nIFTy project was started (Knebe et al., 2015, for a more in depth description of the models). It compares 14 SAM variants, run using the same dark matter only simulation and halo finder (Srisawat et al., 2013), for a broad range of properties. Among all of them, an interesting study case

Table 3.1: List of the different 9 SAMs from the nIFTy project used in this study.

Model Name	Reference	Hot Gas ejection (SNae)
Galacticus	Benson (2012)	No
ySAM	Lee and Yi (2013)	Yes
Morgana	Monaco et al. (2007)	Yes
L-Galaxies	Henriques et al. (2013)	Yes
SAG	Gargiulo et al. (2015)	No
SAGE	Croton et al. (2006)	Yes
Galform KB06	Bower et al. (2006)	No
Galform KF08	Font et al. (2008)	No
Galform GP14	Gonzalez-Perez et al. (2014)	No

was the investigation of the ICM properties. 9 models were available for this study and are presented in Table 3.1.1.

All these models use the same the same cooling radius method for the hot gas (White and Frenk, 1991) and incorporate feedback mechanisms from supernovae (SNae) and black holes. However, as stated in Table 3.1.1, the main difference between their SNae feedback is the possible ejection (and reincorporation) of gas from winds for 4 of these models. It is important to note the all models have not been recalibrated again, even if the underlying DM simulation can be different from their usual one. Their free parameters are set to the best values found in their reference paper.

For this section, the 62.5Mpc/h box from the dark matter only Millennium simulation (Springel, 2005) was used in addition to a flat Λ CDM universe as described in the the 9th-year *WMAP* cosmology (Hinshaw et al., 2013).

3.1.2 Model comparison and the baryon problem discovery

In order to investigate the impact of the different SNae feedback methods, we compare the quantity of hot gas present inside the virial radius for all models, as presented in Fig. 3.1.

As we can see, all the models without an ejection mechanism (except SAG) produce halos too rich in gas at low masses ($M \leq 10^{12}\mathrm{h}^{-1}\mathrm{M}_{\odot}$). The gas ejected prevent the accumulation of hot gas at early time and in small halos, leading to a lower feedback required to prevent cooling in the following timesteps. However, above this mass threshold, the

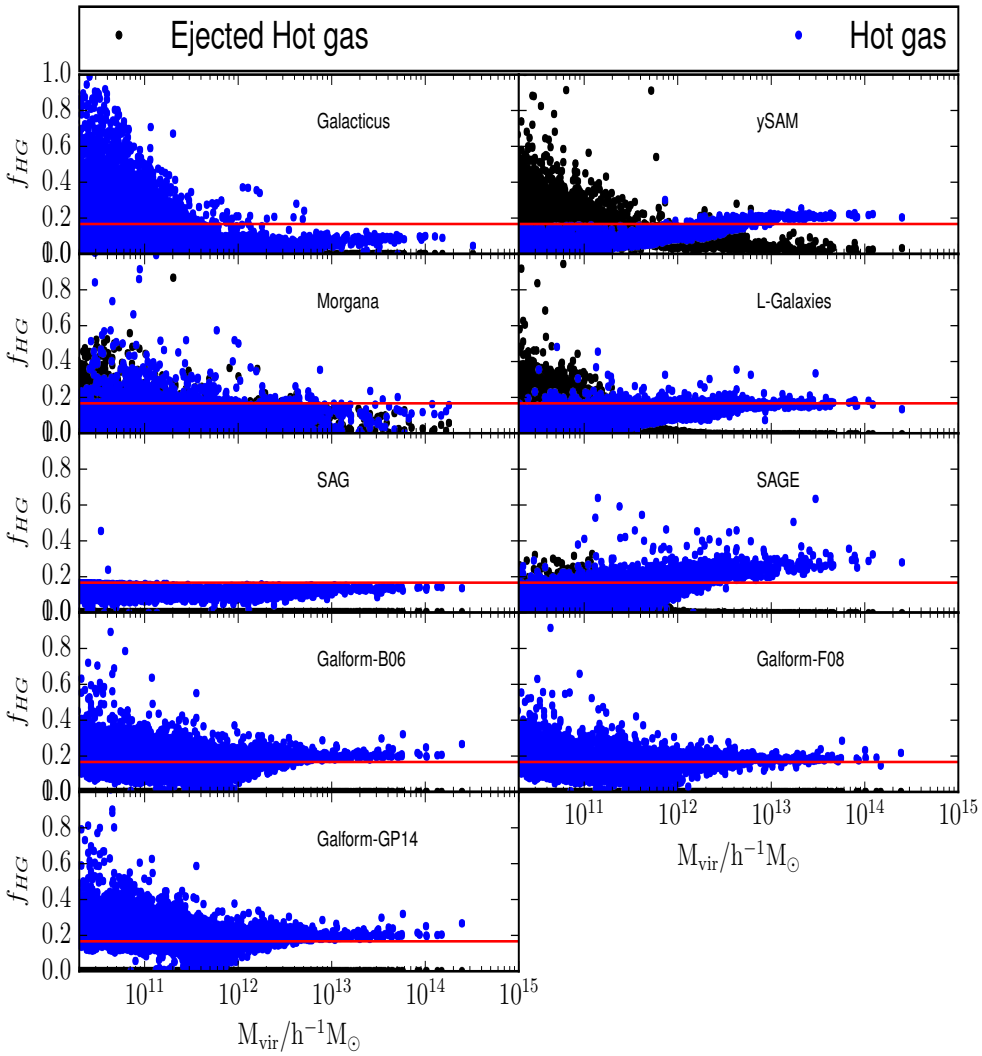

Figure 3.1: Hot gas fraction within r_{200c} (blue dots) and ejected gas fraction (black dots) against M_{200c} at $z = 0$. The red line corresponds to the cosmic mean $\frac{\Omega_b}{\Omega_M} = 0.167$.

SNae feedback becomes inefficient and fails to evacuate the gas from the halo as the gas content strive to reach the cosmic mean value. It is important to note that the relative efficiency of the SNae feedback depends on the model. The SAGE and Morgana models show a struggle in removing the gas and the distribution of ejected gas is similar to that of the hot gas. SAGE, however, is behaving differently due to the nature of its infall formula : the baryon fraction is considered being a free parameter calibrated with the model and is not limited to the cosmic mean. It allows the model to accrete more gas than expected in the other simulations even if this assumption is rather unphysical.
Interestingly, all the models, excluding SAG, are too rich in hot gas content (ejected and not) compared to the cosmic mean, especially at low masses. For high masses, the scatter is reduced but the gas fractions still exceed the mean value, Galacticus being an exception. This hints that the total baryon content is higher than we would expect in SAMs.

Fig. 3.2 shows now the total baryon fraction associated with every halo for all the simulations. According to hydrodynamical simulations without feedback (Crain et al., 2007), the baryon fraction is expected to be rather constant and close to the cosmic mean (except for masses below $M \leq 10^{10}\mathrm{h}^{-1}\mathrm{M}_{\odot}$). As we can clearly see, only SAG manages to produce a baryon content flat and close to the mean value. All the other models over estimate the amount of baryons at low halo masses. As discussed before, with higher masses comes lower baryon fractions although they still remain above the limit. Indeed, the accumulation of baryons is happening in the lower masse range of halo masses and as halos grow with time, the baryon content should not increase due to the infall formula given by Equation 3.1. Thus the baryon fraction excess is expected to decrease.

Knowing the fact that halos shouldn't be able to accrete over the mean limit, it is surprising to observe a strong scatter in the distribution of baryon fractions, with higher values than expected in theory. However, some models have a possible explanation. First of all, as said before, the SAGE model doesn't use the baryon limitation for the infall but consider it a free parameter of the model. Then, the SAG model supposedly allow hot gas to escape from the halo, which is an option unavailable to all the other models.

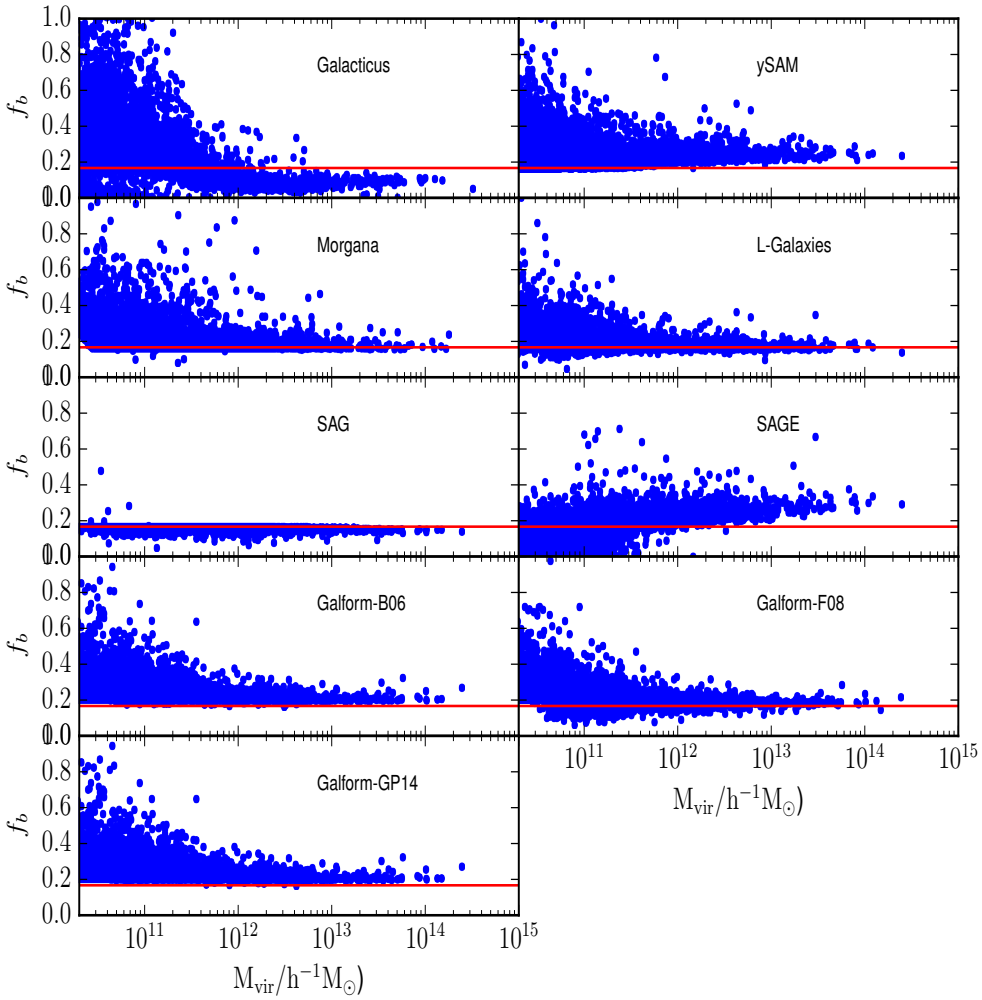

Figure 3.2: Total fraction of baryons associated with their halo against M_{200c} at $z = 0$. The red line corresponds to the cosmic mean $\frac{\Omega_b}{\Omega_M} = 0.167$.

3.1.3 Proposal for the resolution of the excess baryon problem

After highlighting the baryon problem in most of the SAM from the nIFTy study, we investigate the root of the problem and propose a physically motivated solution for the L-Galaxies SAM to deal with the baryonic excess in order to get the baryon fractions right. To achieve this goal, we consider that the diffuse atmosphere and the ejecta phase will be less bounded due to the decrease of the potential well. In this scenario, the gas will be transferred in an external reservoir to keep track of the excess loss and will be reincorporated in priority to the pristine gas during the infall phase once the halo has grown enough.

For the rest of the chapter, we used the 500Mpc/h box from the dark matter only Millennium simulation (Springel, 2005) and a flat Λ CDM universe as described in the the 1st-year *PLANCK* cosmology (Planck Collaboration et al., 2014).
This chapter is structured as follows : in 5.2, we describe the origin of the problem and the solution with the addition of an extra phase to keep track of the excess gas. In 3.3.1, we describe the results obtained with the introduction of the new phase and check on the direct impact of this change on the galaxy population. In 3.3.2, we probe the possible impact of the new phase on the ICM content and metallicity.

3.2 Method

3.2.1 The infall model

The original version of the L-Galaxies SA model dating back to White and Frenk (1991) and beyond, set the baryon density in halos equal to the cosmic mean. For these purposes, the halo was defined to be the mass within a virial radius.[1] The baryonic material within halos was allowed to be in a variety of forms, as shown in Fig. 3.3: the Extra-halo phase that lies outside the dashed line is newly introduced in the paper and will be described below. The Cold and Hot Gas phases represent diffuse gas contained within the virial radius of the halo. The Ejected phase allows for diffuse material that has been ejected beyond the virial radius but is still associated with the halo and may be reincorporated at some later stage. When halos reduced in mass over time any excess material was removed from the Ejected and Hot Gas phases to return the total baryon content to the expected

[1] In common with many SA model papers, we use the term 'virial radius' imprecisely to mean, in our case, R_{200c}, as defined below.

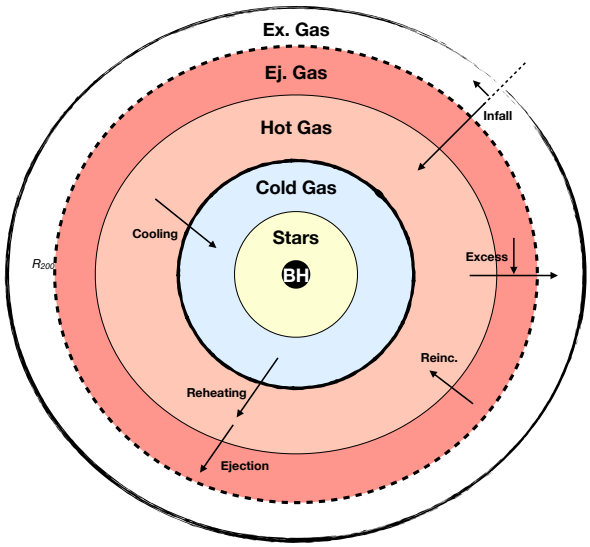

Figure 3.3: The reservoirs of baryonic material and principal gas interactions within each halo in the L-Galaxies SA model. From top to bottom: Extra-halo gas, in excess of the cosmic baryon fraction; Ejected gas, that lies outside the virial radius; Hot gas within the virial radius; Cold gas associated with a galactic disk; Stars (disk, bulge and intracluster, including stellar remnants); central Black hole.

cosmic value. The amount of infall is given by :

$$\Delta M_{\rm infall} = \alpha_{\rm Reion} \frac{\Omega_{\rm b}}{\Omega_{\rm m}} M_{\rm 200c} - M_{\rm b}, \tag{3.1}$$

where $M_{\rm 200c}$ is the virial mass, $M_{\rm b}$ is the total mass of baryons within $R_{\rm 200c}$ $\Omega_{\rm b}$ and $\Omega_{\rm m}$ are respectively the baryon and total mass density parameters, and $\alpha_{\rm Reion}$ is a reduction factor to allow for reduced infall of ionised gas onto low mass halos.[2] If the halo is growing, $\Delta M_{\rm infall}$ of pristine gas is accreted smoothly over the timestep to match the cosmic mean; On the contrary, if the halo mass is decreasing, the infall is prevented to happen. This vision of the infall is simplistic in our model. In reality, the gas accretion onto the halo is more complex and can be smooth or lumpy, depending on the environment near the halo (Voit et al., 2003). If the gas is preheated before the accretion shock the hot gas entropy will raise. It generally leads to higher entropy than predicted by hierarchical accretion models. However, any inhomogeneity in the gas density before the shock will help to lower the entropy of the ICM. In SAMs, we do not have any information about the gas beyond the virial radius. We assume the gas to be shock heated and instantly mixed with the

[2]Throughout this thesis we take $\Omega_{\rm b}/\Omega_{\rm M} = 0.155$ as appropriate for the 1st-year *PLANCK* cosmology (Planck Collaboration et al., 2014) and a baryon reduction factor as calculated by Okamoto et al. (2008).

host halo's hot atmosphere (e.g. through Kelvin-Helmholtz instabilities). A proper study of the gas entropy and the properties of gas beyond the virial radius is needed to better describe the infall mechanism in our SAM. However this type of study would require a project on its own and is beyond the scope of this chapter.

Beginning with Henriques et al. (2013), the model was altered to not allow the baryonic content of halos to decrease. The reason for this was to preserve the metal content of the Universe: the original model merely discarded any excess metals when halos reduced in mass, whereas retaining the metals in halos could lead to metallicities exceeding unity within the residual diffuse gas. Unfortunately, this retention of gas has the effect of allowing halos to attain baryon fractions far in excess of the baryonic mean as previously seen in Figure 3.2. The reason for this is that halos can fluctuate wildly in mass during mergers and can separately accrete baryons that together exceed the total mass of the system. In addition, the overlapping of subhalos around the virial radius can lead to the addition of all its baryonic content to the baryon fraction, even though the substructure is partially located inside R_{200c}.

3.2.2 Baryonic content and halo growth

In principle the infall of gas into halos is very simple: except at early times in very low mass halos, each halo is assumed to have accreted a quantity of baryons that matches the cosmic baryon density. In the absence of gas physics, one might expect that to lead to a gradual increase in baryonic mass within a halo over time. Unfortunately, the growth of halos is not monotonic, both because halos are constantly changing their morphology, and because of deficiencies in halo finding and merger tree construction algorithms (see, e.g., Knebe et al., 2011; Srisawat et al., 2013) which can, for example, misidentify the central halo during a snapshot. Another explanation for this decrease in mass is the pseudo evolution of halos (Diemer et al., 2013). As defined before, the halo properties rely on the background density, which evolves with time. Due to the expansion of the universe, this density is meant to decrease, hence implying a decrease in mass if the halo is isolated. This effect is expected at low redshift ($z < 1$) and for massive halos, as the chances of accretion (through mergers) is reduced.

As clearly shown in Fig. 3.4, the halo masses don't follow a smooth growth at all time. As a consequence, the fraction of baryons is not constant and fluctuate, especially at low redshifts and high masses (for example, due to merger events). When the halo

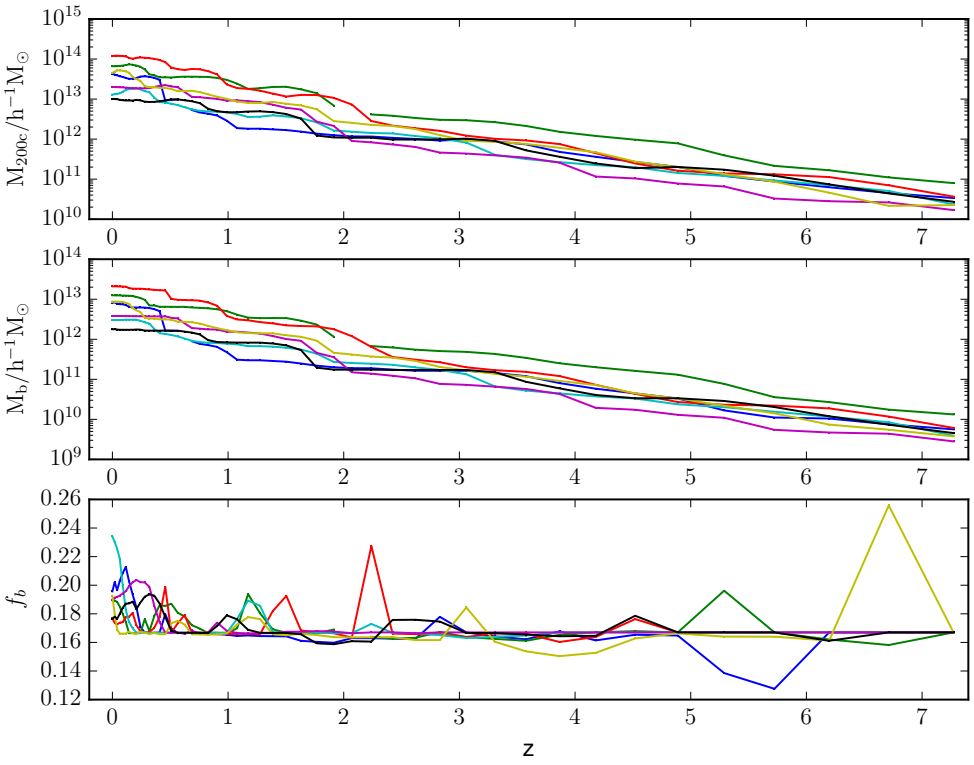

Figure 3.4: The three panels describes the evolution with redshift of three main characteristics for 7 randomly selected halos. These properties are the virial mass, the total mass of baryons associated with the virial mass and the baryon fraction of the halo (top to bottom panel). A discontinuity in the curve symbolises a swap event, meaning that the main halo got considered being a satellite during the snapshot due to a misidentification from the Halo finder.

mass happens to decrease, the amount of baryons remains constant [3] until the halo grows above its previous maximum mass. Thus the accumulation of baryons occurring in most of our halos.

Different solutions can be probed to solve this problem.

• A first solution would be to change the virial radius we use to calculate the total mass and the baryon budget. For example, calculating the total accreted mass inside the splashback radius. However, the knowledge of the environment beyond the virial radius is extremely limited in our SAM, either for the gas outside of the halos or in the specific case where the splashback radius would extend beyond the FoF group. In Yates et al. (2017), it has been proposed to replace the $M_{\rm b}$ in Equation 3.1 with $M_{\rm b,FoF}$, which is the total amount of baryonic mass inside the FoF group. This change is motivated by the possibility of subhalos to (partially) lie outside the virial radius. However it only contributes to a slight change in fractions. Hence it also hints at a limited effect due to possible pseudo-evolution.

• Another solution would be a change of the current halo finder and merger tree code. Discussions with Dr. Srisawat and its study made for nIFTy project (Srisawat et al., 2013) show that the results would lead to a similar problem, as it is known to be a problem with the limitations of these type of codes (e.g. central halo swapping) and our infall assumptions.

• A last solution would be to force the halo to only increase in mass. As much as this appears to be a reasonable solution, it would result in a modified halo mass function with a bias to higher masses and would conflict with pseudo-evolution.

It is clear that neither of the solutions described above is ideal, and so in this work we return to the idea of allowing negative infall onto halos, whilst at the same time introducing an extra gas phase to account for any metals that would otherwise be lost, as described in the following section.

The solution – the extra-halo phase

In the L-Galaxies SA model, the Ejected phase holds material that is associated with a halo but which has been pushed outside of $R_{\rm 200c}$ by the action of feedback. It will be re-incorporated back into the halo at later times. When a halo decreases significantly in mass, or two halos merge to produce a final halo whose mass is less than the sum of the two progenitors, then this arises from a deficiency in the ability of merger trees to fully capture the changing geometries. The excess baryonic contributions that result are

[3] It can happen that the baryon content increases slightly, due to halo mergers and the addition of baryons belonging to the incoming halo.

loosely associated with the FoF group but are not expected to be reincorporated into the halo and so should not be associated with the Ejected phase. Instead, we introduce an additional Extra-halo phase to keep track of these extra baryons and, more importantly, the associated metals.

We consider the change in mass to reduce the virial radius, which means that the potential well of the halo decreases and allows the diffuse gas to be less bounded and able to escape from the halo. We allow consequently a fraction of the hot gas to move to the Ejected phase. Then we fill the Extra-halo phase with the required amount of excess gas, starting from the less bounded reservoir (Ejected phase) to the hot phase. If, at a later stage, a halo grows again in mass, then baryons are accreted[4] preferentially from this Extra-halo phase until it is exhausted before adding primordial material. This whole process is summarised in the schematic shown in Figure 3.3. When coming from the Extra-halo phase, the infalling gas will be shared between the Ejected phase and the hot phase according to the relative weight of these two reservoirs. This arbitrary choice can be justified by the fact that the gas in excess was a mix of these two reservoirs. Moreover, the question of the gas mixing can be important, but we will see in the next section that this choice has no visible impact on the ICM metallicity.

3.3 Results and Discussions

3.3.1 Baryonic correction

The baryon content of halos is shown in Fig. 3.5 for the HWT15 model (top panel) and for the same model including the Extra-halo phase (lower panel). As expected, the baryonic correction removes the upward scatter previously observed in the upper panel at low halo masses, and the enclosed mass is not exceeding the limit as described in Equation 3.1, with the removed gas being stored in the Ejected phase. The results are now in better agreement with predictions and observations (e.g. Crain et al., 2007). The few points above the cosmic mean can't be lowered more. Indeed, it means that the only content remaining in these halos is composed of galactic components (ISM and stars) that we consider bounded to the halo due to their compact structure.

However, it is important to note that both models produces halos with a lower baryon fraction that the expected mean. Although these lower fractions are expected at lower masses due to the reionisation parameter in Equation 3.1, this behaviour should stop as

[4] In the terminology of SA models, 'infall'.

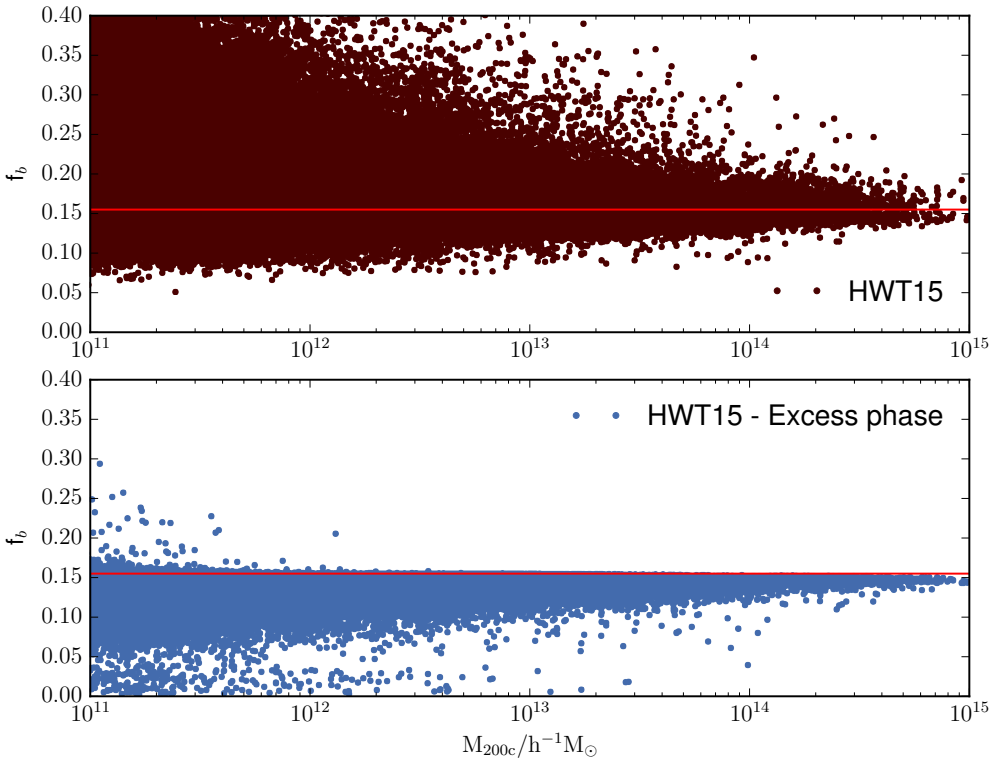

Figure 3.5: Fraction of baryons against their associated virial halo mass for HWT15 (upper panel) and the same model including the baryon correction (lower panel) at $z = 0$. The red line represents the cosmic mean $\Omega_b/\Omega_M = 0.155$ (Planck Collaboration et al., 2014).

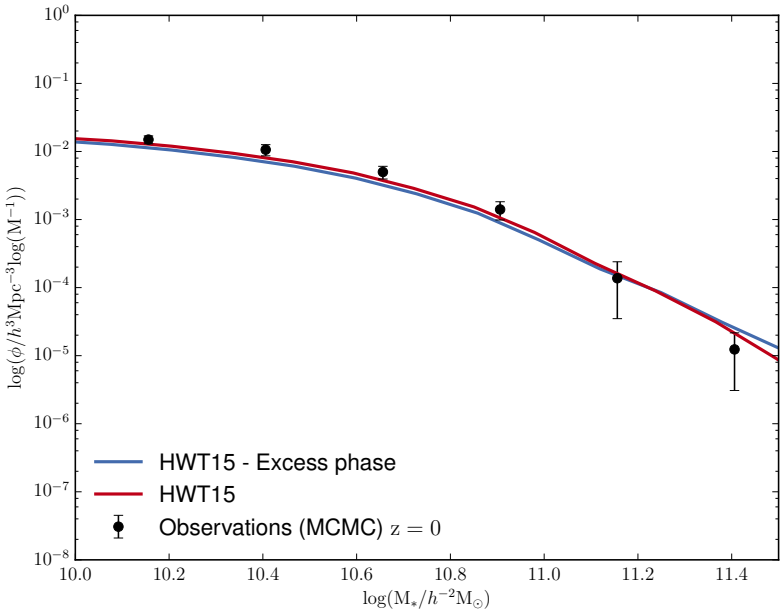

Figure 3.6: Stellar mass function of galaxies for the standard HWT15 model and the same model including the excess phase at $z = 0$ (without AGN ejections). The observations used in the MCMC are a combination of Domínguez Sánchez et al. (2011), Muzzin et al. (2013), Ilbert et al. (2013), and Tomczak et al. (2014).

we increase towards higher halo masses $\geq 10^{11}\mathrm{h}^{-1}\mathrm{M}_{\odot}$. This observation is not a side effect from the new Extra-halo phase as it occurs also in HWT15 and the Hen13 model, or any other SAMs seen in Fig. 3.2. As stated before, taking into account all the baryons inside the FoF group instead of the the virial radius fails to solve this problem as the changes led to a slight change in the baryon content (Yates et al., 2017). Current investigations are still ongoing to to understand the cause of this effect, a bug in the SAM still not being excluded.

Now that the baryon content has been reduced according to expectations, it is important to ensure the galaxy population is not drastically impacted by this severe change. As the gas reservoir has been reduced dramatically for a large range of halo masses, we need to assure galaxies are growing according to expectations. However, as the total amount of baryons bounded to halos remain similar between the two models, one could predict that galactic properties should remain close, as the infall is only delayed for the new model. The galaxy stellar mass function is presented in Fig. 3.6 for the original HWT15 and the one incorporating the Extra-halo phase. As we can see, star formation has been slightly reduced due to a shortage in hot gas for the cooling. At the higher end however, the new

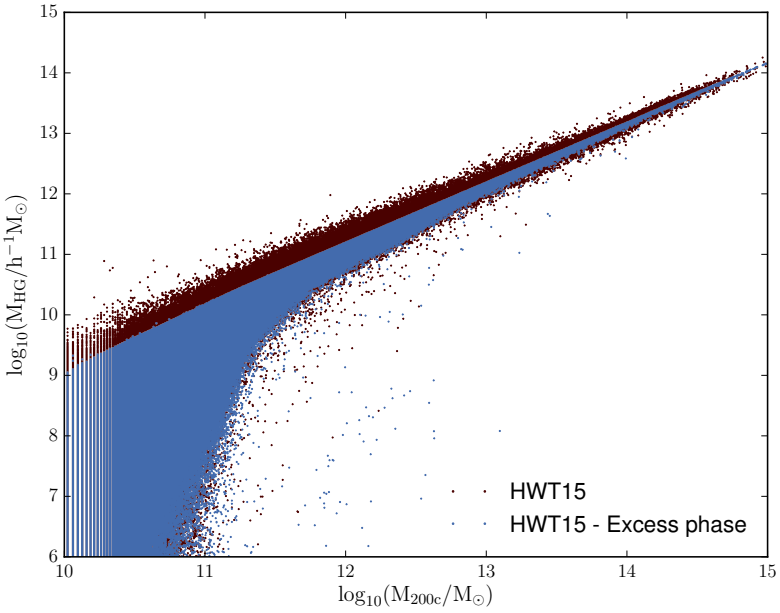

Figure 3.7: Hot gas mass against virial mass for the standard HWT15 model (no baryon ejection feedback) and the same model including the excess phase at $z = 0$.

phase leads to a small increase in the number of massive galaxies. This change can be explained by a reduced efficiency of AGN feedback. Indeed, lowering the available amount of hot gas impacts directly the black hole growth which is then slightly delayed compared to the original model. However these slight differences can be removed by adjusting parameters through MCMC tuning.

For other properties, such as the star formation rate or the gas content of galaxies for example, the two models also show similar results. Hence, this delayed infall and decrease in hot gas has little impact on galaxy properties. This result could be explained by the fact that most of the gas is removed in smaller halos, where SNae feedback is particularly efficient, in addition to halo growth through mergers. Hence the delay for the infall remains small enough. Further investigations would be needed to confirm these hypotheses.

3.3.2 The impact on ICM properties

The new reservoir has a small incidence on star formation due to a modification of the hot gas content, however it is necessary to compare these changes regarding the ICM, as the hot atmosphere and the Ejected are the most impacted by the new implementation. Fig. 3.7 shows the total amount of hot gas inside r_{200c} for our two flavours of the HWT15 model. The Extra-halo reservoir leads to halos with a reduced scatter for the hot gas,

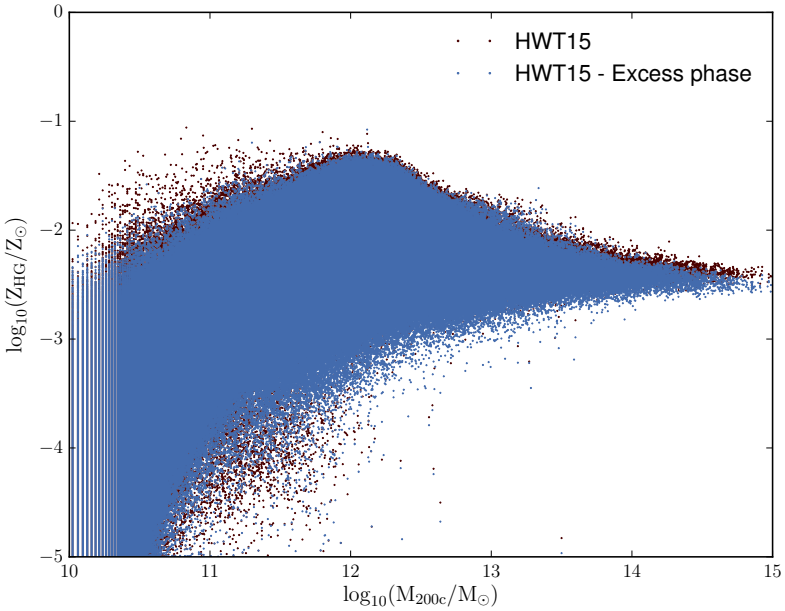

Figure 3.8: ICM total metallicty against virial mass for the HWT15 model (no baryon ejection feedback) and the same model including the excess phase at $z = 0$.

in particularly in the higher mass range of hot gas for a given halo mass. This properly follows the fact that the excess of hot gas is removed from our halo, given that the main trend remains similar to the original model.

One of the main concerns of allowing the hot gas to leave the halo was the conservation of its metallicity. As we can see on Figure 3.8, the hot gas metallicity is similar to the one obtained in the original model. Hence the metallicity is properly conserved in our new infall implementation. This result makes sense as we transfer an equal amount of the fraction of gas and its metallicity when moving the gas through reservoirs The scatter and the means remains similar. Having a reincorporation mixing the reaccreted gas between ejected and hot reservoirs have in addition no impact on the results.

3.4 Conclusions

Starting from the case study of the nIFTy workshop, we have shown in this chapter the weaknesses of SAMs regarding the baryon content of their halos and solved the excess problem by introducing an Extra-halo phase to allow halos to lose their baryonic content when required, while keeping track of it.

All the SAMs from this study agree on a hot gas content close to the cosmic mean at high

masses. However a majority discloses higher gas fractions in low masses halos. A similar trend occurs when taking into account the total mass of baryons enclosed inside the halo for most of the SAMs. This behaviour was even more puzzling because their infall should be limited to the cosmic mean value.

An in depth investigation showed that halo masses, coming from the underlying dark matter only simulation, can actually fluctuate through cosmic time. This could be due to merger events and change in the geometry of the halos but also to the limitations of the halo finder and merger tree codes used. The pseudo-evolution of halos could also be a cause, however its effect seems limited.

A solution for this problem was to allow baryons to leave the halo into an Extra-halo phase were they can be stored with their properties (e.g. metallicity) to be used as infalling gas when the halo grows enough again.

The introduction of this extra phase leads to baryon fractions reduced to the cosmic mean fraction or below, as expected. The impact on galaxy formation is minimal and can easily be adjusted through a MCMC tuning of the parameters. A decrease in the baryon fractions also induced a slight decrease in the hot gas content. Moreover, the metal content is similar to the one obtained previously, which proves an effective conservation mechanism.

However, low baryon fractions are present in the results. Even if this was highlighted in previous version of the model (and other SAMs) and not a consequence of the new infall model, no explanations currently exist to understand this odd behaviour.

Chapter 4

AGN feedback and black hole properties

4.1 Introduction

The hot gas surrounding galaxies in halos is thought to be a key element in their star formation and challenging to model in both hydrodynamical simulations and semi-analytic models (SAMs). In the scenario of hierarchical structure formation (White and Rees, 1978; White and Frenk, 1991), the gas is shock heated during its infall onto the halo. Then it cools down towards the centre and feeds the galaxy with cold gas, leading to star formation. Due to the cooling flow problem (White and Rees, 1978; Fabian, 1994), feedback mechanisms were implemented to regulate gas flows, backed up by strong observational evidence. If supernovae feedback is sufficient to regulate star formation in low mass galaxies (Dekel and Silk, 1986; Cole et al., 1994; Efstathiou, 2000; Governato et al., 2007), it fails at explaining the population of more massive galaxies (Bower et al., 2006; Hopkins et al., 2014). Winds and jets from supermassive black holes are thought to be the main regulation mechanism in massive galaxies and clusters (Hopkins et al., 2005; Bower et al., 2006; Croton et al., 2006; Di Matteo et al., 2008). This feedback has two main roles: quenching the galaxy and regulating the accretion of gas on to the black hole. However, the mechanisms controlling the AGN growth and feedback are still poorly understood in large-scale simulations and different approaches exist, not only for SAMs, but also for hydrodynamical simulations (Vogelsberger et al., 2014; Schaye et al., 2015, e.g.).

X-ray observations (Vikhlinin et al., 2006; Anderson et al., 2007; Sun et al., 2009; Sun, 2012) show that the amount of ICM present inside the virial radius is far below the cosmic mean for all but the most massive dark matter haloes. In low mass halos, cold gas is

heated and expelled from halos by supernovae, but this begins to fail once the virial mass of the halo rises above $\sim 10^{12}\mathrm{M}_{\odot}h^{-1}$. For high mass halos, we need a more energetic heating mechanism and the most obvious candidate for this are AGN jets and winds that are not only powerful enough to reheat the gas currently cooling, but also able to carry away baryons in high velocity outflows (Tremonti et al., 2007; Rupke and Veilleux, 2011). AGN driven outflows have kinetic efficiency that differs depending of the environment but appears to be a fraction of the total AGN luminosity (Cicone et al., 2014; Fiore et al., 2017).

In older SAMs, the feedback from the AGN is mainly used to reduce the cooling of gas on the galaxies. This helps to decrease the star formation by starving the galaxies, but doesn't change the overall baryon content of the halo. Most recent SAMs are now trying to remedy this problem by enabling the AGN feedback to eject gas outside of the virial radius before being reincorporated (Bower et al., 2008; Croton et al., 2016). However, if the mechanical feedback seems a satisfactory solution in lowering the content of baryons, uncertainties remain on the way the supermassive black hole is fed. In the case of most of SAMs (Bower et al., 2006; Croton et al., 2006; Guo et al., 2011; Henriques et al., 2013, 2015; Croton et al., 2016), the black hole is supposed to accrete both during violent merger events, leading to quasars, and also in a continuous manner from the ICM itself, to limit the star formation smoothly over time. Meanwhile other models try to reproduce a feeding of the black hole from a cold accretion disk and galactic disk instabilities (Hopkins and Quataert, 2011; Menci et al., 2014, 2016).

In this chapter we develop a new feedback description for the black holes in the L-Galaxies model from Henriques et al. (2015, hereafter HWT15). We allow the mechanical feedback created by the AGN to reheat part of the gas present in the galaxy and the gas cooling onto the galaxy. If some energy is left, it will be use to eject the gas in a manner similar to the supernovae feedback.[1] We test five different accretion models onto the black holes, constraining the model parameters using the hot gas content of massive halos. We then investigate the affect upon predicted black hole masses and the AGN luminosity function.

For this simulation, we used the 500Mpc/h box from the dark matter only Millennium simulation (Springel, 2005) and a flat Λ CDM universe as described in the the 1st-year *PLANCK* cosmology (Planck Collaboration et al., 2014).

The chapter is structured as follows: in Section 5.2, we describe a modification to

[1]Some studies suggest the possibility of positive feedback triggered by the AGN jets (see, e.g., Molnár et al., 2017) but this will not be investigated in our study.

the infall of primordial gas onto halos, the five different black-hole accretions models considered, our new AGN feedback model allowing ejection of hot gas out of the halo, and how gas reincorporation is modelled. In Section 4.3.1, we describe the results obtained for the constrained properties; in Section 4.3.2, for other galaxy properties; and in Section 4.3.3, for black hole growth and AGN activity. Finally, in Section 5.4, we present our conclusions.

4.2 Method

In this section, we discuss modifications to some of the key physical processes modelled in L-Galaxies which affect the growth of black holes and the corresponding AGN feedback. This includes the modified infall discussed in the previous chapter.

4.2.1 AGN accretion

In the L-Galaxies SA model, black hole growth occurs in two main ways: it happens impulsively during major merger events (the *quasar mode*), in which a fraction of the cold gas is driven onto the central black hole; and also continuously by slow accretion of gas (the *radio mode*).[2] Mergers are main mechanism for black hole formation (we require no seeds) and growth. On the other hand, only the radio mode is used as a feedback mechanism to suppress the gas cooling onto the galaxy, thus quenching star formation. However this description is unrealistic. The goal behind these two modes (and their specific names) was to reproduce the different types of AGN observers could encounter. Quasars are contributing to the luminosity output and are short time events, due to a change in the ISM distribution during a merger. While the radio modeis reproducing the quiet feedback happening to limit the cooling. This description is, however, too simplistic. First of all, it has been proven that quasar driven winds are in fact a major contributor in reducing the cooling from the ICM (McCarthy et al., 2011). Secondly, it is impossible in our SAM to know the local environment of our SMBHs accurately and, as said in the introduction, the unification paradigm indicates that the difference of luminosity is due to the angle of observation rather than a difference of mechanism or feedback.[3]

[2] We note that black hole growth can also occur during disk instability that will also drive gas towards the galactic centre. The existing HWT15 model does not allow for this (although the next version of the L-Galaxies SA model will do so) and so we do not include it here.

[3] It could be useful to rename these modes into more relevant names in future works, such as Merger and Continous modes for example.

The principal aim of this chapter is to contrast different radio mode feedback models and so, to aid this, we use the same quasar accretion model for each:

$$\dot{M}_{\rm BH,Q} = f_{\rm BH} \frac{(M_{\rm sat}/M_{\rm cen})}{1+(V_{\rm BH}/V_{\rm 200c})^2} \frac{M_{\rm cold}}{\Delta t}, \tag{4.1}$$

where $M_{\rm cold}$ is the total cold gas mass of the merging central plus the satellite galaxies, $M_{\rm cen}$ and $M_{\rm sat}$ their respective baryon masses, $V_{\rm 200c}$ is the virial velocity of the halo, Δt the timestep and $f_{\rm BH}$ and $V_{\rm BH}$ are two free parameters indicating the fraction of available accreted cold gas and the velocity at which the efficiency saturates. We adjust these latter two parameters to obtain the best match between predicted and observed stellar mass functions and hot gas fractions, as described in Section 4.3.1 below. This equation is motivated by the fact that mergers are cataclysmic events. The gas distribution of the ISM is completely modified and the probability of gas inflowing towards the center (and, so near the black hole region) dramatically increases.

We consider five models for radio mode accretion, that we can classify in three categories: hot gas accretion using the existing HWT15 algorithm, or the Croton et al. (2016) model; cooling gas accretion using a model inspired by the work of Bower et al. (2008); cold gas accretion using either a classic Bondi-Hoyle, or a gravitational torque approach (Hopkins and Quataert, 2011; Menci et al., 2014). We next describe each of these in turn.

Hot accretion with maximal cooling flow: HotCrot

In HWT15 the sole purpose of black holes was to provide radio-mode AGN feedback to prevent cooling of gas in massive halos hosting clusters of galaxies. However, these authors did not perform some basic checks on the hot gas fractions in clusters or the AGN luminosity function, and we shall see below that it does not reproduce any of these properties very well. The radio mode accretion rate is taken to be

$$\dot{M}_{\rm BH,R} = k_{\rm AGN} \left(\frac{M_{\rm hot}}{10^{11} M_\odot}\right) \left(\frac{M_{\rm BH}}{10^8 M_\odot}\right), \tag{4.2}$$

where $M_{\rm hot}$ is the hot gas mass, $M_{\rm BH}$ is the black hole mass and $k_{\rm AGN}$ an accretion parameter. The precise form of this formula is largely phenomenological but was motivated in Croton et al. (2006) both by Bondi-Hoyle accretion of material cooling out of the hot gas and by accretion from cold clouds. However the black hole growth from 4.2 was regulated in order to only reheat the cooling gas at maximum. Removing this limit in order to evacuate the gas and compute luminosities leads to black hole overaccretions and a poor description of all galaxy properties.

Thus we consider another model based on hot gas accretion, as described in (Croton et al., 2016). This model goes a step further by approximating the density of hot gas surrounding the black hole in order to solve the Bondi-Hoyle equation using the 'maximal cooling flow' method[4] of Nulsen and Fabian (2000). This leads to:

$$\dot{M}_{\rm BH,R} = k_{\rm AGN}\frac{15}{16}\pi G\bar{\mu}m_p\frac{kT}{\Lambda}M_{\rm BH}, \tag{4.3}$$

where k is the Boltzmann constant, $\bar{\mu}m_p$ is the mass per particle, $\Lambda(T,Z)$ is the cooling function, dependent on gas temperature T and metallicity Z, and $k_{\rm AGN}$ is an efficiency parameter. In both this model and the HWT15 method, the accretion rate is proportional to the black hole mass. However, in HotCrot the accretion rate is now largely independent of the hot gas properties: the mass has been replaced by T/Λ, with T being determined by the virial temperature of the halo.

Cooling based accretion: CoolBow

The model developed in Bower et al. (2008) is motivated by the fact that radiative cooling alone can reproduce the observed entropy profiles of clusters of galaxies (see, e.g. Muanwong et al., 2001; Voit and Bryan, 2001) at the expense of having far too much cold gas and star formation. A viable model can be obtained if the majority of that cooling gas can be ejected from the cluster before it forms stars and the model does that by assuming that some fraction of the cooling gas will be accreted onto the central black hole liberating energy that can be used to provide feedback.

The accretion rate is given by

$$\dot{M}_{BH,R} = \frac{L_{\rm radio}}{\eta c^2}, \tag{4.4}$$

where

$$L_{\rm radio} = \min\left[k_{\rm AGN}\eta\dot{M}_{\rm cool}c^2, \epsilon L_{\rm Edd}\right] \tag{4.5}$$

and $L_{\rm Edd}$ is the Eddington luminosity. Here $k_{\rm AGN} = 0.01$ represents the fraction of cooling gas that reaches the black hole and $\eta = 0.1$ is the usual accretion efficiency. $\epsilon = 0.02$ is a limiting factor related to the structure of the accretion disk: at high accretion rates then the disk becomes radiatively efficient and the energy is not available for feedback. This value agrees with a geometrically thin disk.

The rate of ejection of gas from the halo through AGN heating is

$$\dot{M}_{\rm ej} = \frac{L_{\rm radio} - L_{\rm cool}}{0.5V_{\rm 200c}^2}. \tag{4.6}$$

[4]In order to find the local density of gas, we equate the sound travel time across a shell of diameter twice the Bondi radius to the local cooling time.

BMB08 note that the heating rates can often be extreme and lead to complete evacuation of hot gas from the halo. In this specific setup, all the energy is used for mechanical feedback without any contribution to the luminosity (until the hot atmosphere is completely depleted). They impose a limit of no more than 50 per cent of the hot gas being expelled on any given timestep in order to avoid an unrealistic depletion of gas in the hot atmosphere.

However, in this paper we make the following modifications that we feel make the model slightly more self-consistent:

- The black hole will grow in mass according to the amount of mass accreted, regardless of the fraction of the accretion energy used for feedback. This is necessary if we want to compute AGN luminosities. It implies that the black hole is allowed to accrete, up to the Eddington rate, regardless of the feedback it will produce. In addition, we choose not to ignore the distinction between the mass flow rate through the accretion disk and the mass growth rate of the black hole. Therefore we modify Equation 4.4 to read

$$\dot{M}_{BH,R} = \min\left[k_{\rm AGN}(1-\eta)\dot{M}_{\rm cool}, \frac{L_{\rm Edd}}{\eta c^2}\right]. \tag{4.7}$$

- With the above change, then we find it necessary to set $k_{\rm AGN} = 0.001$ in order to limit the accretion on black holes and obtain reasonable masses.

- It is unclear from the text of BMB08 whether or not feedback energy is used to reheat cooling gas that does not make it onto the black hole. From the form of Equation 4.6 it would seem that it should do so as the energy lost by cooling has been subtracted from that available for ejection. In order to be completely consistent, however, we modify the equation to read

$$\dot{M}_{\rm ej} = \frac{L_{\rm radio} - (1-k_{\rm AGN})L_{\rm cool}}{0.5V_{\rm 200c}^2}. \tag{4.8}$$

  As $k_{\rm AGN}$ is small, this makes very little difference to the results.

- We prefer to use a physical timescale when limiting the amount of gas that can be ejected, so we set a maximum ejection rate of $M_{\rm hot}/t_{\rm dyn}$, where $t_{\rm dyn} = R_{\rm 200c}/V_{\rm 200c}$ is the dynamical time of the halo. To be more precise, in time interval Δt we allow ejection of a maximum fraction of hot gas equal to $1 - \exp(-\Delta t/t_{\rm dyn})$ – see Section 4.2.2.

The cold cloud model: ColdC

In the above models the accretion of gas onto the black hole is determined by the large scale gas distribution or cooling rate and is independent of the local environment of the black hole. It would be possible to modify the accretion rates to restrict them to (some multiple of) the Eddington rate but that is only a partial solution. Here we develop a model in which the mass of the black hole and the properties of the cold gas that surrounds it determine the accretion rate.

The Bondi-Hoyle accretion rate onto a black hole sitting in a uniform medium of density ρ and sound speed v is

$$\dot{M}_{\rm BH} \propto \pi R_{\rm Bondi}^2 \rho v, \tag{4.9}$$

with the precise value of the proportionality constant depending upon the equation of state of the gas. Here

$$R_{\rm Bondi} = \frac{2GM_{\rm BH}}{v^2} \tag{4.10}$$

is the Bondi radius. This formula applies equally well to a black hole moving at speed v through a uniform density of cold clouds: the $\pi R_{\rm Bondi}^2$ term represents a capture cross-section, and the product of ρ and v the flux density of material passing through that cross section. Within the cold gas (i.e. interstellar medium) component of the galaxy, the predominant motion is on circular orbits that will not take material close to the black hole. However, gravitational perturbations caused by bars, spiral arms, giant molecular clouds, crossing shells from SNae feedback, etc., will constantly perturb the orbits and scatter some material onto trajectories that do pass within the Bondi radius. We assume that this will occur at a rate that is proportional to the mean gas density within the cold component of galactic disks[5]. Accordingly we take

$$\rho = \frac{M_{\rm cold}}{4\pi R_{\rm disk}^2 a}, \tag{4.11}$$

where $R_{\rm disk}$ is the cold gas disk scale length and a is the disk height scaling parameter.

Our accretion rate is therefore given by

$$\dot{M}_{\rm BH,R} = k_{\rm AGN} \frac{M_{\rm cold}(GM_{\rm BH})^2}{R_{\rm disk}^2 a v^3}. \tag{4.12}$$

We take $a = 0.25\,$kpc and do not allow $R_{\rm disk}$ to drop below that value. The main uncertainty is what value to assign to v. If we take v equal to the typical observed velocity

[5]Here we use the mean density of the gas rather than the density near the black hole as we include all sources of instabilities able to push gas towards the center. This choice might be updated once disk instabilities are properly modelled in our SAM

dispersion in galactic disks, $v = \sigma \approx 10\,\mathrm{km\,s^{-1}}$, then that leads to extraordinarily large Bondi radii of $27\,(M_{\mathrm{BH}}/10^8\,\mathrm{M}_\odot)\,\mathrm{kpc}$, which clearly over-estimates the effective accretion radius of the black hole because the relative velocity of gas on circular orbits is much greater than σ. On the other hand, using the disk circular velocity will underestimate the accretion rate because cold clouds near the centre of the galaxy that have been scattered towards the back hole will have relative velocities less than that. In this paper, we set $v = \sigma$ but with the understanding that the efficiency parameter k_{AGN} will be less than unity.

No matter how large the accretion rate given by Equation 4.12, there will be a limit to how rapidly the cold gas disk can be depleted. We take that limit to be equal to τ_{accrete} times the dynamical time of the disk. Specifically, we limit the fraction of the cold gas that can be accreted in time Δt to $1 - \exp(-\Delta t/\tau_{\mathrm{accrete}} t_{\mathrm{disk}})$, where $\tau_{\mathrm{accrete}} \gg 1$ is a free parameter, $t_{\mathrm{disk}} = R_{\mathrm{disk}}/v_c$, and v_c is the circular speed of the disk. We impose a fixed value of $\tau_{\mathrm{accrete}} = 100$.

The gravitational torque: ColdGT

(Hopkins and Quataert, 2011) developed in their paper a gravitational torque accretion model for their black hole. Gravitational perturbations in the galactic disk triggers angular momentum transport mechanisms that leads to a portion of the ISM being carried towards the centre and feeding the black hole. This leads to a more physical interpretation of the gas flow than the usual Bondi-Hoyle formula. Their analytic result has been adapted for an exponential disk by Menci et al. (2014) who derive

$$\dot{M}_{\mathrm{BH,R}} = k_{\mathrm{AGN}} \alpha(\eta_K) f_d^{19/12} \left(\frac{M_{\mathrm{BH}}}{10^8 M_\odot}\right)^{5/12} \left(\frac{M_{\mathrm{d}}(R_0)}{10^9 M_\odot}\right)^{3/4} \left(\frac{R_0}{100\mathrm{pc}}\right)^{-3/2} \left(\frac{R_{\mathrm{acc}}}{10^{-2} R_{\mathrm{BH}}}\right)^{5/6} \tag{4.13}$$

Here α is a normalization constant depending on the power-law index η_K of the Kennicutt-Schmidt law: we take $\eta_K = 5\ \mathrm{M}_\odot\,\mathrm{yr}^{-1}$. We introduce an additional efficiency parameter k_{AGN} to the original equation in order to fine-tune the model; M_{d} is the mass of the disk (stars + gas), and f_d the disk mass fraction, within scale-length R_0; and $R_{\mathrm{acc}}/R_{\mathrm{BH}} \approx 10^{-2}$ is the ratio of the accretion radius of the black hole to the radius within which its gravitational potential dominates over that of the galaxy as a whole. The accretion rate is proportional to the disk surface density $M_{\mathrm{d}}/\pi R_0^2$ and so relatively insensitive to the precise value of R_0: we set $R_0 = 1\,\mathrm{kpc}$.

4.2.2 Feedback

We next consider feedback of energy from the black hole into the surrounding gas.

The existing HWT15 implementation

In HWT15 , only the feedback power released by radio mode accretion is taken into account :

$$L_{\rm radio} = \frac{\eta}{1-\eta}\dot{M}_{\rm BH,R}c^2, \tag{4.14}$$

where $\eta = 0.1$ is the energy conversion efficiency[6], $\dot{M}_{\rm BH,R}$ the radio mode accretion rate, and c is the speed of light. This power is used to moderate the cooling of hot gas, giving an effective cooling rate of

$$\dot{M}_{\rm cool,eff} = \max\left[\dot{M}_{\rm cool} - 2\frac{L_{\rm radio}}{V_{\rm 200c}^2}, 0\right]. \tag{4.15}$$

When the black hole grows large enough then cooling will switch off completely in this model (the energy liberated by accretion onto the black hole exceeds that required to prevent the gas cooling in the first place).

A new reheating formalism with ejection

As the black hole knows only about its local environment, it cannot know whether or not the gas that it has accreted comes from the quasar or radio mode. We therefore sum the two when determining the black hole response:

$$\dot{M}_{\rm BH} = \dot{M}_{\rm BH,Q} + \dot{M}_{\rm BH,R}. \tag{4.16}$$

As the equation suggests, both modes are contributing to the black hole growth, at all time. The idea can seem odd as one would expect the radio accretion modes being reduced or disturbed by the chaotic merger event taking place. However, first of all these events are rare occurences. Secondly, the contribution from the quasar mode is the most important but occurs rarely and for a short period of time (if cold gas is still present in these galaxies). In this situation, the contribution of the radio mode is small in comparison and makes little to no difference to the final result.

Then the bolometric luminosity of the AGN is

$$L_{\rm AGN,tot} = \frac{\eta}{1-\eta}\dot{M}_{\rm BH}c^2, \tag{4.17}$$

[6]Note that the denominator of $1-\eta$ arises because the rate of mass growth of the black hole is lower than that of the mass flow through the accretion disk. Because the accretion rate itself is highly uncertain, this distinction is often ignored and this factor omitted.

where once again we set $\eta = 0.1$. We assume that a fraction $\eta_{\rm mech}$ of the AGN luminosity can be used for mechanical feedback (Cicone et al., 2014; Fiore et al., 2017), the rest contributing to the observed quasar luminosity, and that the power is limited to a fraction of Eddington, as in Equation 4.5:

$$L_{\rm mech} = \min\left[\eta_{\rm mech} L_{\rm AGN,tot}, \epsilon L_{\rm Edd}\right], \tag{4.18}$$

with $\epsilon = 0.02$, as before.

The feedback is first used to reheat part of the cold gas present in the galaxy. Although we found this step to be crucial in order to prevent runaway growth of black holes at high mass in the Bondi-Hoyle accretion model, it is also motivated by recent observations (see, e.g., Cicone et al., 2013). As the black hole cannot realistically deplete the whole gas disk on a very short timescale, we limit the cold gas heating rate to

$$\dot{M}_{\rm cold} = -\min\left[\frac{L_{\rm mech}}{0.5V_{\rm 200c}^2}, M_{\rm cold}\left(1 - e^{-\Delta t/t_{\rm disk}}\right)\right]. \tag{4.19}$$

If there is any heating power left over, $L'_{\rm mech}$, then it is used to prevent cooling of the hot gas, reducing the amount of gas that is cooling by an amount

$$\dot{M}_{\rm cooling} = \dot{M}_{\rm cooling} - \min\left[\frac{L'_{\rm mech}}{0.5V_{\rm 200c}^2}, \dot{M}_{\rm cooling}\right]. \tag{4.20}$$

Finally, any further excess power, $L''_{\rm mech}$ is used to eject hot gas from the galactic halo. Once again, we restrict the rate at which that gas can be ejected :

$$\dot{M}_{\rm ej} = \min\left[\frac{L''_{\rm mech}}{0.5V_{\rm 200c}^2}, M_{\rm hot}\left(1 - e^{-\Delta t/t_{\rm dyn}}\right)\right], \tag{4.21}$$

where $t_{\rm dyn} = R_{\rm 200c}/v_{\rm 200c}$ is the dynamical time of the halo. In the end, the final bolometric luminosity for our AGN is thus given by :

$$L_{\rm AGN} = L_{\rm AGN,tot} - L_{\rm mech} + L_{\rm leftover} \tag{4.22}$$

Where $L_{\rm leftover}$ is the possible leftover energy after the mechanical feedback occurred.

4.2.3 Reincorporating the ejecta

Gas that is ejected from a galactic halo is not lost forever but will eventually be reincorporated.

In the case of SNR feedback, the L-Galaxies SA model reintegrates gas over a timescale that varies inversely with the halo mass. The model developed for the AGN remains similar to it except that, given the higher energetics of AGN as compared to SNR, we

would expect the reincorporation timescale to be longer and for significant reincorporation to occur only at high masses:

$$\dot{M}_{\rm reinc} = \frac{M_{\rm ej,AGN}}{\tau_{\rm reinc}} \frac{M_{\rm 200c}}{10^{15} h^{-1} M_{\odot}} \tag{4.23}$$

where $M_{\rm ej,AGN}$ is the total amount of ejected gas that was heated by AGN and $\tau_{\rm reinc}$ is a reincorporation timescale parameter for the gas to be re-accreted by in the halo. It is set as a free parameter. It is interesting to note that this equation is depending on $M_{\rm 200c}$ directly, hence z dependent.

In Bower et al. (2008), another description of the reincorporation process is presented, where the ejected gas is reincorporated as the halo grows.

$$\Delta M_{\rm reinc} = M_{\rm ej,AGN} \left(1 - \frac{M_{\rm prog}}{M_{\rm desc}}\right), \tag{4.24}$$

where $M_{\rm prog}$ and $M_{\rm desc}$ are the virial mass of the progenitor and descendant halos respectively.

Preliminary results show no clear differences between these two different types of reincorporation. Although a more in depth study is necessary to conclude definitely on the matter and will be carried in the future improvements of the model.

For the scope of this study and to keep consistency with the SN reincorporation model, we use the equation 4.23 for the AGN reincorporation.

4.3 Results and Discussions

We split our results into three subsections: properties that we set as constraints, some other galaxy-wide properties, and predictions for black hole growth and AGN activity in each of the models.

One of the main motivations for our new black hole growth and feedback models was the desire to better fit the hot gas fractions in massive halos. At the same time, we do not wish to throw away the excellent agreement with the evolving stellar mass function (SMF) of galaxies seen in HWT15. For that reason, all the models have been constrained using MCMC methods to reproduce the observed SMF at $z = 0$ and $z = 2$ in addition to the gas fraction of clusters at low redshift. Additionally, we chose not to constrain the black hole masses as it was done in previous papers due to a change in the resulting bulge fractions which made the MCMC observations unusable. The addition of the Savorgnan et al. (2016) dataset to compare black hole masses to total stellar masses occurred too late in the thesis work to be used as constraints. However, it will be added in the new versions of the model.

Table 4.1: Summary of the five different models described in 5.2. It includes the most relevant AGN accretion and feedback parameters described in Sections 4.2.1 and 4.2.3. The values correspond to the best-fit ones obtained through the MCMC.

Model	Gas Acc.	M_{BH} dep.	f_{BH}	V_{BH}[km/s]	$k_{AGN}[10^{-3}]$	η_{mech}	τ_{Reinc}[Gyr]
HWT15	Hot	M	0.041	750	5.3	-	-
HotCrot	Hot	M	0.031	437.2	5.5	0.75	2.31
CoolBow	Cooling	1	0.027	880.2	1.0	0.11	2.88
ColdC	Cold	M^2	0.16	1256	$3.8\ 10^1$	0.074	3.77
ColdGT	Cold	$M^{\frac{1}{6}}$	0.073	421.1	$6.9\ 10^2$	0.95	5.27

Table 4.3 summarises the best fit for relevant key parameters in all methods investigated.

Although the reincorporation times relatively similar between all models, two distinct feedback behaviours are seen. HotCrot and ColdGT foster strong mechanical feedback efficiency and increased merger-driven accretion to compensate lower BH accretion rates. The opposite case is occurring for the two other models whose low values for mechanical efficiency seem to be more in agreement with what is found in Cicone et al. (2014) and Fiore et al. (2017).

4.3.1 Constrained properties

The gas fraction of halos is shown in Fig. 4.1. The data points with error bars show the observational constraints that we use which are derived from the observations in Vikhlinin et al. (2006), Anderson et al. (2007) and Sun et al. (2009). Note that the observations refer to the gas content within R_{500} whilst all the virial properties in L-Galaxies are calculated for R_{200}. The results presented here have been rescaled following a NFW profile for dark matter and isothermal-β profile for the ICM.[7] It is clear from Fig. 4.1 that all models correct the excess hot gas content found in HWT15. In that model supernovae feedback starts to become inefficient above $M_{500} \approx 10^{11} M_\odot$ but the AGN feedback is used only to prevent cooling of gas, leading to an accumulation of hot gas inside the halo. In order to maintain a reduced gas content, it is necessary for the AGN to be able to remove part of the hot atmosphere, as has been implemented in the four other models.

Below $M_{500} \approx 10^{13}$ $M_\odot$ observational constraints on the hot gas content become very

[7]The adjustments to the gas content developed in Yates et al. (2017) are not implemented here, to remain consistent with the cooling prescription.

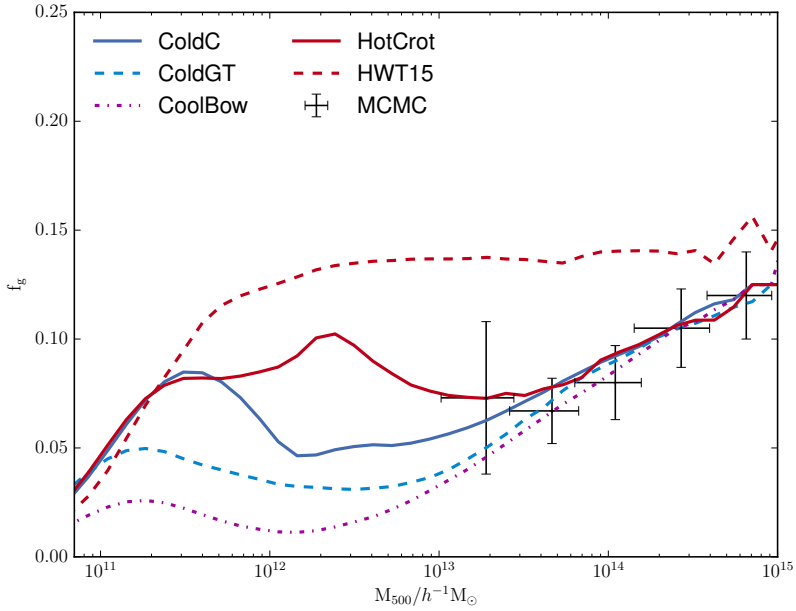

Figure 4.1: Hot gas fraction of halos against virial mass for the different models tested at $z = 0$. The virial mass has been rescaled from R_{200} to R_{500} for an easier comparison with observations. The binning of the observations used in the MCMC is made using data from Vikhlinin et al. (2006), Anderson et al. (2007) and Sun et al. (2009).

weak and we see here that there is a divergence in the model predictions. The CoolBow and ColdGT models produce a strong and continuous feedback over a wide mass range due to their independence or weak dependence black hole mass. The other two models need time to build up their central black holes before accretion and feedback become effective. Which of these two behaviours better matches real galaxies remains at present undetermined.

The stellar mass function for all the models is presented in Fig. 4.2 at $z = 2$ (top panel) and $z = 0$ (bottom panel). To derive the MCMC constraints combined data from Li and White (2009) and Baldry et al. (2012) for $z = 0$ and from Domínguez Sánchez et al. (2011), Ilbert et al. (2013), Muzzin et al. (2013) and Tomczak et al. (2014) for $z = 2$. All models reproduce the general shape of the SMF but CoolBow under-produces stars over most of the mass-range, presumably due to the early onset of AGN feedback as the black hole growth doesn't depend on any galaxy properties. Those results seem in contradiction with those of Bower et al. (2008) which reproduces the luminosity adequately. However, these differences can be explained by the fact that, even if based on the same accretion model for the black hole, the changes made for the CoolBow formula and its implementation

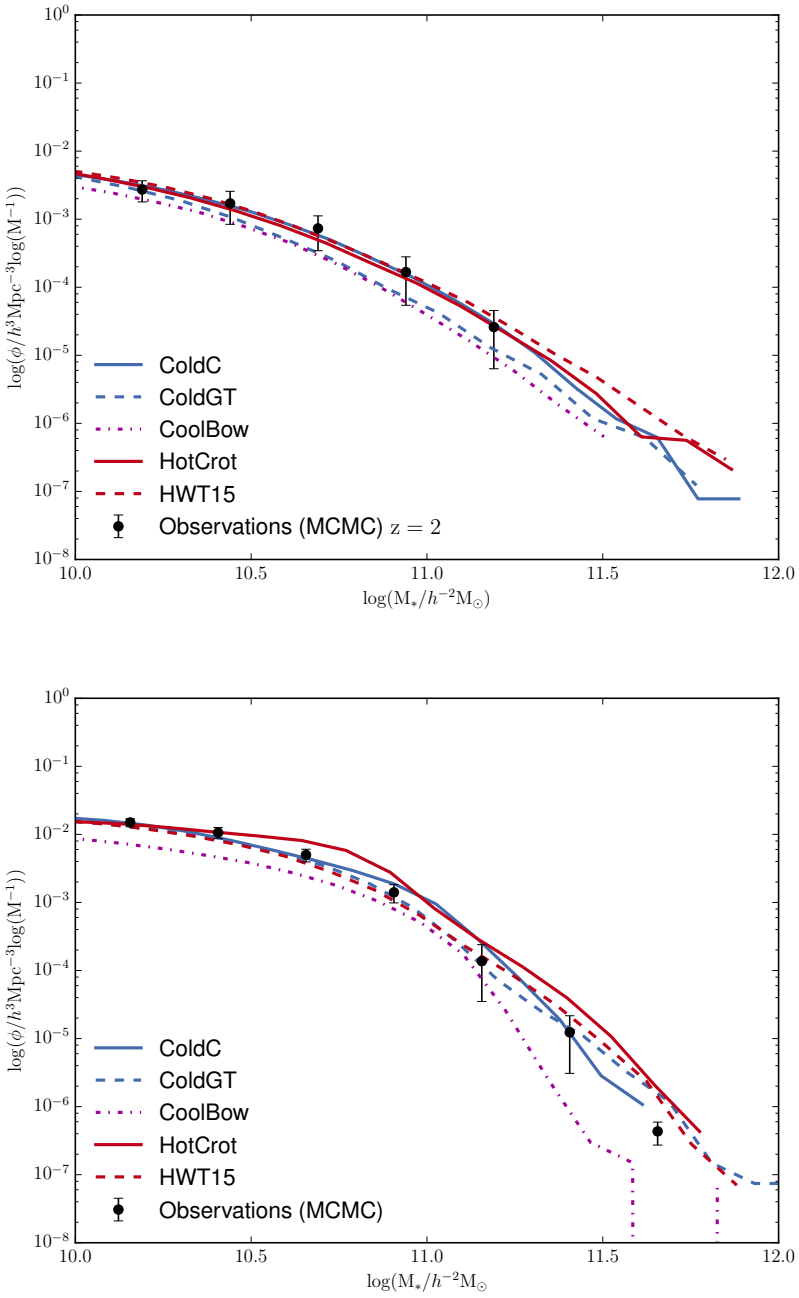

Figure 4.2: Stellar mass function of galaxies at $z = 2$ (top panel) and $z = 0$ (bottom panel) for all the model tested. The observations used in the MCMC are a combination of Domínguez Sánchez et al. (2011), Muzzin et al. (2013), Ilbert et al. (2013), and Tomczak et al. (2014) for $z = 2$, Li and White (2009) and Baldry et al. (2012) for $z = 0$.

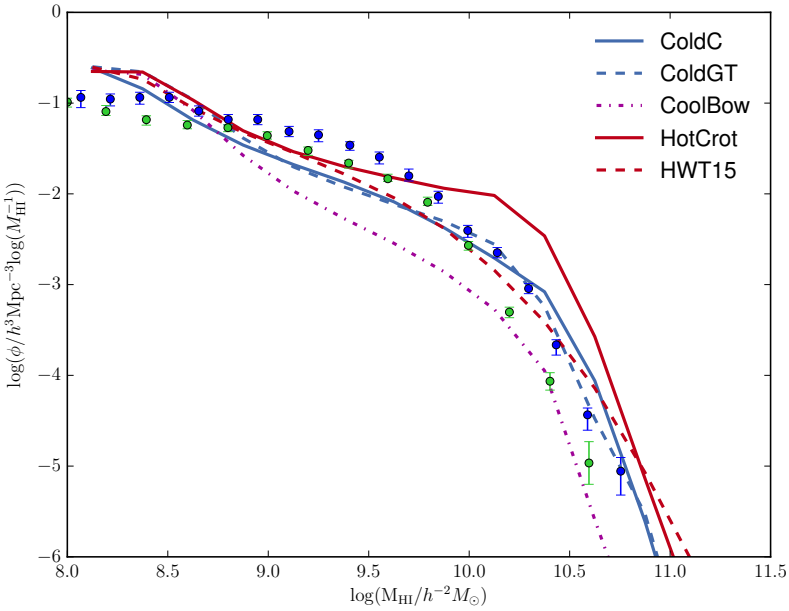

Figure 4.3: HI mass function of galaxies at $z = 0$ for the different accretion models. The observational datasets come from Zwaan et al. (2005) and Haynes et al. (2011).

differ dramatically from the original paper. By contrast, HotCrot over-produces stars at the knee of the mass function because black hole growth is relatively delayed.

4.3.2 Other galaxy properties

The principal impact of our models is to affect the gas content of halos, using the hot gas content as a constraint. In Fig. 4.3 we show the impact on the HI mass function and contrast with observations from Zwaan et al. (2005) and Haynes et al. (2011). It can be seen that the original HWT15 model provides only an approximate fit to the observational data:[8] for that reason it is more instructive to compare the new models to the former rather than the latter. The models based on cold gas content reproduce fairly well the previous results obtained in HWT15 . The two other models reveal contrasting behaviours. In keeping with the findings from the previous section, the delayed black hole growth in the HotCrot model means that it tends to accumulate more cold gas at the knee of the mass function than is observed, which in return leads to higher galaxy masses due to increased star formation (Fig. 4.2). In the case of CoolBow however, the early onset of feedback leads to a depletion of cold gas and less massive galaxies.

[8]This has been discussed in Martindale et al. (2017) and is improved by moving to a galaxy formation model that relies on molecular gas content rather than HI.

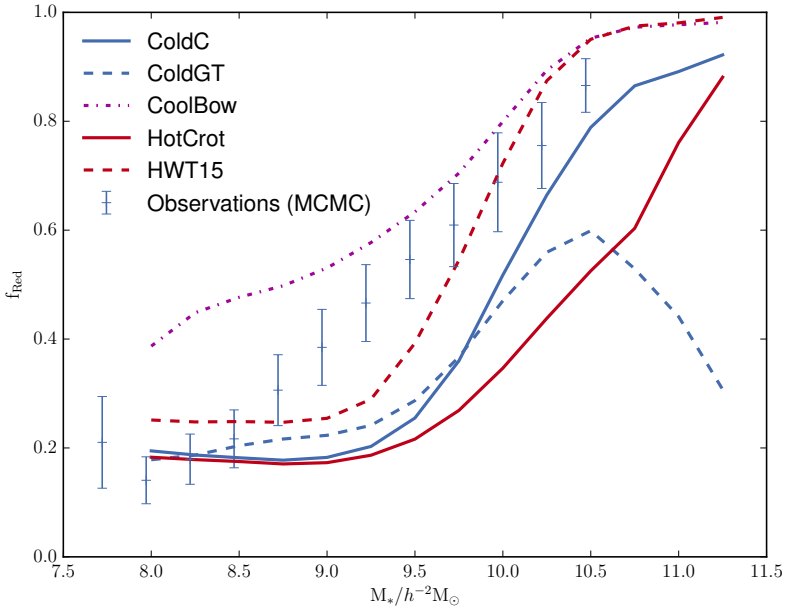

Figure 4.4: Fraction of passive (red) galaxies for all the models against stellar mass at $z = 0$, compared to a combination of observations from Bell et al. (2003) and Baldry et al. (2012).

The feedback has an impact on the quenching of galaxies as well. The fraction of red galaxies is obtained by the separation method of red and blue galaxies described in HWT15 and is presented in Fig. 4.4. As shown in the figure, the results agree with the above trends: CoolBow produces more passive galaxies than expected and HotCrot galaxies are bluer. ColdC in this case leads to slightly more active galaxies than was obtained in HWT15 while following a similar trend. The most intriguing result here is for ColdGT which shows the expected increase in passive fraction up to a stellar mass of $M_* \approx 3 \times 10^5 h^{-2}$ $M_\odot$, but above which star formation activity again rises. This is suggestive of a feedback becoming inefficient and allowing part of the gas to cool onto the galaxy, hence enhancing the production of stars.

Moreover, a potential problem with the fraction of predicted bulge dominated galaxies is investigated in Appendix A.

4.3.3 Black hole growth and AGN activity

In addition to having a strong impact on the ICM, the implementation of the new models also modifies heavily the way black holes are evolving.

Fig. 4.5 describes the black hole and total stellar mass relation for the different accretion

methods. In the HWT15 model black hole growth is mostly via the QSO mode associated with merging galaxies. In that model, with its lack of feedback, the normalisation is arbitrary. The other models all have significant growth from radio mode accretion. For the CoolBow and the ColdGT models, the weak dependence of black hole accretion rates on black hole mass means that there is a strong degeneracy in the product of the radio mode accretion rate $k_{\rm AGN}$ and the feedback efficiency $\eta_{\rm mech}$, resulting again in arbitrary mass normalisation for the black holes. However, in the HotCrot and ColdC models then the normalisation is fixed by the radio mode feedback requirements.

Apart for CoolBow, the models mostly manage to reproduce the mean trend and scatter in the observational data above $M_* \approx 3 \times 10^5 h^{-1}$ M$_\odot$, with various degrees of fidelity. Given the difficulties in making these observations and their inherent uncertainties, all are acceptable. At lower masses, the observed relation seems to flatten, although this could partly be due to observational bias. The original HWT15 model fails to produce any high mass black holes at low stellar mass, as does HotCrot. The other models all do so, however, with the cold cloud accretion models, ColdC and ColdGT, producing a wide spread of black hole masses at a given stellar mass. The distribution of masses for ColdGT is smoother: we can see a bimodality for ColdC where the black hole masses transition from low to high masses; it is not clear which of these better mimics reality. Although, ColdGT seem to lack massive enough black holes at the high mass end which then doesn't provide enough feedback to stop completely the cooling anymore, hence increasing star formation in massive galaxies as discussed before.

The hot gas based models are similar, the accretion is mainly depending on the mergers, with a scatter on black hole masses less important than in the other models and a deficit of high mass black holes.

In the CoolBow model, the black holes masses are concentrated in a narrow band that varies only slowly with stellar mass, between $10^{7.5} - 10^8 {\rm M}_\odot {\rm h}^{-1}$ over the plotted range. This early growth and saturation of black hole mass is different to that observed in Bower et al. (2008) and comes from the removal of the $0.02{\rm L}_{\rm Edd}$ limit in our prescription for black hole growth.

Fig. 4.6 and Fig. 4.7 show the ratio of the two different accretion modes against stellar mass and black hole mass for all the models involved and support the idea previously detailed. Indeed the hot gas based models are dominated by the merger accretion for most masses compared to other models. In addition we can see that the for ColdC the relative importance of the two modes is smoother than in the case of ColdGT . In ColdC the bi-

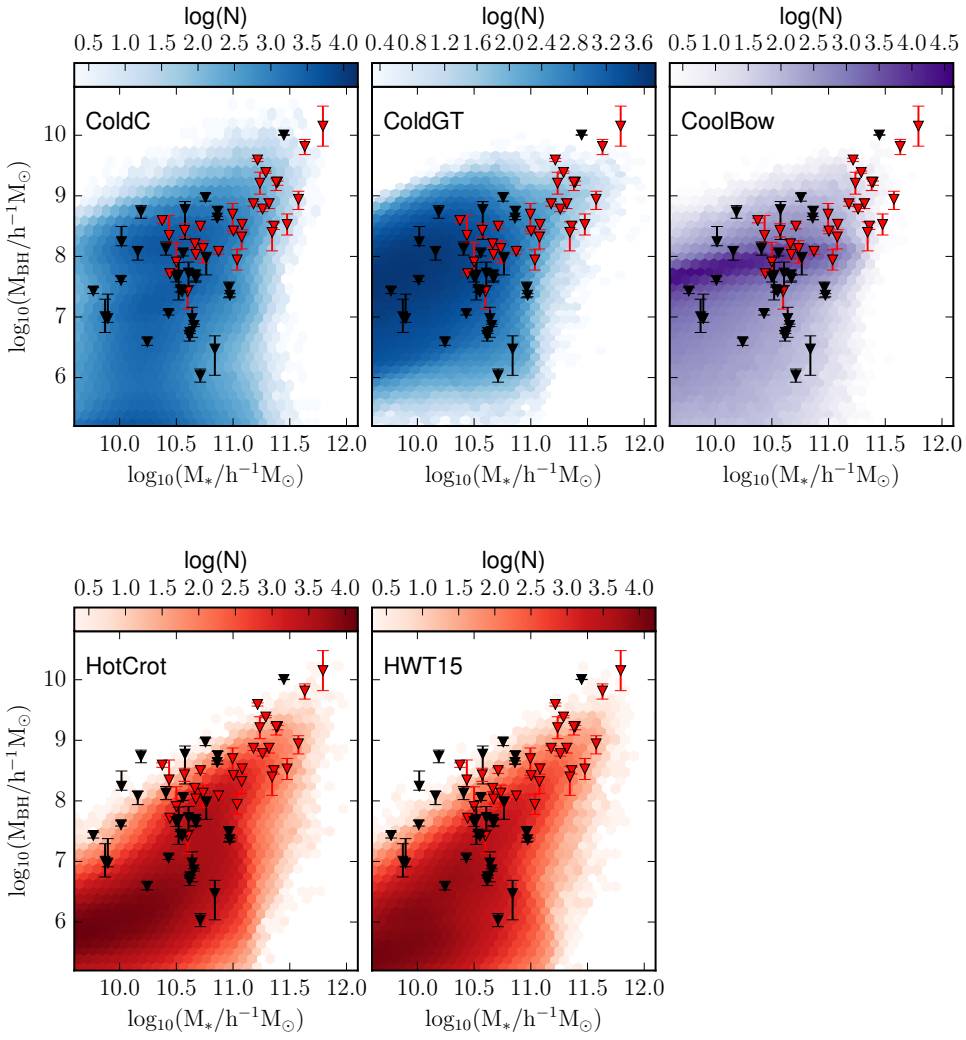

Figure 4.5: Black hole mass against stellar mass for the different accretion models at $z = 0$. The observations for early types (red) and late types (black) galaxies are taken from (Savorgnan et al., 2016). Following the method used in Bower et al. (2017), we convert the mid-IR photometry given by Savorgnan et al. (2016) to stellar mass using the calibration of Meidt et al. (2014).

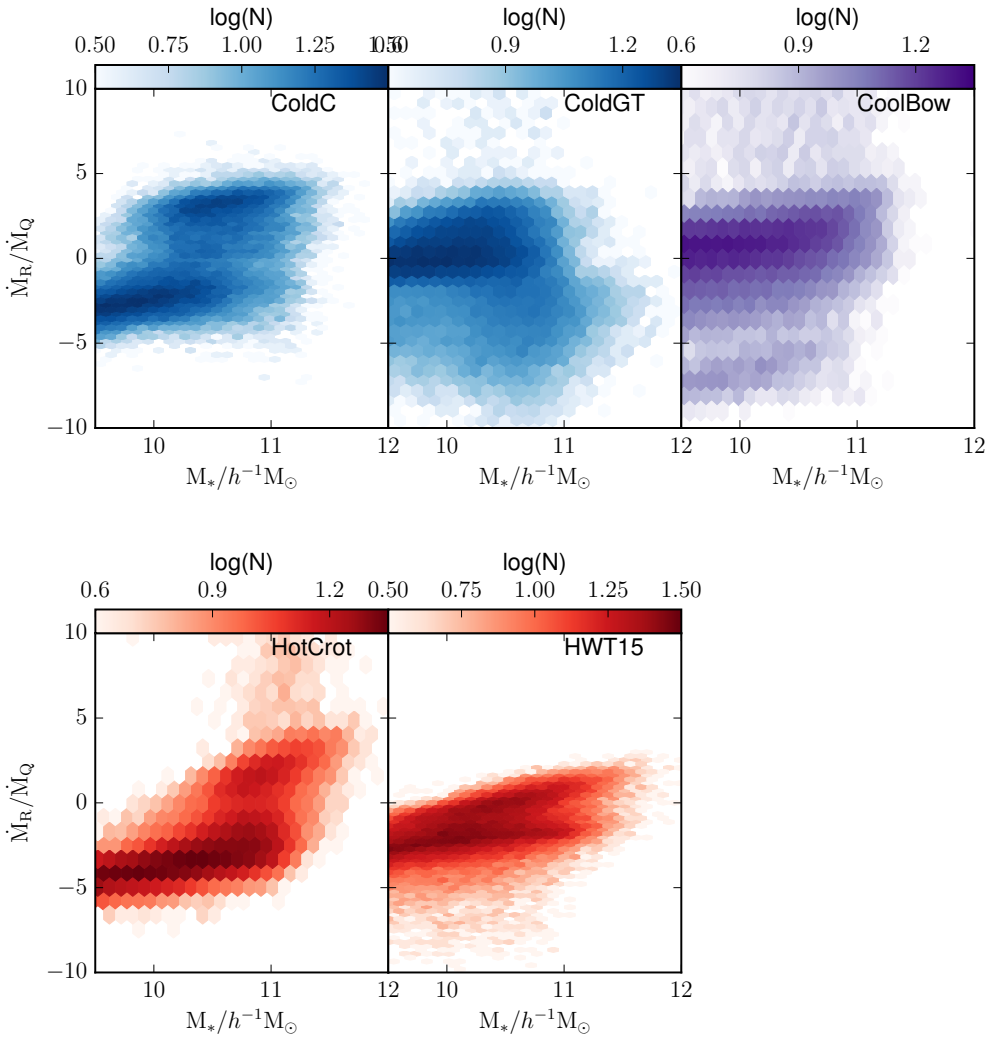

Figure 4.6: Ratio of the radio and quasar accretion modes against stellar mass for all the different models at $z = 0$.

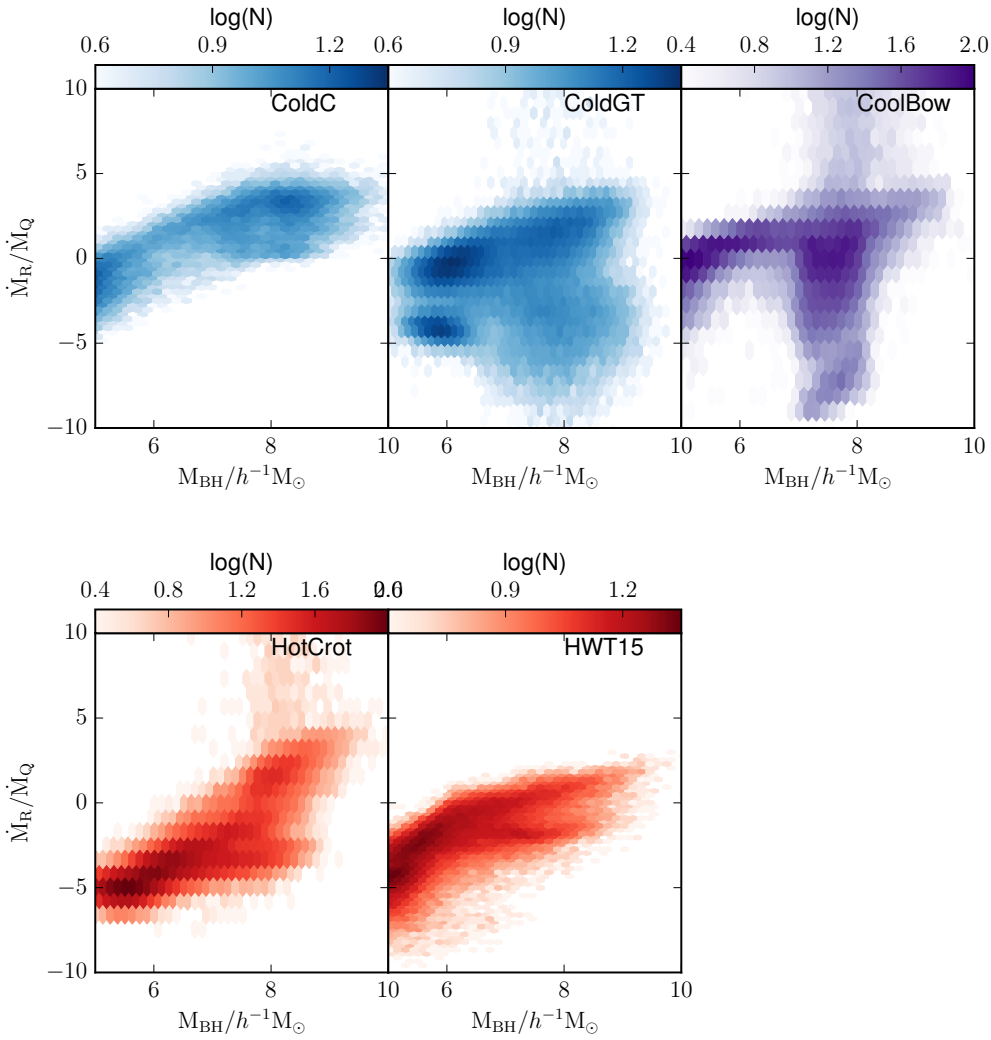

Figure 4.7: Ratio of the radio and quasar accretion modes against black hole mass for all the different models at $z = 0$.

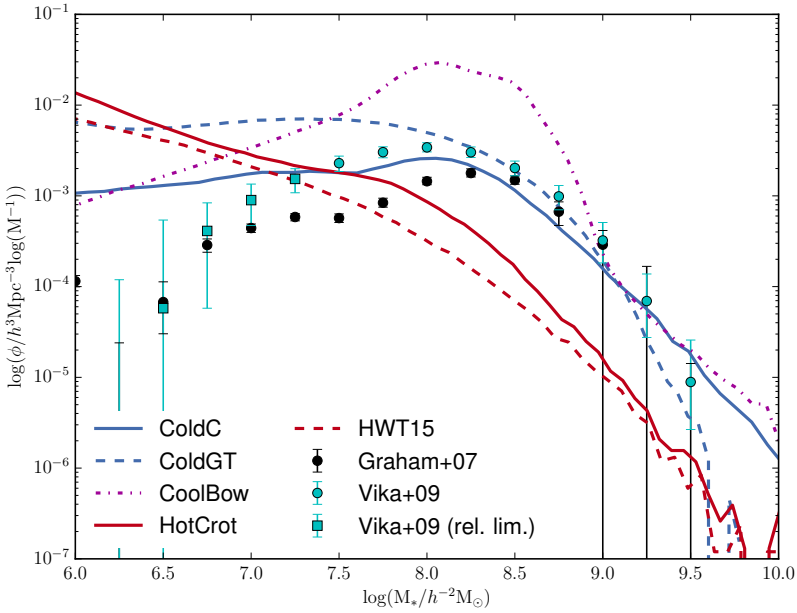

Figure 4.8: Black hole mass function for the different accretion models, compared to observational data from Graham et al. (2007) and Vika et al. (2009).

.

modality previously seen actually comes from the turning point between the domination of the merger accretion or the cold cloud one, while it has a more chaotic behaviour in the case of ColdGT and a merger driven accretion for high black hole masses, certainly coming from the approximation of the radius R_0 becoming too small at those masses. The CoolBow case is interesting, as the scatter in the ratio only happens when black holes are of masses around between $10^{7.5} - 10^8 M_\odot h^{-1}$ as previously seen, due to an accretion only depending on the hot gas properties.

The local black hole mass function presented in Fig. 4.8 supports these previous observations. Only the cold cloud accretion models provide a close match to the observed trend, each performing well at masses above $10^8 h^{-1}$ $M_\odot$. At lower masses, ColdGT predicts a higher density of low mass black holes while ColdC is predicting the opposite. However, at low masses observational data become unreliable thus it is difficult to be certain which behaviour is better.

The QLF has the potential to be a strong constraint on black hole accretion modes, but the precise mapping between mass accreted and observed luminosity power is very uncertain. In all our models (except HWT15), we simply set the quasar luminosity to be the difference between $0.1\dot{M}_{\rm BH}c^2$ and the work done in mechanical heating (Equation 4.22).

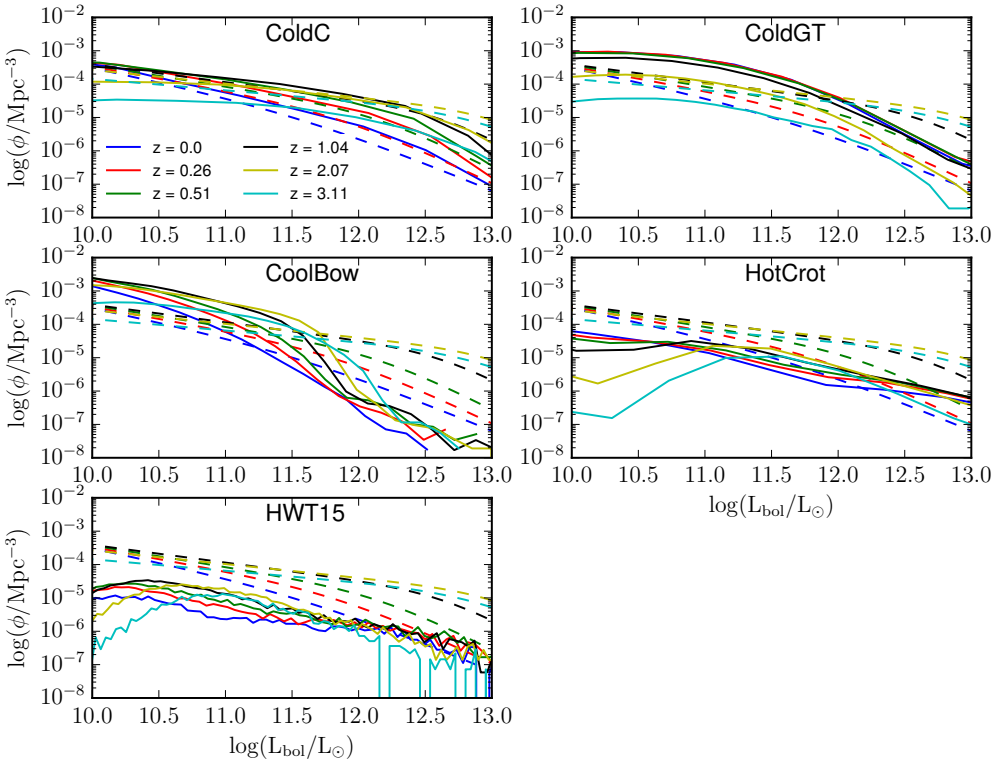

Figure 4.9: Quasar bolometric luminosity function for all the models, compared with the observational data from (Hopkins et al., 2008), for 6 different redshifts, as indicated.

Fig. 4.9 compares the predicted quasar bolometric luminosity function (QLF) to the observational fits of Hopkins et al. (2008) at six different redshifts, as indicated. In HWT15 only the quasar mode was assumed to contribute and that leads to a significant underestimate of the QLF at $z = 0$. Furthermore, there is little evidence of evolution, in contrast to the observations that show a significant enhancement in the number density of bright quasars out to $z = 1$. In the models presented in this paper, all AGN contribute if they are powerful enough, with the different accretion modes leading to a wide variety of behaviours. Concentrating on the bright end of the QLF, above 10^{10} 10^{13} $L_{\odot}$, the cold cloud accretion models match the slope of the QLF best at $z = 0$: ColdC has approximately the correct normalisation; quasars in ColdGT are a few times too bright. Of the models that we consider, only ColdC and CoolBow have the observed increase in normalisation of the QLF between $z = 0$ and $z = 1$; above that redshift, none of the models fit the data particularly well.

4.4 Conclusions

Throughout this work, we have studied the effect of an improved feedback implementation for our AGN in the L-Galaxies SA model, coupled with different black hole accretion methods, in order to better reproduce the ICM gas fraction.

We consider 4 different, physically-motivated models for black hole accretion[9], 2 of which accrete directly from cooling gas, and 2 which accrete from cold clouds in the ISM. Compared to HWT15 , these all give a better agreement with the gas content observed in groups and clusters of galaxies. However, the different models have varying degrees of success in matching other galaxy properties:

- CoolBow, in which some fraction of cooling gas is accreted onto the black hole, builds up its black holes too quickly, leading to ejection of gas in Milky Way-sized halos, a reduction in cold gas content, and under-formation stars. This comes mainly from the fact that the accretion is completely independent of the black hole properties. In this situation, the black hole grows rapidly and reaches a value of approximately 10^8 $M_\odot$in low mass galaxies, before saturating and subsequently growing only very slowly. The black hole - bulge mass relation is therefore too flat and the quasar luminosity function too steep.

- HotCrot, that is closest in spirit to the original HWT15 model, estimates the accretion that would be expected from a cooling flow out of the hot gas, directly onto the black hole. It shows the opposite effect to CoolBow: black hole growth occurs quite late, there is an excess of cold gas in Milky Way-sized halos, and the stellar mass function is slightly too high at the knee. There is a hint that the black hole masses might be too low in dwarf galaxies, and the quasar luminosity function at $z = 0$ is too flat.

- ColdGT is derived from the assumption that gravitational perturbations in the galactic disk trigger angular momentum transport mechanisms that leads to a portion of the ISM being carried towards the centre and feeding the black hole. It provides a reasonable match to all galaxy properties except that there is an excess of cold gas in the most massive galaxies, meaning that they are not properly quenched.

[9]It can be argued that the improvement seen is not due to a better understanding of the physics of accretion, but is rather just due to a more flexibly set of parametric functions. A more in depth investigation of this accretion mechanism and the different free parameters is necessary and will be pursued in future works.

The quasar luminosity function at $z = 0$ has the correct slope, albeit with too high a normalisation, but is unevolving with redshift out to $z = 1$.

- ColdC provides the best all round fit to both the galaxy properties and the normalisation and evolution of the quasar luminosity function. In this model, the accretion is again from cool clouds, but with a much stronger dependence upon the mass of the central black hole. The model predicts a wide spread in black hole masses in dwarf galaxies, with many in excess of 10^8 $M_\odot$; however, this is not inconsistent with current observations and may even be required. The rise in the fraction of passive galaxies also seems to arise at slightly too large a stellar mass.

In conclusion, simultaneously matching galaxy properties, the hot gas content of halos, and the luminosity evolution of quasars presents significant challenges for models of galaxy formation. Of all the models for black hole growth and feedback that we consider here, the ColdC model, while being far from perfect, provides a reasonable overall match to all the observations that we consider. We will investigate further the predictions of this model for the properties of the ICM in the next chapter.

Chapter 5

ICM and X-ray properties

5.1 Introduction

The intracluster medium (ICM) is a key component to understand galaxy formation and the physics of groups and clusters of galaxies. Indeed, the available content of gas in the halo and its density distribution will have a direct impact on the cooling rates and, consequently, on the amount of feedback required to quench star formation. The gas from this hot atmosphere cools towards the centre of the halo while emitting in the X-ray spectrum due to bremsstrahlung radiation supplying galaxies with colder gas that can be used for star formation. These cooling flows are regulated by supernovae (SNae) winds at low halo masses (Dekel and Silk, 1986; Cole et al., 1994; Efstathiou, 2000; Governato et al., 2007) and AGN jets at higher masses (Bower et al., 2006; Hopkins et al., 2014). Impacted by the SNae feedback, the ICM is enriched in metals and becomes an important tracer of the recycling mechanisms taking place in galaxies.
For the past 20 years X-ray astronomy has been providing large surveys to investigate the diverse properties of groups and clusters with the use of Chandra (Vikhlinin et al., 2006, 2009) and XMM-Newton (Lloyd-Davies et al., 2011a; Mehrtens et al., 2012) telescopes, even leading to possible constraints on cosmological parameters (see, e.g., Sahlén et al., 2009). While properties derived from X-ray observations following different assumptions can lead to a scatter in the estimations (see, e.g., Bartalucci et al., 2017), these surveys remain a crucial source of information to understand the underlying Physics of the ICM and evaluate our simulations. Indeed, our models can be compared to these crucial data to investigate the reliability of their ICM and their cooling rates.

The cooling radius method presented in (White and Frenk, 1991) has been widely adopted by most of the SAMs. In this scenario, the gas density profile is assumed to follow

that of a singular isothermal sphere. Only the hot gas within a specific radius r_{cool} will then be allowed to cool. It has the advantage of reproducing two observed phenomena. If the radius is larger than the virial radius, the shock-heated gas doesn't have the time to reach an hydrostatic equilibrium state and, as a consequence, is cooled instantly. In the second situation, the gas reach the hydrostatic equilibrium and a cooling flow is introduced carrying the X-ray emitting gas towards the center.
While the results have been proven sufficient, the method is far from perfect. First of all, only the gas within the radius will be able to cool and to produce a luminosity, leaving a fraction of the hot atmosphere out of the contribution. In addition, the gas profile is unrealistic, which results in the impossibility to calculate a proper analytical solution for the cooling. Observers, on the contrary, generally use a flatter profile at low radii (by assuming, for example, a β profile and a core radius).

In this chapter, we propose a new cooling formalism in the L-Galaxies model from Henriques et al. (2015) in order to give a more reliable and self-consistent method to compute the cooling of the gas and its intrinsic X-ray luminosity. We assume a new density profile for the gas, based on a β model and derive the cooling directly from the X-ray luminosity emitted by the gas. We then then analyse the effect upon the different observable ICM properties when this new cooling method is coupled with the new AGN feedback developed in Chapter 4 (hereafter FTH18). The best fit parameters from the MCMC runs for HWT15 and FTH18 are summarised in Table B.
For this simulation, we used the 500Mpc/h box from the dark matter only Millennium simulation (Springel, 2005) and a flat Λ CDM universe as described in the the 1st-year *PLANCK* cosmology (Planck Collaboration et al., 2014).

The chapter is structured as follows: in Section 5.2, we describe and compare the original cooling method with the new prescription. In Section 5.3.1, we describe the results obtained for the predicted X-ray luminosities; in Section 5.3.2, for the hot gas content and evolution; and in Section 5.3.3, for the ICM metallicity. Finally, in Section 5.4, we present our conclusions.

5.2 Method

In this section we first describe the existing L-Galaxies cooling algorithm and its deficiencies. We then present our new method before comparing the their impact on the

cooling gas.

5.2.1 The existing cooling algorithm

The cooling model that is used in the current version of L-Galaxies is described in detail in the supplementary material that accompanies Henriques et al. (2015). We reiterate the essential points below.

The singular isothermal sphere

For simplicity, the density profile of the ICM is assumed to be that of a singular isothermal sphere (SIS),

$$\rho_{\rm g} = f_{\rm g} \frac{200\rho_{\rm c}}{3} \frac{1}{x^2}, \tag{5.1}$$

where $f_{\rm g} = M_{\rm g}/M_{\rm 200c}$ and $x = r/r_{\rm 200c}$. Here $M_{\rm g}$ is the gas mass and $M_{\rm 200c}$ the total mass within a radius $r_{\rm 200c}$Àlthough an infinite density at the centre of the halo is not an accurate representation of real halos, this is expected to make little difference to the cooling rates in practice

In a SIS, the gas mass contained within radius r is

$$m_{\rm g} = f_{\rm g} M_{\rm 200c} x. \tag{5.2}$$

The specific energy of the gas is constant and equal to

$$\epsilon = \frac{3k_{\rm B}T}{2\mu m_{\rm H}}, \tag{5.3}$$

The equation of hydrostatic support leads quickly to the relation

$$\frac{k_{\rm B}T_{Vir}}{\mu m_{\rm H}} = \frac{1}{2}{v_{\rm c}}^2 = \frac{GM_{\rm 200c}}{2r_{\rm 200c}} = \frac{200\pi}{3} G\rho_{\rm c}{r_{\rm 200c}}^2, \tag{5.4}$$

where $v_{\rm c}$ is the circular speed of the halo.
The calculation of dynamical times for a SIS can be found in Appendix C.1

The cooling radius method

After being shock-heated as it infalls onto the halo, the gas is accreted towards the centre via cooling flows. In order to reproduce this behaviour, a cooling radius is calculated for which the mass enclosed is able to cool.

Assuming the gas cooling from the SIS is in a quasi-static regime (White and Frenk, 1991; Springel et al., 2001), we can calculate a cooling time by dividing its thermal energy

by its cooling rate per unit volume :

$$t_{\rm cool}(r) = \frac{5\mu m_{\rm H} k_{\rm B} T_{\rm Vir}}{2\rho_{\rm hot}(r)\Lambda(T_{\rm hot}, Z_{\rm hot})} \tag{5.5}$$

where $\mu m_{\rm H}$ is the mean particle mass, $k_{\rm B}$ is the Boltzmann constant and $\rho_{\rm hot}$ the hot gas density derived from Equation 5.4 The cooling rate per unit volume of the gas is ${n_{\rm g}}^2\Lambda(T, Z)$, where $n_{\rm g} = \rho_{\rm g}/\mu m_{\rm H}$ is the number density of particles in the gas and the cooling function, Λ, is a function of temperature and metallicity, Z. For simplicity, the model assumes a constant temperature for the gas $T_{\rm hot} = T_{\rm Vir}$. One might naively expect that the gas in the centre of the halo will be able to cool to low temperatures more effectively than that at larger radii, leading to a positive temperature gradient in the gas as a function of radius. That in turn would give a density increase at the halo centre (to maintain pressure support) and a central luminosity spike. However, X-ray observations of quasi-steady cooling in groups and clusters of galaxies (e.g. Ettori et al., 2013) show only mild temperature gradients so that, to a good approximation, $T(r) \approx$ constant, as in the SIS. Instead the gas is thought to have a multiphase structure (i.e. there is a mixture of densities at any given radius) leading to a multiphase cooling flow model (Thomas, 1988). In such a model, the mean temperature of the gas remains fixed also in time and only the density changes as gas cools out of the flow.

The cooling radius is determined by equating the cooling time to the dynamical time of the halo given by $t_{\rm dyn,h} = \frac{r_{\rm 200c}}{v_{\rm c}}$ [1] :

$$r_{\rm cool} = \left(\frac{t_{\rm dyn,h} {\rm M_{HG}} \Lambda(T_{\rm Vir}, Z_{\rm hot})}{6\pi\mu m_{\rm H} k_{\rm B} T_{\rm Vir} r_{\rm 200c}} \right)^{1/2} \tag{5.6}$$

From this calculation, two different cooling regimes can be observed (White and Rees, 1978; White and Frenk, 1991). If $r_{\rm cool} \geq r_{\rm 200c}$, the cooling rate is defined by :

$$\dot{\rm M}_{\rm cool} = \frac{\rm M_{HG}}{t_{\rm dyn,h}} \tag{5.7}$$

In this scenario, the cooling time is short enough for the gas to cool directly towards the centre at the free-fall rate. It is usually the case for small halos and at early times.

If $r_{\rm cool} < r_{\rm 200c}$, the cooling rate is however defined by :

$$\dot{\rm M}_{\rm cool} = \frac{\rm M_{HG}}{t_{\rm dyn,h}} \frac{r_{\rm cool}}{r_{\rm 200c}} \tag{5.8}$$

Although this method produces satisfactory results, it is not exempt of issues.

[1] If the halo masses are too small, the shock heated gas cools rapidly and loses pressure support, hence a hot atmosphere in the hydrostatic equilibrium cannot be maintained.

The first problem with this model is the use of an unrealistic description of the gas density with the SIS, as stated before.

Another problem with the model is that the total amount of mass cooled is only correctly estimated when the timestep is sufficiently small that $M_{HG,fin} \approx M_{HG,ini}$. This is an unnecessary restriction introduced to minimise execution time in the code and can easily be replaced by integrated versions of the cooling equations that use a variable cooling rate as the density of the remaining gas decreases over time (so called variable cooling model in Figure 5.1. For more detail, please refer to Appendix C.2).

In addition to previous point, the X-ray luminosities are given by the formula (White and Frenk, 1991) :

$$L \sim 2.5\dot{M}_{cool}v_c^2 \tag{5.9}$$

They are calculated after the feedback has been processed, leading to non luminous groups and clusters as the feedback prevent most of the cooling. However this choice is difficult to understand as the gas will emit while cooling (reheated after or not). Thus we modified the HTW15 model to calculate the luminosities before any feedback is taking place.

A more serious objection to the cooling model is that it seems to depend only upon the behaviour of the gas within the cooling radius: why should gas outside that radius not contribute? A direct integration of the expected luminosity in a SIS profile leads to an infinite result, hence the use of Equation 5.9 which again depends only upon the emission within the cooling radius. In the following section we develop a new version of the model that does not have this deficiency.

5.2.2 The new cooling algorithm

Fundamental to our new cooling algorithm is the use of a density profile for the ICM that more closely mimics that of observed clusters. In particular, we use a model that has a finite central density. That then gives a finite luminosity and we derive the rate of mass deposition from this luminosity, rather than the other way around.

The isothermal-beta model

We again assume that the total matter content of the halo can be approximated by an SIS. However, we adopt a density profile for the gas that tends to a constant within core

radius a:

$$\rho_{\rm g} = \frac{\rho_0}{1+y^2}, \tag{5.10}$$

where $y = r/a$. We call this the isothermal-beta model as it is derived from a class of density profiles $\rho_{\rm g} \propto (1+y^2)^{-\beta}$, with $\beta = \frac{2}{3}$, giving the usual $1/r^2$ dependence of the isothermal sphere at large radii, $r \gg a$.

The mass profile of the gas is

$$m_{\rm g} = 4\pi\rho_0 a^3 (y - \arctan y) = M_{\rm g} \frac{y - \arctan y}{Y - \arctan Y}, \tag{5.11}$$

where $Y = y(r_{\rm 200c})$. Hence the gas fraction within $r_{\rm 200c}$ is

$$f_{\rm g} = \frac{4\pi\rho_0 a^3 (Y - \arctan Y)}{M_{\rm 200c}}. \tag{5.12}$$

For our work, we take $Y = 10$ in agreement with clusters observations (e.g. Sanders et al., 2018).

We again assume an isothermal temperature for the gas. This is not strictly valid because the core gas would not be in hydrostatic equilibrium within an SIS potential at this temperature. However, we know that the background potential does not itself truly follow an SIS and, as the core is small compared to the virial radius, this seems a reasonable approximation to adopt.

The luminosity of the hot gas halo (integrating now out to infinite radius) is

$$L = \int_0^\infty {n_{\rm g}}^2 \Lambda \, 4\pi r^2 \, {\rm d}r = \frac{\rho_0^2 \Lambda \, \pi^2 a^3}{(\mu m_{\rm H})^2}. \tag{5.13}$$

It is important to note that a fundamental assumption of our model is that feedback ejects gas only. In order to create a core, the cluster needs energy. A possibility could be to use part of the feedback in raising entropy in the core rather than gas ejection. Doing such a change would enable us to create and modify the core radius instead of having an arbitrary value suitable for clusters only. This improvement is required to understand the distribution of radial profiles of clusters (e.g. cool core vs. non-cool core) and the large intrinsic scatter in X-ray scaling relations.

The cooling model

In a quasi-static cooling flow, in which the gas cools at constant pressure, then the mass-deposition rate is (Thomas, 1988)

$$\dot{M}_{\rm g} = \frac{L}{H}, \tag{5.14}$$

where $H = 5k_{\rm B}T/2\mu m_{\rm H}$ is the specific enthalpy of the gas. The reason for using enthalpy instead of energy is that the parcels of cooling gas remain in pressure equilibrium with their surroundings and therefore have pressure work done on them as they cool.

Combining Equation 5.14 with Equations 5.12 and 5.13 and the characteristic cooling timescale $\tau_{\rm cool} = \frac{9\mu m_{\rm H} k_{\rm B} T}{400\rho_{\rm c}\Lambda}$ gives

$$\dot{f_{\rm g}} = -\frac{{f_{\rm g}}^2}{{\tau_{\rm cool}}'}, \tag{5.15}$$

where

$${\tau_{\rm cool}}' = \frac{3\mu m_{\rm H} k_{\rm B} T}{20\pi\rho_{\rm c}\Lambda}\frac{(Y - \arctan Y)^2}{Y^3} \tag{5.16}$$

$$= \frac{20}{3\pi}\frac{(Y - \arctan Y)^2}{Y^3}\tau_{\rm cool}. \tag{5.17}$$

As for the SIS, the quasi-static cooling flow assumptions break down when the cooling time at the edge of the halo is less than the dynamical time. We therefore impose the same limit on the cooling rate, meaning that the expression for the gas fraction again splits into two cases. For ${\tau_{\rm cool}}' \geq \tau_{\rm dyn} f_{\rm g0}$,

$$f_{\rm g} = f_{\rm g0}\left(1 + \frac{f_{\rm g0}\Delta t}{{\tau_{\rm cool}}'}\right)^{-1}; \tag{5.18}$$

whereas for ${\tau_{\rm cool}}' < \tau_{\rm dyn} f_{\rm g0}$,

$$f_{\rm g} = \begin{cases} f_{\rm g0} e^{-\Delta t/\tau_{\rm dyn}}, & \Delta t \leq t_{\rm eq}; \\ \frac{{\tau_{\rm cool}}'}{\tau_{\rm dyn}}\left(1 + \frac{\Delta t - t_{\rm eq}}{\tau_{\rm dyn}}\right)^{-1}, & \Delta t > t_{\rm eq}; \end{cases} \tag{5.19}$$

where $t_{\rm eq} = \tau_{\rm dyn}\ln(\tau_{\rm dyn} f_{\rm g0}/{\tau_{\rm cool}}')$.

In this case, the fraction of gas cooled is independent of the dynamical time of the halo (as it should be). This can potentially lead to very different estimates of the rate of deposition of hot gas in the cooling flow regime. Fig. 5.1 shows the amount of gas cooled using the existing model (solid, red curves), the existing model modified to use a variable cooling rate (dotted, red curves) and for the new model (solid, blue curves). We see that the amount of cooled gas is less than in the existing SIS model both in the limit of short and long cooling times. However, when $\tau_{\rm dyn} f_{\rm g} \approx {\tau_{\rm cool}}'$ then the cooling rate has approximately doubled leading to greater deposition of gas for short timesteps.

Fig. 5.2 shows the cooling rate of the hot gas against the virial mass (upper panel) and the hot gas mass (lower panel) for the HWT15 model and the same model with the new cooling implementation. Fortunately, it is clearly visible on this figure that the previous concern is actually a rare scenario in our simulation. Both cooling models are perfectly

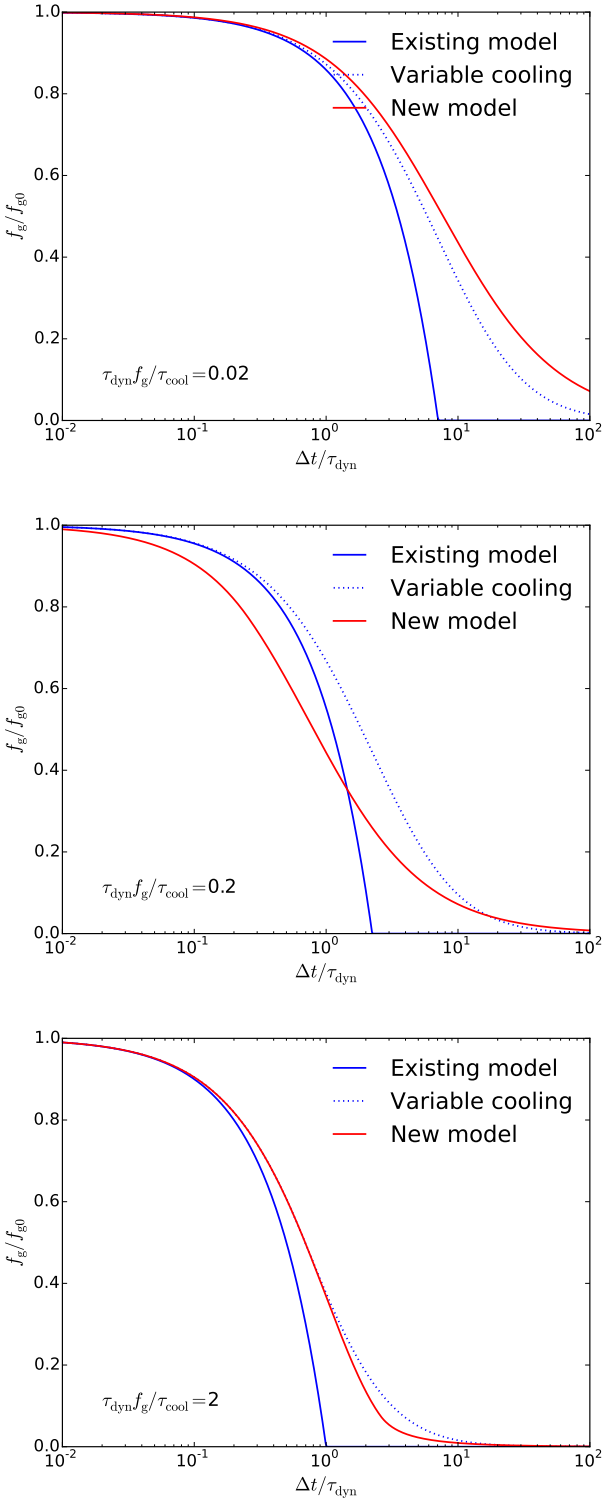

Figure 5.1: The amount of gas remaining as a function of time using the existing SIS model with a fixed cooling rate (solid, blue curve) and variable cooling rate (dotted, blue curve), and for the new isothermal-beta model model (solid, red curve), for the cases where $\tau_{\rm cool}/\tau_{\rm dyn} f_{\rm g} = 0.02$ (upper panel), 0.2 (middle panel) and 2 (lower panel). We have taken $Y = 10$.

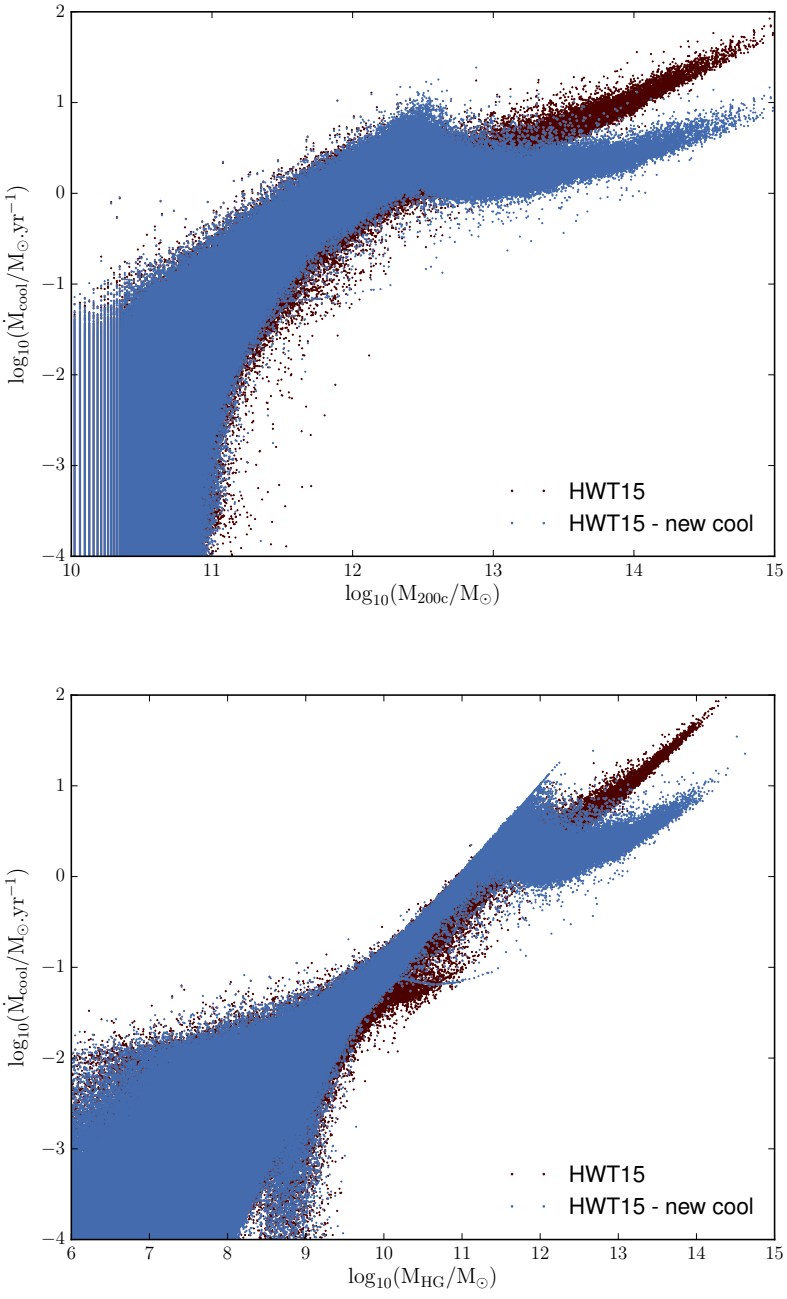

Figure 5.2: Cooling rate of hot gas against the virial mass (top panel) and hot gas mass (bottom panel) at $z = 0$. The red points correspond to the original HWT15 model and the blue ones to the same model but with the new cooling implementation. The cooling rate has been calculated before the any feedback is applied.

similar for small to medium halo and hot atmosphere masses. However, when we reach the range of group and cluster masses, we observe a distinct break in the cooling rates for the new β model. The cooling radius method provide cooling rates increasing along a sharp slope while the new model gives us lower cooling rates as the halo mass increases. The sharp break observed for the new model is due to the change of regimes that occurs between small halos and group size objects. For small objects, our cooling model is similar to the cooling radius method, with a rapid cooling mechanism. However, as the halo grows, the impact of the core is revealed and the cooling flows decrease as expected.[2] This will lead to some implications for the amount of feedback needed to suppress star formation in groups and clusters of galaxies or their predicted X-ray luminosities.

5.3 Results

We exposed the problems of the previous cooling method and proposed a solution by modifying the density profile of the hot gas to be an isothermal-β model which has a finite central density. In this new scenario, the cooling rate of the gas is self-consistently calculated and used to determine the rate of mass deposition in the cooling flow regime. In addition, it produces reliable and self-consistent X-ray luminosities. In this section we discuss the ICM results produced by the new cooling model coupled with the AGN feedback implementation described in the previous chapter.

5.3.1 X-ray properties

We explained previously the differences between the two different cooling methods and highlighted a decrease in the cooling rate for high mass objects in the β model. In Fig. 5.3, we present the X-ray luminosity predictions corresponding to these cooling flows and compare them to observational datasets from Maughan et al. (2008), Pratt et al. (2009) Vikhlinin et al. (2009) and a recent XCS (XMM Cluster Survey) sample. The method for the measurements and selection of the XCS data sample is detailed in Appendix D.1. The clusters simulated in the HWT15 model are 4 to 30 times more luminous than the ones from the new prescription. The flatter profile obtained in the cooling rates also decreased the expected luminosities of the hot gas in these groups and clusters, bringing them closer to observations. This result is indeed expected due to the introduction of a core size based on observations. However the new luminosity distribution appears less steep than the observational trend and lies on the upper end of the observations. It is

[2] However this sharp transition is still under investigation.

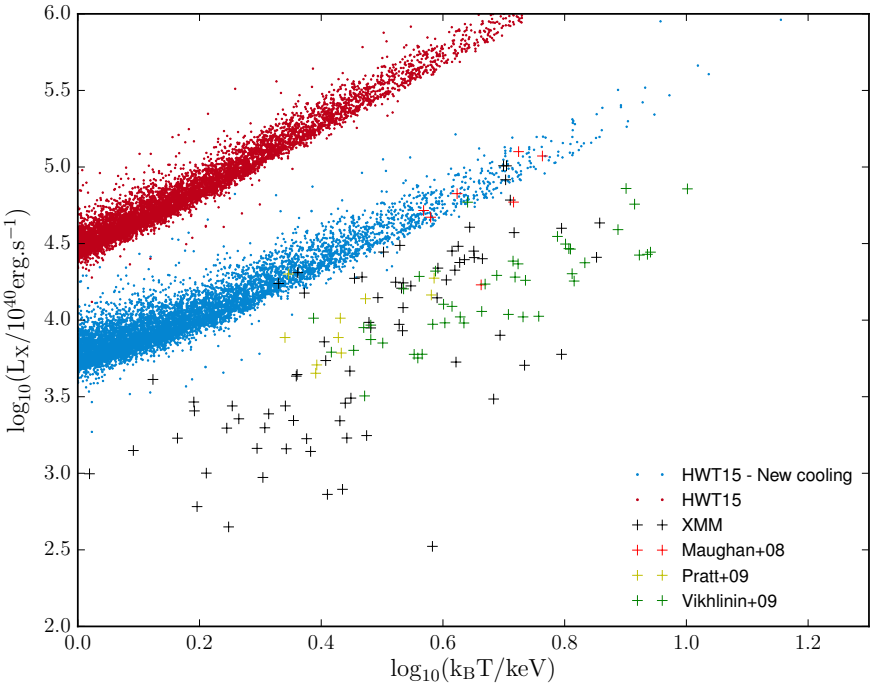

Figure 5.3: Bolometric X-ray luminosities against temperature for the original HTW15 model and the one including the β cooling method (without AGN feedback) at $z = 0$. The observational data are taken from Maughan et al. (2008), Pratt et al. (2009) Vikhlinin et al. (2009) and an XCS sample (XMM). The method for the measurements and selection of the XCS data sample is detailed in Appendix D.1.

important to note that the break observed in Fig. 5.2 is not appearing on the plot due to the range of temperatures considered, which are not low enough. As expected from previous chapters, the cooling rates with the new prescription are still too high due to groups and clusters being too rich in hot gas and especially gas available to cool. The current AGN feedback description as implemented in the HWT15 is the main mechanism to regulate the cooling flows in the most massive objects by reheating the cooling gas. However, in this configuration the reheated gas is allowed to cool again at the following timestep. As a consequence, the total amount of gas available to cool at each timestep is similar (or increases, due to the infall of new gas), leading to an overestimation of the cooling rates and their associated luminosity. In order to reduce the luminosity further, we need the AGN feedback to reheat and/or remove the gas from the hot atmosphere with a mechanism similar to the SNae feedback. As a consequence, we continue the results analysis focusing on the FTH18 model.

Fig. 5.4 shows our X-ray luminosity predictions against observations in four different

redshift bins in the range 0 - 1 for the FTH18 model. The simulated luminosities now reproduce the observational trend at all redshifts involved. Moreover, there seems to be no particular mass-luminosity evolution below $z = 1$. The amount of gas cooling thus appears to be in agreement with the expectations from real groups and clusters. However, our luminosities lie on the high end of the observations for low cluster masses and groups. Moreover, it presents an overall weaker slope than suggested by the observational trend. Hence it could hint to a cooling too proficient and/or a hot gas content higher than what would be observationally expected at low masses. It could also hint at a limit of the β model description for smaller halo size.

In addition, it is important to keep in mind that the isothermal approximation made for the gas could also be an issue. As the observational temperatures are computed inside r_{500c}, our temperatures could be underestimated. However it would not affect the general trend of our results, especially at low temperatures. Finally, our results lack the observed scatter at all redshifts. This result is not surprising considering we use an arbitrary fixed core radius. The radial core profiles of true clusters and groups have more variety, which cannot be reproduce here. The impact of the core radius variation will be investigated in future work and was beyond the scope of this chapter. As noticed before, using the feedback mechanism to modify the core entropy could be a necessity in order to reproduce this observational scatter.

5.3.2 Gas content of clusters

As discussed in the previous chapter, our model is properly constrained to reproduce the observed gas content at $z = 0$, as it can be seen on Fig. 5.5. Powerful AGN winds enable us to remove gas from the halo and reduce the gas content of the halo. In comparison, a sample of clusters taken from the C-Eagle simulation (Barnes et al., 2017) show a slightly larger gas content for clusters and lie on top of the observational data. The explosive type of AGN feedback (dT9) implemented in the simulation is efficient at low masses but struggles to properly evacuate the gas when masses reach the clusters mass range.

If we look at the evolution of the gas content in our model between $z = 0$ and $z = 0.9$ as shown in Fig. 5.6, we see that the hot gas content becomes flatter and higher between 10^{12} to $10^{14} M_\odot/h$ as the redshift increases. This is because of the hot gas relying on AGN feedback to remove the gas from halos more massive than $10^{12} M_\odot/h$. The black holes to build up between $z = 1$ and present in order to produce powerful winds. Above $10^{14} M_\odot/h$, the gas content is not affected by the redshift evolution. This is because the gas ejection is

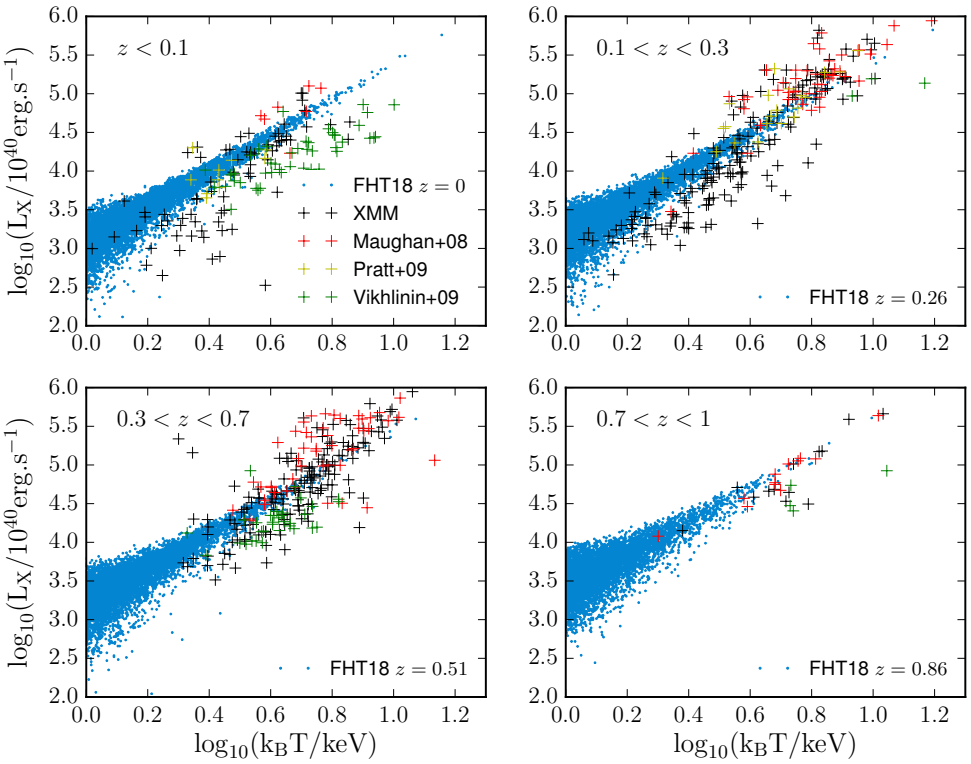

Figure 5.4: Bolometric X-ray luminosities against temperature for the FTH model, binned by redshifts for $0 < z < 1$. The observational data are taken from Maughan et al. (2008), Pratt et al. (2009) Vikhlinin et al. (2009) and an XCS sample (XMM). The method for the measurements and selection of the XCS data sample is detailed in Appendix D.1.

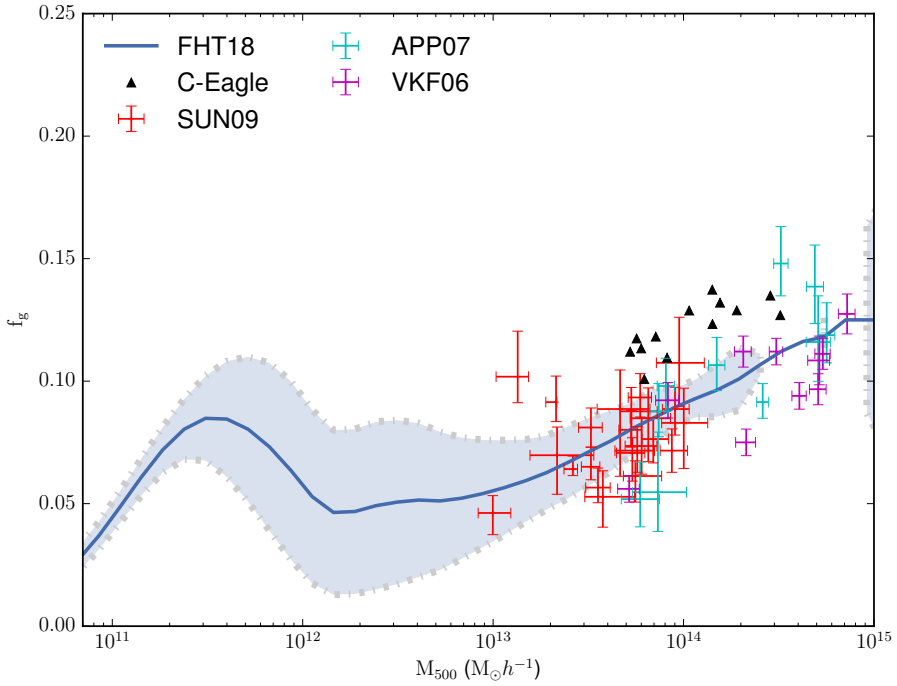

Figure 5.5: Hot gas fraction against the virial mass M_{500c} for the FTH18 and C-EAGLE models at $z = 0$. The blue shaded area encloses 68% of the population around the mean value. The observational data are taken from Vikhlinin et al. (2006), Anderson et al. (2007) and Sun et al. (2009).

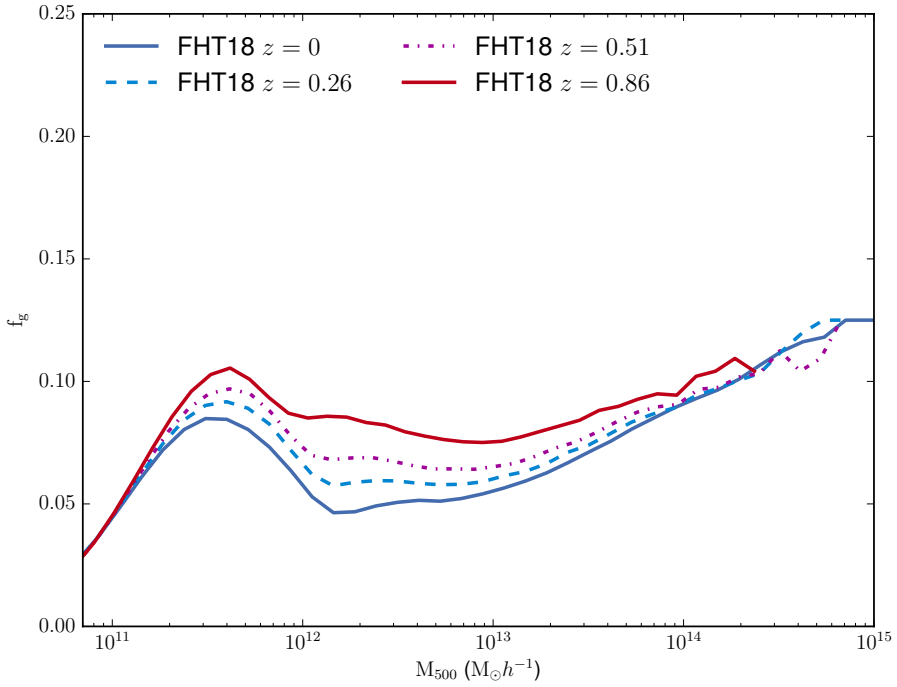

Figure 5.6: Hot gas fraction against the virial mass M_{500c} for the FTH18 for $0 < z < 0.9$.

built up at lower masses. Moreover, this result correlates with the previous observations made from Fig. 5.4 where the cooling luminosity remains similar throughout this range of redshifts for high mass halos (high temperatures).

As observations struggle to give reliable data for higher redshifts, it is difficult to infer which behaviour the gas is expected to follow. Simulations have a large set of recipes for feedback and reincorporation of gas parameters. Although they lead to solutions agreeing well with the observations at $z = 0$, differences can emerge from their predictions at higher redshifts. In this context we compare our gas content predictions to the ones of the cluster sample from the C-Eagle simulation and present the results in Fig. 5.7, for $z = 1$ (top panel) and $z = 2$ (bottom panel). At $z = 1$, the two simulations are in good agreement for the gas content expected in massive objects. However, our fractions distribution increases slowly with halo mass at the high mass end ($10^{14}\mathrm{M}_\odot/h$) but tends to become flat for lower masses. Contrary to C-Eagle clusters which show a steeper slope instead.

By $z = 2$, our gas fractions are mostly flat for the whole range of masses while C-Eagle clusters show a weak increase with masses. More interestingly, our halos contain in average twice the amount of hot gas compared to C-Eagle clusters. If the AGN feedback, being inefficient at high redshift, is the cause for our high fractions, it is not the only possible explanation. Indeed, our infall assumptions, described in Equation 3.1, forces our

halos to constantly maintain a baryon fraction close to the 0.155 which includes a high concentration of hot gas inside the halo if no feedback is able to eject it.
On the other hand, hydrodynamical simulations have the advantage of being able to track gas particles inside and outside of their halos. The gas content allowed inside the virial radius is thus highly dependent on the feedback mechanisms but also on the amount of gas infalling and/or being reincorporated in the halo through proper physical mechanisms. Thus our SAM seems to predict a higher baryonic (mostly hot gas) content at high redshifts than what is expected in the simulations.

Additional observational data for lower halo masses will be necessary in order to properly conclude on these discrepancies between simulations. Moreover, a proper comparison with the BAHAMAS simulation (McCarthy et al., 2017) will be done to confirm this trend as part of future work on this project.

5.3.3 Metallicities

The metallicity has an impact on the cooling function, and also gives information on the accuracy of our SNae feedback. As the FTH18 model doesn't contain the chemical enrichment method developed in Yates et al. (2017), we cannot detail the abundance of each individual element. We are also unable to estimate the metallicity of our gas at a specific radius, such as r_{500}. In order to get a rough estimate of the Fe abundance and the total metallicity of the gas to compare directly with observations, we proceed as follows.
We consider all metals to follow a distribution similar to the one observed for Fe and described in Yates et al. (2017). This arbitrary choice for the profile has a relatively small importance as the density profiles of metals are similar for Fe, Si or O (see e.g. Mernier et al., 2017; Vogelsberger et al., 2018).
Moreover, we approximate the amount of H in the hot phase to be $\approx 0.75 M_{HG}$ in order to extract the Fe content out of our total metallicity, in agreement with our assumptions for the pristine gas composition.

We present the total metallicity (within r_{500}) of the HWT15 model (upper panel) and our FTH18 model (bottom panel) against the temperature in Fig. 5.8. The method for the measurements and selection of the XCS data sample is detailed in Appendix D.2. The FTH18 model presents a lower metal content in the ICM which fits the observations better compared to the previous HWT15 model. This difference can be explained by the SNae winds method used in the model. In this setup, the SNae feedback is enriching the

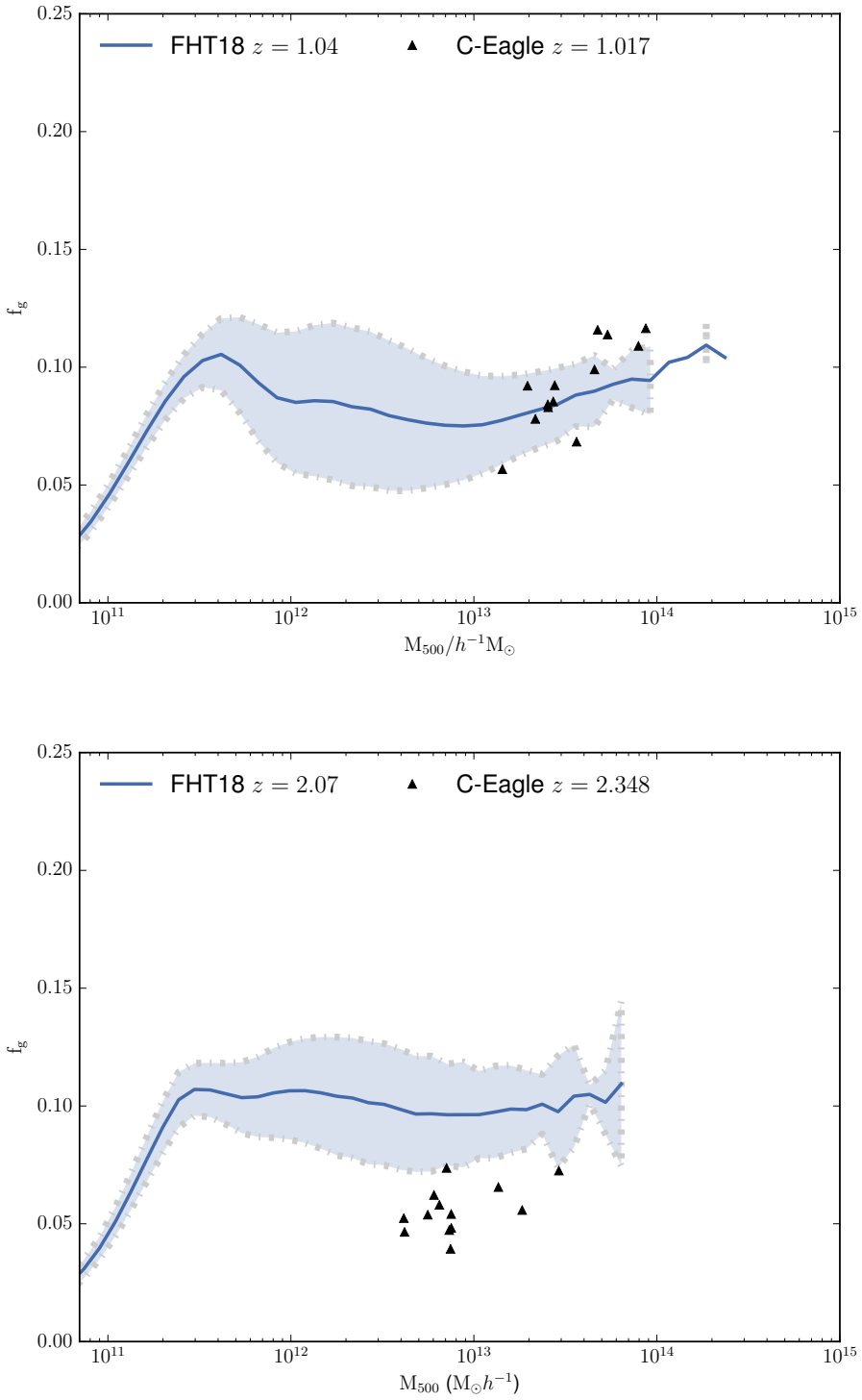

Figure 5.7: Hot gas fraction against the virial mass M_{500c} for the FTH and C-EAGLE models at $z = 1$ (top panel) and $z = 2$ (bottom panel) . The blue shaded area encloses 68% of the population around the mean value

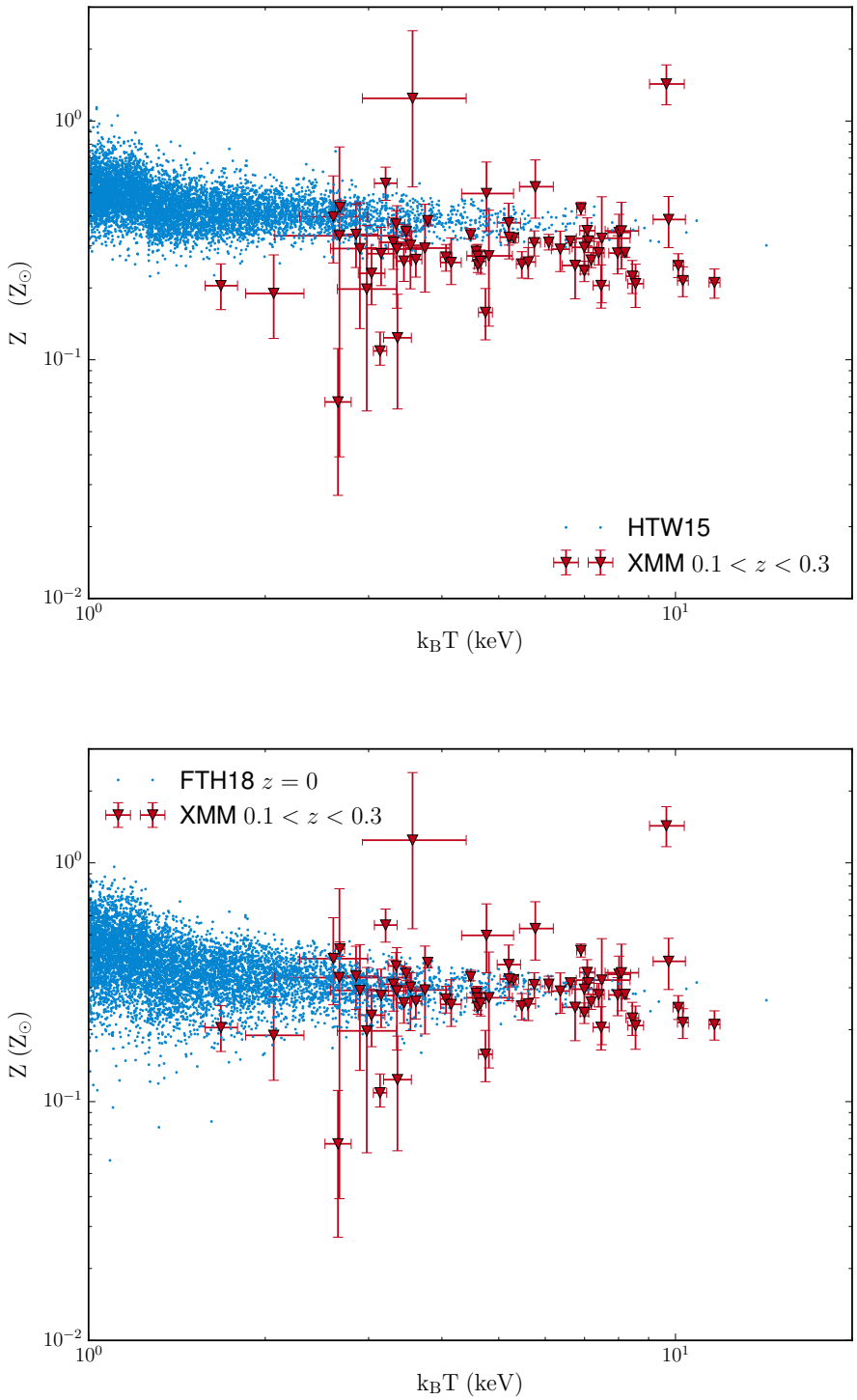

Figure 5.8: ICM metallicity within r_{500} against the temperature for the HWT15 (upper panel) and the FTH18 (bottom panel) models at $z = 0$. The method for the measurements and selection of the XCS data sample is detailed in Appendix D.2.

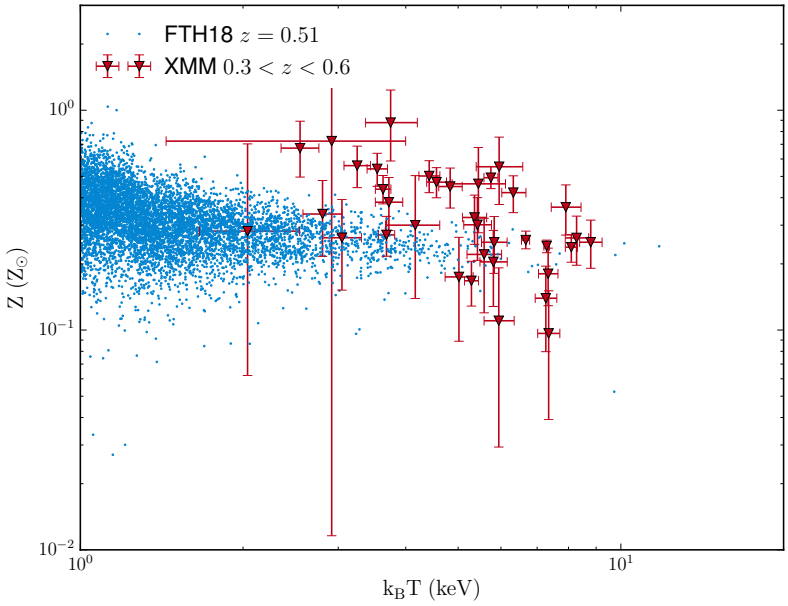

Figure 5.9: ICM metallicity inside r_{500} against the temperature for FTH18 model at $z = 0.5$. The method for the measurements and selection of the XCS data sample is detailed in Appendix D.2.

interstellar medium (ISM) and the amount of metals created depends on a yield parameter which value is set by the MCMC. Then a fraction of the ISM and its metals is reheated to be part of the ICM. In the FTH18 model, the yield parameter has been lowered by 15% as seen in Table B, thus reducing the amount of metals initially created and released by SNae winds.

Although the FTH18 model seems to fit better the observations at $z < 0.3$, it seems to underproduce metals in the ICM at higher redshift, as it can be seen in Fig. 5.9. While the observations suggest an increased metal content at higher redshifts, our predictions remain similar to those at $z = 0$. It could hint at the existence of a dilution by infall mechanism occurring at low metallicity gas and low redshift, that our model struggles to reproduce.

In addition, it is interesting to note that the observations suggest a weak negative slope as the temperature increases while our distribution of metals remains flat.

Fig. 5.10 shows the inferred Fe content of our groups and clusters in the case of the HTW15 model (upper panel) and our new model (bottom panel). The results are similar to the previous example due to the assumptions made that remains similar : the HWT15

model is overpredicting the amount of Fe in the ICM compared to the FTH18 model. However, both models contain more Fe than expected for the smallest groups (lowest temperatures), even if the FTH18 model is in better agreement with the data due to a large scatter. Thus the enrichment of the ICM done by supernovae winds appears too strong in the range of group of galaxies. Moreover, it is important to note that in both cases the Fe distribution with temperature is flat and does not follow any of the weak observational trends detailed in Yates et al. (2017). This could have serious implications for our feedback mechanisms and the enrichment method currently used for our models.

To summarise, the new FTH18 model reproduces fairly well most of the ICM properties. However, it is clear from these results that the metal enrichment and recycling of the ICM is poorly predicted by our SAM besides all the new improvements. This hints that our SNae and gas recycling need an improved description in order to get a more realistic behaviour for our metals. It is crucial to correctly model the ICM enrichment in future versions of the model, as it impacts heavily the cooling rates and is implicitly linked to the metallicity of the ISM.

5.4 Conclusions

In this work we update the current cooling model in the L-Galaxies SAM with a new description. This improvement is aimed at describing the observable properties of the ICM in a more realistic manner. To achieve this goal, we developed a physically motivated cooling mechanism based on an isothermal β model for the gas to replace the cooling radius method present in most SAMs. This change leads to X-ray luminosities self-consistently calculated and a cooling independent of the timestep size, while defining a more realistic density profile for the gas similar to the one assumed for cluster observations (see, e.g., Sanders et al., 2018).

Changing the cooling mechanism alone leads to a decrease in the cooling rates for the group and cluster sized objects du to the presence of a core. However, our computed luminosities still remain too high compared to the observed clusters.

With an appropriate feedback and a lowered gas content in the halo, as provided by the FTH18 model, we achieve a better agreement with the observations up to $z = 0.8$. In addition, we observe that our bolometric X-ray luminosity doesn't evolve in this range of redshifts. However, our X-ray predictions are brighter than what would be observationally expected at low temperatures due to a sharper slope in the distribution of observations. This could imply a gas content too large and/or a density profile not adapted to these

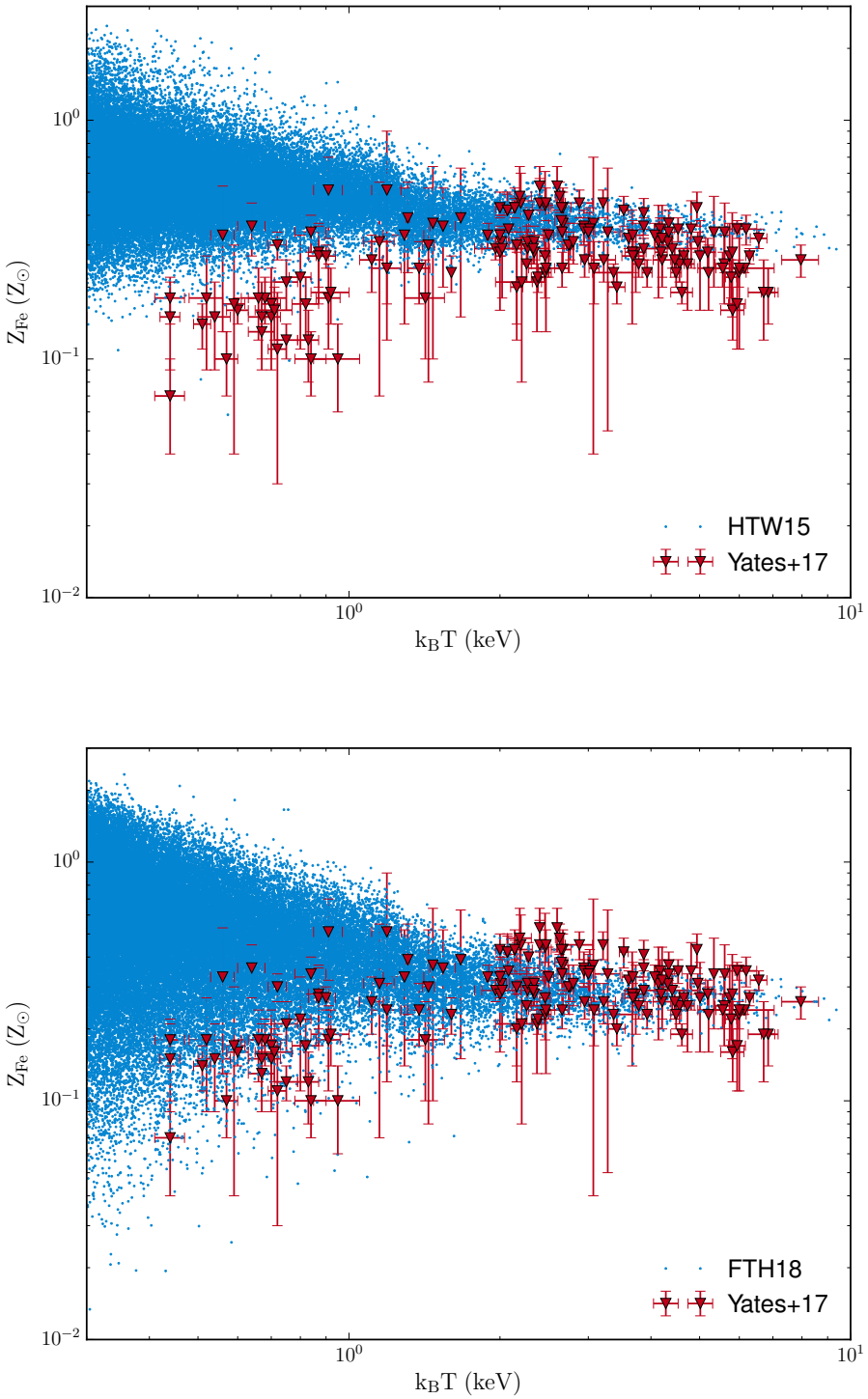

Figure 5.10: Fe metallicity within r_{500} against the temperature for the HWT15 (upper panel) and the FTH18 (bottom panel) models at $z = 0$. The observations are taken from Yates et al. (2017) and include several observational datasets.

objects.

Regarding the gas content, the new FTH18 model shows a correct gas fraction at $z = 0$ as its parameters were constrained to reproduce the observations. However, comparing it with with clusters from the C-Eagle simulations, we highlight two different trends emerging. As the redshift increases, the fraction of hot gas decreases slowly down to 5% at $z = 2$ for the C-Eagle clusters (on a very limited mass range) while the FTH18 model shows an inverse trend. The gas fractions increases for masses from 10^{11} to $10^{13}\mathrm{M}_{\odot}\mathrm{h}^{-1}$ and the distribution flattens. Due to the nature of the code and a baryon content matching the cosmic mean at every snapshot, SAMs are more rich in gas at higher redshifts. Indeed the evacuation of the gas can only be achieved when the black hole is massive enough to produce an efficient feedback with AGN jets. On the contrary, in the hydrodynamical simulations the amount of gas rely on the gas density distribution, temperature and speed for the infall/reincorporation mechanisms but also on the type of AGN feedback implemented. High redshift and low masses observations will be compulsory to state on the most plausible scenario, in addition to a comparison with other simulations.

The last property of the gas investigated was the metallicity. The FTH18 model is producing an environment in better agreement with the observations than its predecessor for the total metallicity content but also the iron metallicity. However, the ICM is too poor in metals at redshift $z \geq 0.3$. Moreover, the Fe distribution doesn't reproduce the weak observational negative slope described in Yates et al. (2017). This hints to a SNae feedback failing to enrich the ICM in a realistic manner.

To conclude, The FTH18 model, combining a β isothermal cooling model coupled with AGN winds able to eject the gas, achieves to reproduce the different global observables for the ICM (content, metallicity and luminosities) of groups and clusters of galaxies at z = 0. However, improvements can still be made in the enrichment of gas through SNae feedback (direct ejection of gas instead of mixing during reheating events). Different profiles for the gas density could be tried to see the impact on the ICM properties, especially for low temperature ICM objects.

Chapter 6

Conclusion

The work of this thesis focuses on the ICM component and feedback mechanisms through AGN feedback of the L-Galaxies SAM. As explained throughout this work, the hot gas is one of the key components in galaxy formation because its characteristics will determine the cooling rates and the amount of feedback required to regulate it. The goal of this thesis has been to reliably predict hot gas properties in order to compare with observations. As the observational data is limited in the redshift range, we focused on comparisons within the low redshift case in this thesis work.

To achieve a more realistic prediction of hot gas behaviour, three main characteristics of the gas have been investigated and improved: infall, gas content and cooling rates. Implementing these changes has solved a long running problem intrinsic to the code, leading to an improved and physically motivated description of the black hole growth and gas behaviour (cooling and feedback). This has resulted in an overall better agreement with observations in a large range of galaxy properties. We briefly summarise the main achievements below.

6.1 Summary

All but one SAM from the nIFTy comparison project displays an important baryon content problem. The overaccretion of baryons in the model was found to be due to the halo evolution through time, and their properties extracted through halo finder and merger tree codes. Due to changes of shape and sometimes misidentifications, the halo masses fluctuate but the baryon content in the SAMs is only allowed to increase.

As a consequence an Extra-halo phase was created in order to keep track of the gas in excess and its metallicity, and to achieve mass conservation while removing gas out from

the halo. Including this extra reservoir managed to clear the high gas fractions while impacting the galaxy properties minimally.
Although the content of baryons has been properly reduced through this method, there is still no viable explanation for gas fractions lower than the cosmic mean.

Although the baryon content of halos has been decreased, the hot atmosphere was found to be still too rich in gas compared to observations of groups and clusters. As the SNae feedback is not efficient enough for the high masses range, the AGN feedback was modified to include jets capable of removing gas from the halo (similar to the SNae winds). Four different black hole accretion methods were tested with this improved feedback, as the old implementation was working to reheat the gas only. After tuning the parameters through a MCMC method, all models reproduced the correct hot gas fraction as they were constrained to. However, differences exist between them.
• HotCrot , based on hot gas accretion, produces black holes smaller than observationally expected and a feedback too inefficient at high masses, leading to larger galaxies.
• CoolBow on the other hand is too efficient to accrete gas on black holes especially in small galaxies due to a formula based on the cooling gas only, without black hole mass dependence. This leads to a feedback too powerful, reducing dramatically the amount of gas allowed to cool. Hence lowering star formation.
• ColdGT based on cold gas, manages to produce an overall good agreement with galaxy and ICM properties. However, the lack of high mass black holes reduces the feedback in large galaxies and consequently leads to bluer galaxies. In addition, it produces higher luminosities than expected by predictions from Hopkins et al. (2008).
• ColdC is finally the model that manages to agree the best with all galaxy properties. A cold cloud accretion seems also to be the best description to produce accurate AGN properties.
However, all models fail to reproduce a correct bulge fraction for the galaxies. This problem is due to the change of feedback impacting the cold gas of galaxies too. Underestimating the disk instability contribution to BH growth in the HWT15 model seems to be a plausible cause and is investigated in Irodotou et al. (2018).

In addition to the feedback change, a new description for the cooling mechanism, analytical and more physical, has been developed to replace the previous cooling radius method. The gas profile was changed to an isothermal β density profile. Then the total

X-ray luminosity of the gas can be calculated directly and the cooling rate derived analytically from the formula. This leads to a cooling rate reduced at high masses (i.e. groups and clusters) compared to the previous version of the model. However, the X-ray predictions were still too high due to the gas content. The addition of the previous best model of feedback (ColdC accretion) was compulsory in order to solve this issue.

Comparing with observations (including the most recent XMM dataset), the model produces X-ray luminosities in agreement with the expectations up to $z \leq 1$. Moreover, there is no trace of apparent luminosity evolution with redshift, just as suggested by the observations. However the luminosities might be higher than the expected observational trend at low masses, certainly due to the density profile not being accurate enough at low masses.

If the gas fraction at $z = 0$ reproduces the observations it was constrained with, the evolution of the gas fraction with redshift is different from what could be expected from hydrodynamical simulations such as C-Eagle. Indeed, in our case the gas content is increasing for low to medium halo masses up to a global flat trend around 0.13 by $z = 2$. On the other hand, the predictions from C-Eagle show a fraction increasing with halo mass at all redshifts with values around 0.5 by $z = 2$. These differences can be explained by the nature of the different codes, as the content of hot gas is lower inside the C-Eagle simulation. But also by the black hole growth model. Indeed, in the FTH18 model, the AGN feedback is not efficient enough at $z = 2$ to remove the hot atmosphere as the black holes are still too small. However, a proper comparison with observations will be needed to tell apart which behaviour is more realistic. To conclude, the metallicities seem to be in better agreement than the previous HWT15 model due to a change in the yield parameter, up to $z = 0.6$. However, it doesn't reproduce the weak trends from the observations (Yates et al., 2017), which implies the need for a better description of the enrichment (Yates et al., 2017) or a more accurate description of the SNae feedback.

6.2 Future work and improvements

A new version of the HWT15 model (Hen18) is currently being developed, including an improved description of the galactic disk and the ISM through the separation of the disk in rings. The infall correction has already been included in the development version of the code and merged with the Yates et al. (2017) correction. Once the paper including the FTH18 model has been reviewed and accepted, it will be implemented as the main

recipe for AGN feedback and cooling methods in the new version. As the Hen18 model is also including an improved model for the disk instabilities and mergers (Irodotou et al., 2018), more tests have to be run to investigate if it solves the bulges problem developed in the A. In addition, a comparison of the AGN luminosities with bolometric corrected observations from Lusso et al. (2012) will be included in the new model.
The implementation of the feedback mechanism into the new model will also be a perfect occasion to dig more in depth into the black hole accretion mecanisms. Indeed, the ring description enables us to track the gas flowing towards the center more accurately. This will lead to the creation of a proper accretion disk around the black hole with a more detailed accretion. Depending on the success, a proper thin/thick disk distinction could also be made to help with the observational comparison.

Finally, even if the ICM description has been greatly improved, further work can be pursued on several ideas.
• The current infall correction is working but has revealed the flaws of the imported virial properties via halo finders and merger trees. As discussed before, these errors are due to limitations intrinsic to the nature of the code itself. Hence a new approach could be investigated, where the merger trees are swapped for merger bushes. The fundamental change made in this case is that progenitors will not have a unique descendent anymore, but possibly several. This method will be more challenging as it requires tracking and storing more information, but it will help to track more accurately the halos during mergers and the change of shape, or mass, induced. Therefore it will be easier to move baryons from different halos and hopefully solve the baryon problem without resorting to the use of an external reservoir.
• Although the global properties of the ICM are agreeing well with observations of low redshift clusters and groups in the new model, it fails to give radial information such as temperature or entropy gradients. The use of hydrodynamical codes, able to track particles, is generally required in order to compare with observations. However, with the relative success of the disk rings introduction in the Hen18 model, it would be worth investigating a similar shell-like structure for the ICM too. Dividing the the hot atmosphere into spherical shells would help tracking the gas more accurately and produce a more accurate feedback and reincorporation, in addition to a larger set of properties to compare with observational datasets. However, the implementation of such a structure is not trivial, especially due to the intrinsic nature of the SAM. First of all, the boundary conditions are problematic, as we have currently no information in the code about the

outside of the halo (above r_{200c}). Then, the feedback and reincorporation mechanisms, although being localised events, will impact each shell homogeneously, which could lead to unrealistic results due to this forced assumption.

• Another important improvement could be made towards the black hole growth and AGN luminosities. As we have seen before, the characteristic at low redshift are agreeing with observations and predictions. However, the FTH18 model seems to fail reproducing predictions at higher redshifts. This could be due to two factors : a black hole growth too slow at high redshift, or a hot gas content too high inside halos, as discussed before. Moreover, our predicted AGN luminosities are currently bolometric and difficult to compare to observations. A possible improvement could be to assume an energy density distribution for the AGN. Thus we would be able to compare our predicted luminosities with direct observations without involving k corrections.

Appendix A

The bulge fraction problem

A.1 Description of the problem

We have seen in Chapter 4.3.2 that all models reproduce with rather good agreement most of the galaxy properties in general.

However, the new feedback mechanism has an unexpected impact on the bulge growth of galaxies. As clearly shown on Figure A.1, all the models without exceptions fail to reproduce the fraction of bulge dominated galaxies. The fact that the total stellar mass is in agreement with observations indicates that the mechanism involved in the bulge growth failed during the runs of our new version of the model.

The feedback, having an impact on the cold gas reservoir and galaxy growth at earlier time could be a cause. In addition, the reduction of the hot gas atmosphere could have impacted the stellar growth at higher redshifts. However, as seen previously in Fig 4.2 and 4.3, it doesn't seem to be a valid reason.
. In addition, bulges are not growing only through merger events, as stated in Section 2.2.3, but also through disk instabilities.

A.2 Disk instabilities

The creation of a central bar in galaxies is coming from dynamical instabilities in the disk. They occur when the self-gravity of the disk is dominant over the gravitational effects of the bulge and halo. In order to stabilise the disk, stars and gas are channeled towards the

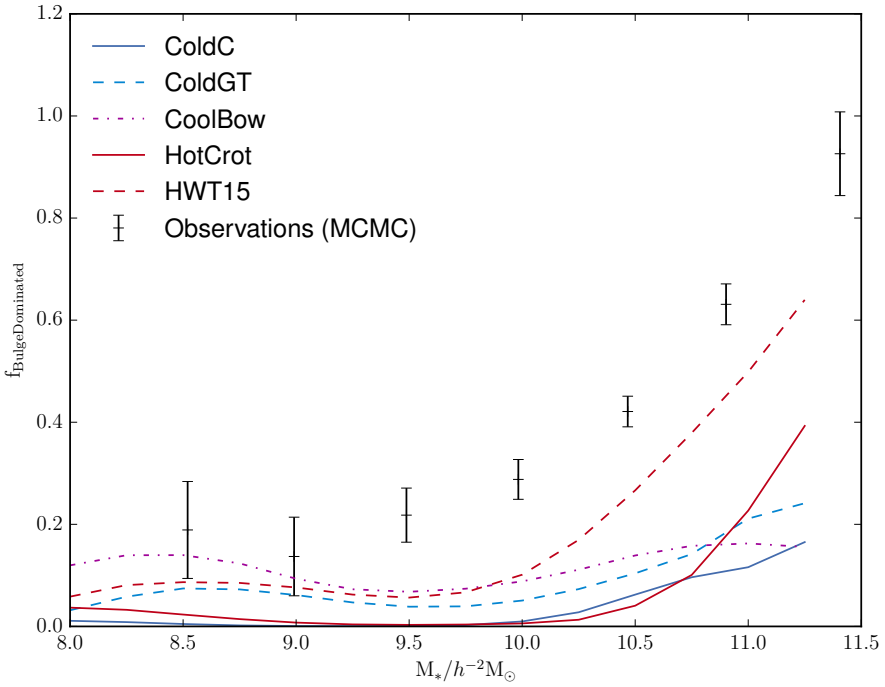

Figure A.1: Fraction of bulge dominated galaxies against stellar mass for all the models presented in Section 4.2.1 at $z = 0$. The observational dataset is given by Conselice (2006).

central bulge. The criterion used for the disk instability is described in Guo et al. (2011) :

$$V_{max} = \sqrt{\frac{GM_{*,d}}{3R_{*,d}}} \tag{A.1}$$

where $M_{*,d}$ and $R_{*,d}$ are the stellar mass and exponential scale-lengths of the disk. V_{max} is the maximum circular velocity of the disk, which is assumed to also be the circular velocity of the galaxy.

However, as the bulge growth was dominated by merger events in the previous version of the code, the contribution of this mode was not a concern. The work presented in Tonini et al. (2016) shows that, on the contrary, disk instabilities are the main mechanism in bulge growth for medium sized galaxies.

Going through the precursor work made for this instability criterion (Efstathiou et al., 1982), it has been found that the criterion has been modified in De Lucia et al. (2004) to replace the disk radius by the exponential scale-length, which is one third of its value. Moreover, other constants seem to have been omitted during process. Indeed, the Toomre

criterion of stability (Toomre, 1964) is defined by :

$$Q = \frac{\kappa \sigma_R}{3.36 G \Sigma} \geq 1 \tag{A.2}$$

where κ is the epicyclic frequency, σ_R the velocity dispertion and Σ the surface density of the disk.

Rearranging for the critical mass of star $\mathrm{M_{*,crit}}$ ($Q = 1$) gives us the following relations :

$$\mathrm{M_{*,crit}} = \pi \frac{\mathrm{R_{*,d}}^2}{9} \Sigma_{crit} = 0.10 \frac{\mathrm{R_{*,d}}}{G} \mathrm{R_{*,d}} \kappa \sigma_R \tag{A.3}$$

Assuming $\sigma_R < \mathrm{V_{rot}}$ and $\mathrm{V_{rot}} \approx \mathrm{V_{max}}$ we obtain the final relation :

$$\mathrm{M_{*,crit}} = \alpha \frac{\mathrm{V_{max}}^2 \mathrm{R_{*,d}}}{G} \tag{A.4}$$

where the constant $\alpha << 1$.

In this appendix, we propose to investigate briefly the impact of a boosted disk instability criterion by setting $\alpha = 0.1$.

A.3 Discussion

The results for one of the model with the disk instability criterion from Equation A.4 is presented in Figure A.2.

It is clear from that figure that an increase in the transfer of stars through disk instabilities is necessary in order to get a better agreement with the observations. Moreover, it doesn't only give a better description for the bulge dominated galaxies, but for all the different morphologies. However, the bulge dominated fraction is still underpredicted for the highest range of galaxy masses.

The implementation of the new feedback raised a weakness of the model regarding to the dominant merger driven growth of bulges. A possible solution to this problem could be a more prominent role of the disk instabilities, as we have just shown. Following this discovery, a more detailed prescription for mergers and disk instabilities is being currently developed and described in Irodotou et al. (2018).

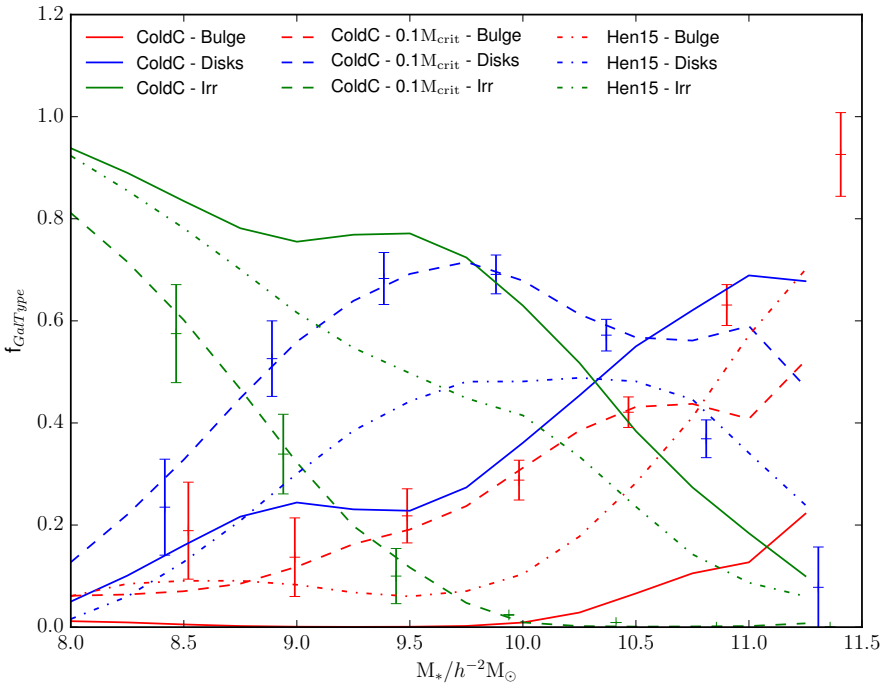

Figure A.2: Fraction of different morphological types as a function of stellar mass for the FTH18 model (solid lines), the FTH18 model including our boosted DI criterion (dashed lines) and the HWT15 model (dotted lines) at $z = 0$. Red lines show the fractions of ellipticals ($M_{bulge}/M_* \geq 0.7$), blue lines show the fraction of normal spirals ($0.01 \geq M_{bulge}/M_* \leq 0.7$) and green lines represent the pure discs or extreme late-types ($M_{bulge}/M_* \leq 0.01$). The observational datasets are given by Conselice (2006).

Appendix B

Models parameters

Table B.1: Free parameters of the L-Galaxies SAM and their best fit value obtained through MCMC tuning for the HWT15 and FTH18 models.

Parameters	HWT15	FTH18	Units
α_{SF} (SF eff)	0.025	0.035	-
$M_{crit,0}$ (Gas mass threshold)	0.24	0.20	$10^{10}M_{\odot}$
$\alpha_{SF,burst}$ (SF burst eff)	0.60	0.50	-
$\beta_{SF,burst}$ (SF burst slope)	1.9	0.63	-
k_{AGN}(AGN eff)	5.3×10^{-3}	10^{-2}	-
f_{BH} (BH growth eff)	0.041	0.016	-
V_{BH} (Quasar growth scale)	750	1256	km/s
ϵ (Mass-loading eff)	2.6	7.6	-
V_{reheat} (Mass-loading scale)	480	430	km/s
β_1 (Mass-loading slope)	0.72	0.13	-
η (SNae ej eff)	0.62	1.3	-
V_{eject} (SNae ej scale)	100	97	km/s
β_2 (SNae ej slope)	0.80	0.63	-
γ (Ej reinc)	3.0	1.6	10^{10}yr
$M_{r.p.}$ (Ram-presure threshold)	1.2	4.0	$10^{10}M_{\odot}$
R_{merger} (Major-merger threshold)	0.1	0.46	-
$\alpha_{friction}$ (Dynamical friction)	2.5	3.0	-
y (Metal yield)	0.046	0.039	-
η_{mech} (Mechanical feedback eff)	-	0.074	-
τ_{Reinc} (AGN ej reinc)	-	3.8	Gyr

Appendix C

SIS dynamical times and variable cooling

C.1 The cooling and dynamical times

We take the cooling rate per unit volume of the gas to be ${n_{\rm g}}^2\Lambda(T,Z)$, where $n_{\rm g}=\rho_{\rm g}/\mu m_{\rm H}$ is the number density of particles in the gas and the cooling function, Λ, is a function of temperature and metallicity, Z. The specific cooling rate of the gas in a SIS is then

$$\frac{{\rm d}\epsilon}{{\rm d}t}=-\frac{n_{\rm g}}{\mu m_{\rm H}}\Lambda, \tag{C.1}$$

which leads to a characteristic cooling timescale for the gas of

$$t_{\rm cool}\equiv\frac{\epsilon}{|{\rm d}\epsilon/{\rm d}t|}=\frac{3k_{\rm B}T}{2n_{\rm g}\Lambda}. \tag{C.2}$$

We can write this as

$$t_{\rm cool}=\tau_{\rm cool}\frac{x^2}{f_{\rm g}}, \tag{C.3}$$

where

$$\tau_{\rm cool}=\frac{9\mu m_{\rm H}k_{\rm B}T}{400\rho_{\rm c}\Lambda}. \tag{C.4}$$

The adiabatic sound speed in the gas is $(5k_{\rm B}T/3\mu m_{\rm H})^{1/2}\approx v_{\rm c}$. Hence the characteristic dynamical time for gas to flow a distance r is

$$t_{\rm dyn}=\frac{r}{v_{\rm c}}=\tau_{\rm dyn}x, \tag{C.5}$$

where $\tau_{\rm dyn}=r_{\rm 200c}/v_{\rm c}$.

C.2 Variable cooling

In the existing L-GALAXIES model, this is implemented by finding the radius, $r_{\rm cool}$, at which $t_{\rm cool}(r_{\rm cool}) = \tau_{\rm dyn}$ and setting the cooling rate to be

$$\dot{M}_{\rm g} = -\frac{m_{\rm g}(r_{\rm cool})}{\tau_{\rm dyn}} = \dot{M}_{\rm g,max} x_{\rm cool}, \tag{C.6}$$

where $x_{\rm cool} = r_{\rm cool}/r_{\rm 200c}$. Now, from Equation C.4, we see that $x_{\rm cool} = (\tau_{\rm dyn} f_{\rm g}/\tau_{\rm cool})^{1/2}$. Hence the final expression for the cooling rate is

$$\dot{M}_{\rm g} = \dot{M}_{\rm g,max} \min\left[1, \left(\frac{\tau_{\rm dyn} f_{\rm g}}{\tau_{\rm cool}}\right)^{\frac{1}{2}}\right]. \tag{C.7}$$

Over timestep Δt the amount of gas that has cooled and been deposited is estimated assuming the cooling rate to be constant over the timestep, but restricting the total amount of gas cooled to be no larger than that initially present:

$$|\Delta M_{\rm g}| = \min\left[M_{\rm g}, |\dot{M}_{\rm g}|\Delta t\right]. \tag{C.8}$$

We can rewrite this in terms of the hot gas mass fraction. Starting with initial gas fraction $f_{\rm g0}$, the remaining gas fraction after time Δt is

$$f_{\rm g} = f_{\rm g0} \max\left[0, 1 - \frac{\Delta t}{\tau_{\rm dyn}}, 1 - \left(\frac{\tau_{\rm dyn} f_{\rm g0}}{\tau_{\rm cool}}\right)^{\frac{1}{2}} \frac{\Delta t}{\tau_{\rm dyn}}\right]. \tag{C.9}$$

As stated before, the problem with the model is that the total amount of mass cooled is only correctly estimated is sufficiently small $f_{\rm g} \approx f_{\rm g0}$. This is an unnecessary restriction introduced to minimise execution time in the code and can easily be replaced by integrated versions of the cooling equations that use a variable cooling rate as the density of the remaining gas decreases over time. Equation C.7 can be rewritten as

$$\dot{f}_{\rm g} = -\begin{cases} \dfrac{f_{\rm g}}{\tau_{\rm dyn}}, & \tau_{\rm cool} \leq \tau_{\rm dyn} f_{\rm g}; \\ \dfrac{{f_{\rm g}}^{\frac{3}{2}}}{(\tau_{\rm dyn}\tau_{\rm cool})^{\frac{1}{2}}}, & \tau_{\rm cool} > \tau_{\rm dyn} f_{\rm g}. \end{cases} \tag{C.10}$$

When $\tau_{\rm cool} > \tau_{\rm dyn} f_{\rm g0}$ the lower of these expressions integrates to give

$$f_{\rm g} = f_{\rm g0}\left(1 + \left(\frac{\tau_{\rm dyn} f_{\rm g0}}{\tau_{\rm cool}}\right)^{\frac{1}{2}} \frac{\Delta t}{2\tau_{\rm dyn}}\right)^{-2}. \tag{C.11}$$

The condition $\tau_{\rm cool} \leq \tau_{\rm dyn} f_{\rm g}$ is trickier, because after some of the gas has cooled, the cooling time drops and the cooling rate switches from the upper to the lower expression:

$$f_{\rm g} = \begin{cases} f_{\rm g0} e^{-\Delta t/\tau_{\rm dyn}}, & \Delta t \leq t_{\rm eq}; \\ \dfrac{\tau_{\rm cool}}{\tau_{\rm dyn}}\left(1 + \dfrac{\Delta t - t_{\rm eq}}{2\tau_{\rm dyn}}\right)^{-2}, & \Delta t > t_{\rm eq}; \end{cases} \tag{C.12}$$

where $t_{\rm eq} = \tau_{\rm dyn} \ln(\tau_{\rm dyn} f_{\rm g0}/\tau_{\rm cool})$.

Fig. C.1 shows the difference between the two approaches for the cases where $\tau_{\rm cool}/\tau_{\rm dyn} f_{\rm g} = 0.2$ and 2. The amount of gas cooled is the same for timesteps that are short compared to the dynamical time but, whereas the fixed cooling rate scheme exhausts all the gas after one dynamical time, the variable cooling rate approach leaves residual gas even at late times.

We note in passing that it could be argued that the cooling radius should be determined not by the location where the cooling time of the gas equals the dynamical time of the halo, $\tau_{\rm dyn}$, but rather the local dynamical time, $t_{\rm dyn}$. That would have the effect of modifying Equation C.12 as follows:

$$f_{\rm g} = \begin{cases} f_{\rm g0} e^{-\Delta t/\tau_{\rm dyn}}, & \Delta t \leq t_{\rm eq}; \\ \frac{\tau_{\rm cool}}{\tau_{\rm dyn}} \left(1 + \frac{\Delta t - t_{\rm eq}}{3\tau_{\rm dyn}}\right)^{-3}, & \Delta t > t_{\rm eq}; \end{cases} \tag{C.13}$$

In practice, the two are very similar.

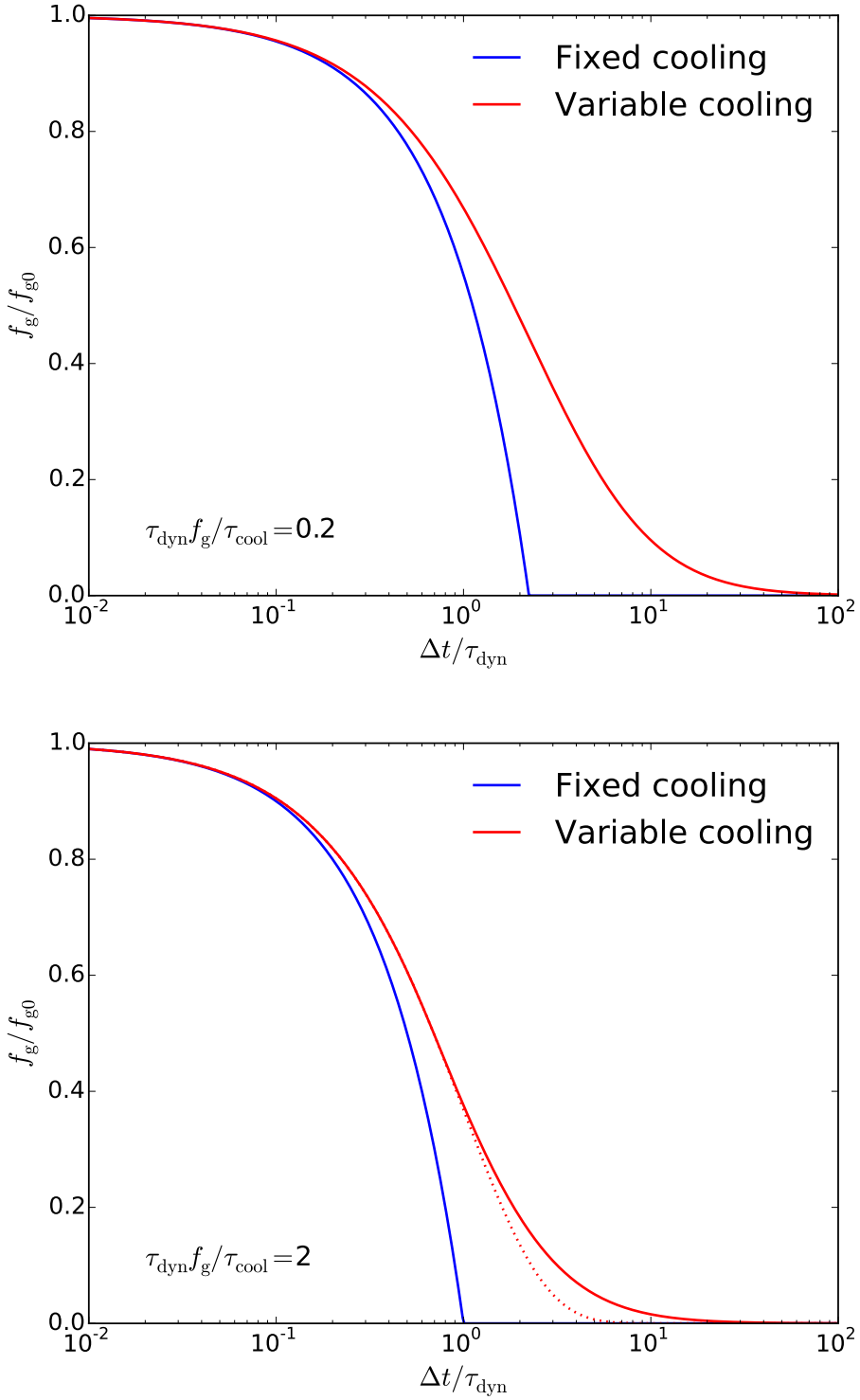

Figure C.1: The amount of gas remaining in the SIS model after time Δt using a fixed cooling rate (lower, blue curve) and variable cooling rate (upper, red curve), for the cases where $\tau_{\rm cool}/\tau_{\rm dyn} f_{\rm g} = 0.2$ (upper panel) and 2 (lower panel). The dotted red line in the lower panel shows the exponential branch of the solution given in Equation C.12.

Appendix D

XCS Methodology: Cluster Sample and X-ray Data Analysis

D.1 Luminosity-Temperature Measurements

The X-ray cluster sample used to compare with the model is a subset of the *XMM* Cluster Survey's second data release (XCS DR2), containing galaxy clusters in the SDSS DR13 footprint. 418 clusters were used, all with associated X-ray luminosity ($L_{\rm X}$), temperature ($T_{\rm X}$) and redshift measurements (Manolopoulou et al. in prep). These clusters were selected from the overall sample for having a signal-to-noise ratio (SNR) greater than 15 and $z > 0.05$, to ensure good quality spectral fits. The X-ray Post Processing Pipeline (`XCS3P`) was used to derive the X-ray spectral properties of the clusters, specifically their X-ray temperature ($T_{\rm X}$) bolometric luminosity ($L_{\rm X}$) and total average metallicity (Z). An overview of `XCS3P`, including methodology tests, can be found in Lloyd-Davies et al. (2011b).

Cluster spectra were extracted and fitted using the XSPEC package (Arnaud (1996)). The fits were performed in the 0.3-7.9 keV band with an absorbed MeKaL model (`wabs` × `mekal`) using the c-statistic. The `wabs` component accounts for absorption due to neutral hydrogen along the line of sight to the cluster, while the `mekal` component models the emission from a hot diffuse gas enriched with various elements. Relative abundances of these elements are defined in relation to the solar abundance ($Z_{\odot}$). During the fitting process for the luminosity and temperature, the abundance is fixed at $0.3Z_{\odot}$ - a typical value for X-ray clusters (Kravtsov and Borgani (2012)). The redshift is also fixed, leaving the `mekal` temperature and normalisation free to vary.

The spectral extraction region is initially equivalent to the X-ray Automated Pipeline

Algorithm `XAPA` region placed on the detected cluster. The radius corresponding to this aperture is used to calculate an initial temperature for the cluster. This temperature is used to estimate r_{500} via the $T_X - r_{500}$ relation from (Arnaud et al., 2005). A new region is then created with the r_{500} value as the major axis, and another temperature is extracted. The process is repeated until the r_{500} converges (the ratio of the new to old r_{500} defined to be >0.9 and < 1.1). For each iteration, a coefficient of variation of the T_X is calculated. This coefficient is defined as the ratio of the standard deviation (σ) to the mean (μ), given by $C_v = \sigma(T_{\rm X})/\mu(T_{\rm X})$. In the analysis, we adopted a value of $C_v < 0.25$ as an indicator of a reliable measurement. The background is accounted for by including a background annulus centred on the cluster, which has an inner and outer radius of $1.05r_{500}$ and $1.5r_{500}$, respectively.

The luminosities and temperatures in the plot are measured in an r_{500} aperture

D.2 Abundance-Temperature Relation

In order to reliably measure the overall metal content, the clusters must have a significant number of soft band photon counts. A subsample of 120 clusters from the overall XCS-SDSS sample was created by selecting clusters with more than 2000 counts, at $z > 0.1$. The model fitting process was kept the same, only this time, the abundance was treated as an additional free parameter. All other properties were fixed. The average abundance for the cluster was fitted simultaneously with the temperature, between lower and upper bounds of $0.01Z_{\odot}$ and $3.0Z_{\odot}$.

Bibliography

Anderson, S. F., Margon, B., Voges, W., Plotkin, R. M., Syphers, D., Haggard, D., Collinge, M. J., Meyer, J., Strauss, M. A., Agüeros, M. A., Hall, P. B., Homer, L., Ivezić, Ž., Richards, G. T., Richmond, M. W., Schneider, D. P., Stinson, G., Vanden Berk, D. E., and York, D. G. (2007). A Large, Uniform Sample of X-Ray-emitting Active Galactic Nuclei from the ROSAT All Sky and Sloan Digital Sky Surveys: The Data Release 5 Sample. *AJ*, 133:313–329. xiv, xvi, 23, 40, 51, 52, 77

Arnaud, K. A. (1996). XSPEC: The First Ten Years. In Jacoby, G. H. and Barnes, J., editors, *Astronomical Data Analysis Software and Systems V*, volume 101 of *Astronomical Society of the Pacific Conference Series*, page 17. 101

Arnaud, M., Pointecouteau, E., and Pratt, G. W. (2005). The structural and scaling properties of nearby galaxy clusters. II. The M-T relation. *A&A*, 441:893–903. 102

Baldry, I. K., Driver, S. P., Loveday, J., Taylor, E. N., Kelvin, L. S., Liske, J., Norberg, P., Robotham, A. S. G., Brough, S., Hopkins, A. M., Bamford, S. P., Peacock, J. A., Bland-Hawthorn, J., Conselice, C. J., Croom, S. M., Jones, D. H., Parkinson, H. R., Popescu, C. C., Prescott, M., Sharp, R. G., and Tuffs, R. J. (2012). Galaxy And Mass Assembly (GAMA): the galaxy stellar mass function at z ¡ 0.06. *MNRAS*, 421:621–634. xiv, 23, 52, 53, 55

Barbosa, D., Bartlett, J. G., Blanchard, A., and Oukbir, J. (1996). The Sunyaev-Zel'dovich effect and the value of {OMEGA}_0_. *A&A*, 314:13–17. 7

Barnes, D. J., Kay, S. T., Bahé, Y. M., Dalla Vecchia, C., McCarthy, I. G., Schaye, J., Bower, R. G., Jenkins, A., Thomas, P. A., Schaller, M., Crain, R. A., Theuns, T., and White, S. D. M. (2017). The Cluster-EAGLE project: global properties of simulated clusters with resolved galaxies. *MNRAS*, 471:1088–1106. 14, 75

Bartalucci, I., Arnaud, M., Pratt, G. W., Démoclès, J., van der Burg, R. F. J., and Mazzotta, P. (2017). Resolving galaxy cluster gas properties at z = 1 with XMM-Newton and Chandra. *A&A*, 598:A61. 64

Baugh, C. M. (2006). A primer on hierarchical galaxy formation: the semi-analytical approach. *Reports on Progress in Physics*, 69:3101–3156. xiii, 5, 7, 14

Bell, E. F., McIntosh, D. H., Katz, N., and Weinberg, M. D. (2003). The Optical and Near-Infrared Properties of Galaxies. I. Luminosity and Stellar Mass Functions. *ApJS*, 149:289–312. xiv, 55

Benson, A. J. (2012). G ALACTICUS: A semi-analytic model of galaxy formation. *New Astron.*, 17:175–197. 25

Bertschinger, E. (1983). Cosmological self-similar shock waves and galaxy formation. *ApJ*, 268:17–29. 8

Bertschinger, E. (1985). The self-similar evolution of holes in an Einstein-de Sitter universe. *ApJS*, 58:1–37. 8

Binney, J. and Tremaine, S. (2008). *Galactic Dynamics: Second Edition*. Princeton University Press. 4

Biviano, A. (2000). From Messier to Abell: 200 Years of Science with Galaxy Clusters. In *Constructing the Universe with Clusters of Galaxies*. 7

Bondi, H. (1952). On spherically symmetrical accretion. *MNRAS*, 112:195. 11

Bower, R. G., Benson, A. J., Malbon, R., Helly, J. C., Frenk, C. S., Baugh, C. M., Cole, S., and Lacey, C. G. (2006). Breaking the hierarchy of galaxy formation. *MNRAS*, 370:645–655. 15, 25, 40, 41, 64

Bower, R. G., McCarthy, I. G., and Benson, A. J. (2008). The flip-side of galaxy formation: A combined model of Galaxy Formation and Cluster Heating. *MNRAS*, 390:1399–1410. 41, 43, 44, 50, 52, 56

Bower, R. G., Schaye, J., Frenk, C. S., Theuns, T., Schaller, M., Crain, R. A., and McAlpine, S. (2017). The dark nemesis of galaxy formation: why hot haloes trigger black hole growth and bring star formation to an end. *MNRAS*, 465:32–44. xv, 57

Boylan-Kolchin, M., Springel, V., White, S. D. M., Jenkins, A., and Lemson, G. (2009). Resolving cosmic structure formation with the Millennium-II Simulation. *MNRAS*, 398:1150–1164. 15

Chabrier, G. (2003). Galactic Stellar and Substellar Initial Mass Function. *PASP*, 115:763–795. 20

Cicone, C., Maiolino, R., Sturm, E., Gracia-Carpio, J., Feruglio, C., Neri, R., Aalto, S., Davies, R., Fiore, F., Fischer, J., Garcia-Burillo, S., Gonzalez-Alfonso, E., Hailey-Dunsheath, S., Piconcelli, E., and Veilleux, S. (2013). VizieR Online Data Catalog: AGN feedback from CO observations (Cicone+, 2014). *VizieR Online Data Catalog*, 356. 49

Cicone, C., Maiolino, R., Sturm, E., Graciá-Carpio, J., Feruglio, C., Neri, R., Aalto, S., Davies, R., Fiore, F., Fischer, J., García-Burillo, S., González-Alfonso, E., Hailey-Dunsheath, S., Piconcelli, E., and Veilleux, S. (2014). Massive molecular outflows and evidence for AGN feedback from CO observations. *A&A*, 562:A21. 10, 11, 41, 49, 51

Cole, S., Aragon-Salamanca, A., Frenk, C. S., Navarro, J. F., and Zepf, S. E. (1994). A Recipe for Galaxy Formation. *MNRAS*, 271:781. 40, 64

Cole, S., Lacey, C. G., Baugh, C. M., and Frenk, C. S. (2000). Hierarchical galaxy formation. *MNRAS*, 319:168–204. 15

Colless, M., Dalton, G., Maddox, S., Sutherland, W., Norberg, P., Cole, S., Bland-Hawthorn, J., Bridges, T., Cannon, R., Collins, C., Couch, W., Cross, N., Deeley, K., De Propris, R., Driver, S. P., Efstathiou, G., Ellis, R. S., Frenk, C. S., Glazebrook, K., Jackson, C., Lahav, O., Lewis, I., Lumsden, S., Madgwick, D., Peacock, J. A., Peterson, B. A., Price, I., Seaborne, M., and Taylor, K. (2001). The 2dF Galaxy Redshift Survey: spectra and redshifts. *MNRAS*, 328:1039–1063. 15

Conselice, C. J. (2006). The fundamental properties of galaxies and a new galaxy classification system. *MNRAS*, 373:1389–1408. xvi, 92, 94

Crain, R. A., Eke, V. R., Frenk, C. S., Jenkins, A., McCarthy, I. G., Navarro, J. F., and Pearce, F. R. (2007). The baryon fraction of ΛCDM haloes. *MNRAS*, 377:41–49. 27, 34

Croton, D. J., Springel, V., White, S. D. M., De Lucia, G., Frenk, C. S., Gao, L., Jenkins, A., Kauffmann, G., Navarro, J. F., and Yoshida, N. (2006). The many lives of active

galactic nuclei: cooling flows, black holes and the luminosities and colours of galaxies. *MNRAS*, 365:11–28. 15, 16, 25, 40, 41, 43

Croton, D. J., Stevens, A. R. H., Tonini, C., Garel, T., Bernyk, M., Bibiano, A., Hodkinson, L., Mutch, S. J., Poole, G. B., and Shattow, G. M. (2016). Semi-Analytic Galaxy Evolution (SAGE): Model Calibration and Basic Results. *ApJS*, 222:22. 41, 43, 44

De Lucia, G. and Blaizot, J. (2007). The hierarchical formation of the brightest cluster galaxies. *MNRAS*, 375:2–14. 15, 16

De Lucia, G., Kauffmann, G., and White, S. D. M. (2004). Chemical enrichment of the intracluster and intergalactic medium in a hierarchical galaxy formation model. *MNRAS*, 349:1101–1116. 15, 16, 92

De Lucia, G., Tornatore, L., Frenk, C. S., Helmi, A., Navarro, J. F., and White, S. D. M. (2014). Elemental abundances in Milky Way-like galaxies from a hierarchical galaxy formation model. *MNRAS*, 445:970–987. 21

Dekel, A. and Silk, J. (1986). The origin of dwarf galaxies, cold dark matter, and biased galaxy formation. *ApJ*, 303:39–55. 20, 40, 64

Di Matteo, T., Colberg, J., Springel, V., Hernquist, L., and Sijacki, D. (2008). Direct Cosmological Simulations of the Growth of Black Holes and Galaxies. *ApJ*, 676:33–53. 40

Diemer, B., More, S., and Kravtsov, A. V. (2013). The Pseudo-evolution of Halo Mass. *ApJ*, 766:25. 31

Domínguez Sánchez, H., Pozzi, F., Gruppioni, C., Cimatti, A., Ilbert, O., Pozzetti, L., McCracken, H., Capak, P., Le Floch, E., Salvato, M., Zamorani, G., Carollo, C. M., Contini, T., Kneib, J.-P., Le Fèvre, O., Lilly, S. J., Mainieri, V., Renzini, A., Scodeggio, M., Bardelli, S., Bolzonella, M., Bongiorno, A., Caputi, K., Coppa, G., Cucciati, O., de la Torre, S., de Ravel, L., Franzetti, P., Garilli, B., Iovino, A., Kampczyk, P., Knobel, C., Kovač, K., Lamareille, F., Le Borgne, J.-F., Le Brun, V., Maier, C., Mignoli, M., Pelló, R., Peng, Y., Perez-Montero, E., Ricciardelli, E., Silverman, J. D., Tanaka, M., Tasca, L. A. M., Tresse, L., Vergani, D., and Zucca, E. (2011). The evolution of quiescent galaxies at high redshifts (z ¿ 1.4). *MNRAS*, 417:900–915. xiv, 23, 36, 52, 53

Efstathiou, G. (2000). A model of supernova feedback in galaxy formation. *MNRAS*, 317:697–719. 40, 64

Efstathiou, G., Lake, G., and Negroponte, J. (1982). The stability and masses of disc galaxies. *MNRAS*, 199:1069–1088. 92

Ettori, S., Donnarumma, A., Pointecouteau, E., Reiprich, T., Giodini, S., Lovisari, L., and Schmidt, R. (2013). Mass profiles of galaxy clusters from x-ray analysis. *SSRv*, 177:119. 67

Fabian, A. C. (1994). Cooling Flows in Clusters of Galaxies. *ARA&A*, 32:277–318. 40

Fielding, D., Quataert, E., McCourt, M., and Thompson, T. A. (2017). The impact of star formation feedback on the circumgalactic medium. *MNRAS*, 466:3810–3826. 10

Fiore, F., Feruglio, C., Shankar, F., Bischetti, M., Bongiorno, A., Brusa, M., Carniani, S., Cicone, C., Duras, F., Lamastra, A., Mainieri, V., Marconi, A., Menci, N., Maiolino, R., Piconcelli, E., Vietri, G., and Zappacosta, L. (2017). AGN wind scaling relations and the co-evolution of black holes and galaxies. *A&A*, 601:A143. 41, 49, 51

Font, A. S., Bower, R. G., McCarthy, I. G., Benson, A. J., Frenk, C. S., Helly, J. C., Lacey, C. G., Baugh, C. M., and Cole, S. (2008). The colours of satellite galaxies in groups and clusters. *MNRAS*, 389:1619–1629. 15, 25

Gargiulo, I. D., Cora, S. A., Padilla, N. D., Muñoz Arancibia, A. M., Ruiz, A. N., Orsi, A. A., Tecce, T. E., Weidner, C., and Bruzual, G. (2015). Chemoarchaeological downsizing in a hierarchical universe: impact of a top-heavy IGIMF. *MNRAS*, 446:3820–3841. 25

Geller, M. J. and Beers, T. C. (1982). Substructure within clusters of galaxies. *PASP*, 94:421–439. 15

Gonzalez-Perez, V., Lacey, C. G., Baugh, C. M., Lagos, C. D. P., Helly, J., Campbell, D. J. R., and Mitchell, P. D. (2014). How sensitive are predicted galaxy luminosities to the choice of stellar population synthesis model? *MNRAS*, 439:264–283. 15, 25

Governato, F., Willman, B., Mayer, L., Brooks, A., Stinson, G., Valenzuela, O., Wadsley, J., and Quinn, T. (2007). Forming disc galaxies in ΛCDM simulations. *MNRAS*, 374:1479–1494. 40, 64

Graham, A. W., Driver, S. P., Allen, P. D., and Liske, J. (2007). The Millennium Galaxy Catalogue: the local supermassive black hole mass function in early- and late-type galaxies. *MNRAS*, 378:198–210. xv, 60

Guo, F.-K., Hidalgo-Duque, C., Nieves, J., and Pavón Valderrama, M. (2013). Consequences of heavy-quark symmetries for hadronic molecules. *Phys. Rev. D*, 88(5):054007. 15, 16

Guo, Q., White, S., Boylan-Kolchin, M., De Lucia, G., Kauffmann, G., Lemson, G., Li, C., Springel, V., and Weinmann, S. (2011). From dwarf spheroidals to cD galaxies: simulating the galaxy population in a ΛCDM cosmology. *MNRAS*, 413:101–131. 15, 16, 19, 41, 92

Harrison, C. M., Costa, T., Tadhunter, C. N., Flütsch, A., Kakkad, D., Perna, M., and Vietri, G. (2018). AGN outflows and feedback twenty years on. *Nature Astronomy*, 2:198–205. 10, 11

Haynes, M. P., Giovanelli, R., Martin, A. M., Hess, K. M., Saintonge, A., Adams, E. A. K., Hallenbeck, G., Hoffman, G. L., Huang, S., Kent, B. R., Koopmann, R. A., Papastergis, E., Stierwalt, S., Balonek, T. J., Craig, D. W., Higdon, S. J. U., Kornreich, D. A., Miller, J. R., O'Donoghue, A. A., Olowin, R. P., Rosenberg, J. L., Spekkens, K., Troischt, P., and Wilcots, E. M. (2011). The Arecibo Legacy Fast ALFA Survey: The α.40 H I Source Catalog, Its Characteristics and Their Impact on the Derivation of the H I Mass Function. *AJ*, 142:170. xiv, 54

Henriques, B., White, S., Thomas, P., Angulo, R., Guo, Q., Lemson, G., and Springel, V. (2013). Simulations of the galaxy population constrained by observations from z=3 to the present day: implications for galactic winds and the fate of their ejecta. *MNRAS*, 431:3373. 10, 15, 16, 21, 25, 31, 41

Henriques, B., White, S., Thomas, P., Angulo, R., Guo, Q., Lemson, G., Springel, V., and Overzier, R. (2015). Galaxy formation in the planck cosmology - !. matching the observed evolution of star-formation rates, colours and stellar masses. *MNRAS*, 451:2263. v, 15, 16, 18, 23, 41, 65, 66

Hinshaw, G., Larson, D., Komatsu, E., Spergel, D. N., Bennett, C. L., Dunkley, J., Nolta, M. R., Halpern, M., Hill, R. S., Odegard, N., Page, L., Smith, K. M., Weiland, J. L., Gold, B., Jarosik, N., Kogut, A., Limon, M., Meyer, S. S., Tucker, G. S., Wollack, E., and Wright, E. L. (2013). Nine-year Wilkinson Microwave Anisotropy Probe (WMAP) Observations: Cosmological Parameter Results. *ApJS*, 208:19. 25

Hopkins, P. F., Hernquist, L., Cox, T. J., Di Matteo, T., Martini, P., Robertson, B.,

and Springel, V. (2005). Black Holes in Galaxy Mergers: Evolution of Quasars. *ApJ*, 630:705–715. 40

Hopkins, P. F., Hernquist, L., Cox, T. J., and Kereš, D. (2008). A Cosmological Framework for the Co-Evolution of Quasars, Supermassive Black Holes, and Elliptical Galaxies. I. Galaxy Mergers and Quasar Activity. *ApJS*, 175:356–389. xv, 61, 87

Hopkins, P. F., Kereš, D., Oñorbe, J., Faucher-Giguère, C.-A., Quataert, E., Murray, N., and Bullock, J. S. (2014). Galaxies on FIRE (Feedback In Realistic Environments): stellar feedback explains cosmologically inefficient star formation. *MNRAS*, 445:581–603. 40, 64

Hopkins, P. F. and Quataert, E. (2011). An analytic model of angular momentum transport by gravitational torques: from galaxies to massive black holes. *MNRAS*, 415:1027–1050. 11, 41, 43, 47

Hu, J.-W., Cai, R.-G., Guo, Z.-K., and Hu, B. (2014). Cosmological parameter estimation from CMB and X-ray cluster after Planck. *J. Cosmology Astropart. Phys.*, 5:020. 7

Hubble, E. and Humason, M. L. (1931). The Velocity-Distance Relation among Extra-Galactic Nebulae. *ApJ*, 74:43. 2

Ilbert, O., McCracken, H. J., Le Fèvre, O., Capak, P., Dunlop, J., Karim, A., Renzini, M. A., Caputi, K., Boissier, S., Arnouts, S., Aussel, H., Comparat, J., Guo, Q., Hudelot, P., Kartaltepe, J., Kneib, J. P., Krogager, J. K., Le Floc'h, E., Lilly, S., Mellier, Y., Milvang-Jensen, B., Moutard, T., Onodera, M., Richard, J., Salvato, M., Sanders, D. B., Scoville, N., Silverman, J. D., Taniguchi, Y., Tasca, L., Thomas, R., Toft, S., Tresse, L., Vergani, D., Wolk, M., and Zirm, A. (2013). Mass assembly in quiescent and star-forming galaxies since z = 4 from UltraVISTA. *A&A*, 556:A55. xiv, 23, 36, 52, 53

Irodotou, D., Thomas, P., and Henriques, B. (2018). Mergers and disk instabilities. *MNRAS*. 87, 89, 93

Kauffmann, G. (1996). Disc galaxies at z=0 and at high redshift: an explanation of the observed evolution of damped Lyalpha absorption systems. *MNRAS*, 281:475–486. 19

Kereš, D., Katz, N., Weinberg, D. H., and Davé, R. (2005). How do galaxies get their gas? *MNRAS*, 363:2–28. 5

Knebe, A., Knollmann, S. R., Muldrew, S. I., Pearce, F. R., Aragon-Calvo, M. A., Ascasibar, Y., Behroozi, P. S., Ceverino, D., Colombi, S., Diemand, J., Dolag, K., Falck,

B. L., Fasel, P., Gardner, J., Gottloeber, S., Hsu, C.-H., Iannuzzi, F., Klypin, A., Lukic, Z., Maciejewski, M., McBride, C., Neyrinck, M. C., Planelles, S., Potter, D., Quilis, V., Rasera, Y., Read, J. I., Ricker, P. M., Roy, F., Springel, V., Stadel, J., Stinson, G., Sutter, P. M., Turchaninov, V., Tweed, D., Yepes, G., and Zemp, M. (2011). Haloes gone mad: The halo-finder comparison project. *MNRAS*, 415:2293. 31

Knebe, A., Pearce, F. R., Thomas, P. A., Benson, A., Blaizot, J., Bower, R., Carretero, J., Castander, F. J., Cattaneo, A., Cora, S. A., Croton, D. J., Cui, W., Cunnama, D., Lucia, G. D., Devriendt, J. E., Elahi, P. J., Font, A., Fontanot, F., Garcia-Bellido, J., Gargiulo, I. D., Gonzalez-Perez, V., Helly, J., Henriques, B., Hirschmann, M., Lee, J., Mamon, G. A., Monaco, P., Onions, J., Padilla, N. D., Power, C., Pujol, A., Skibba, R. A., Somerville, R. S., Srisawat, C., Vega-Martinez, C. A., and Yi, S. K. (2015). nifty cosmology: Comparison of galaxy formation models. *MNRAS*, 451:4029. 15, 24

Kravtsov, A. V. and Borgani, S. (2012). Formation of Galaxy Clusters. *ARA&A*, 50:353–409. 101

Lacey, C. G., Baugh, C. M., Frenk, C. S., Benson, A. J., Bower, R. G., Cole, S., Gonzalez-Perez, V., Helly, J. C., Lagos, C. D. P., and Mitchell, P. D. (2016). A unified multi-wavelength model of galaxy formation. *MNRAS*, 462:3854–3911. 15

Larson, R. B. (1974). Effects of supernovae on the early evolution of galaxies. *MNRAS*, 169:229–246. 20

Lee, J. and Yi, S. K. (2013). On the Assembly History of Stellar Components in Massive Galaxies. *ApJ*, 766:38. 25

Li, C. and White, S. D. M. (2009). The distribution of stellar mass in the low-redshift Universe. *MNRAS*, 398:2177–2187. xiv, 23, 52, 53

Limber, D. N. (1959). Effects of Intracluster Gas and Duct upon the Virial Theorem. *ApJ*, 130:414. 7

Lloyd-Davies, E. J., Romer, A. K., Mehrtens, N., Hosmer, M., Davidson, M., Sabirli, K., Mann, R. G., Hilton, M., Liddle, A. R., Viana, P. T. P., Campbell, H. C., Collins, C. A., Dubois, E. N., Freeman, P., Harrison, C. D., Hoyle, B., Kay, S. T., Kuwertz, E., Miller, C. J., Nichol, R. C., Sahlén, M., Stanford, S. A., and Stott, J. P. (2011a). The XMM Cluster Survey: X-ray analysis methodology. *MNRAS*, 418:14–53. 6, 64

Lloyd-Davies, E. J., Romer, A. K., Mehrtens, N., Hosmer, M., Davidson, M., Sabirli, K., Mann, R. G., Hilton, M., Liddle, A. R., Viana, P. T. P., Campbell, H. C., Collins, C. A., Dubois, E. N., Freeman, P., Harrison, C. D., Hoyle, B., Kay, S. T., Kuwertz, E., Miller, C. J., Nichol, R. C., Sahlén, M., Stanford, S. A., and Stott, J. P. (2011b). The XMM Cluster Survey: X-ray analysis methodology. *MNRAS*, 418:14–53. 101

Lusso, E., Comastri, A., Simmons, B. D., Mignoli, M., Zamorani, G., Vignali, C., Brusa, M., Shankar, F., Lutz, D., Trump, J. R., Maiolino, R., Gilli, R., Bolzonella, M., Puccetti, S., Salvato, M., Impey, C. D., Civano, F., Elvis, M., Mainieri, V., Silverman, J. D., Koekemoer, A. M., Bongiorno, A., Merloni, A., Berta, S., Le Floc'h, E., Magnelli, B., Pozzi, F., and Riguccini, L. (2012). Bolometric luminosities and Eddington ratios of X-ray selected active galactic nuclei in the XMM-COSMOS survey. *MNRAS*, 425:623–640. 89

Martindale, H., Thomas, P. A., Henriques, B. M., and Loveday, J. (2017). Towards a consistent model for both the hi and stellar mass functions of galaxies. *MNRAS*, 472:1981. 54

Martizzi, D., Fielding, D., Faucher-Giguère, C.-A., and Quataert, E. (2016). Supernova feedback in a local vertically stratified medium: interstellar turbulence and galactic winds. *MNRAS*, 459:2311–2326. 10

Maughan, B. J., Jones, C., Forman, W., and Van Speybroeck, L. (2008). Images, Structural Properties, and Metal Abundances of Galaxy Clusters Observed with Chandra ACIS-I at 0.1 ¡ z ¡ 1.3. *ApJS*, 174:117–135. xv, xvi, 73, 74, 76

Mayer, L., Kazantzidis, S., Escala, A., and Callegari, S. (2010). Direct formation of supermassive black holes via multi-scale gas inflows in galaxy mergers. *Nature*, 466:1082–1084. 11

McCarthy, I. G., Frenk, C. S., Font, A. S., Lacey, C. G., Bower, R. G., Mitchell, N. L., Balogh, M. L., and Theuns, T. (2008). Ram pressure stripping the hot gaseous haloes of galaxies in groups and clusters. *MNRAS*, 383:593–605. 22

McCarthy, I. G., Schaye, J., Bird, S., and Le Brun, A. M. C. (2017). The BAHAMAS project: calibrated hydrodynamical simulations for large-scale structure cosmology. *MNRAS*, 465:2936–2965. 14, 79

McCarthy, I. G., Schaye, J., Bower, R. G., Ponman, T. J., Booth, C. M., Dalla Vecchia,

C., and Springel, V. (2011). Gas expulsion by quasar-driven winds as a solution to the overcooling problem in galaxy groups and clusters. *MNRAS*, 412:1965–1984. 42

McConnell, N. J. and Ma, C.-P. (2013). Revisiting the Scaling Relations of Black Hole Masses and Host Galaxy Properties. *ApJ*, 764:184. 23

Mehrtens, N., Romer, A. K., Hilton, M., Lloyd-Davies, E. J., Miller, C. J., Stanford, S. A., Hosmer, M., Hoyle, B., Collins, C. A., Liddle, A. R., Viana, P. T. P., Nichol, R. C., Stott, J. P., Dubois, E. N., Kay, S. T., Sahlén, M., Young, O., Short, C. J., Christodoulou, L., Watson, W. A., Davidson, M., Harrison, C. D., Baruah, L., Smith, M., Burke, C., Mayers, J. A., Deadman, P.-J., Rooney, P. J., Edmondson, E. M., West, M., Campbell, H. C., Edge, A. C., Mann, R. G., Sabirli, K., Wake, D., Benoist, C., da Costa, L., Maia, M. A. G., and Ogando, R. (2012). The XMM Cluster Survey: optical analysis methodology and the first data release. *MNRAS*, 423:1024–1052. 6, 64

Meidt, S. E., Schinnerer, E., van de Ven, G., Zaritsky, D., Peletier, R., Knapen, J. H., Sheth, K., Regan, M., Querejeta, M., Muñoz-Mateos, J.-C., Kim, T., Hinz, J. L., Gil de Paz, A., Athanassoula, E., Bosma, A., Buta, R. J., Cisternas, M., Ho, L. C., Holwerda, B., Skibba, R., Laurikainen, E., Salo, H., Gadotti, D. A., Laine, J., Erroz-Ferrer, S., Comerón, S., Menéndez-Delmestre, K., Seibert, M., and Mizusawa, T. (2014). Reconstructing the Stellar Mass Distributions of Galaxies Using S^4G IRAC 3.6 and 4.5 μm Images. II. The Conversion from Light to Mass. *ApJ*, 788:144. xv, 57

Menci, N., Fiore, F., Bongiorno, A., and Lamastra, A. (2016). Relative growth of black holes and the stellar components of galaxies. *A&A*, 594:A99. 41

Menci, N., Gatti, M., Fiore, F., and Lamastra, A. (2014). Triggering active galactic nuclei in hierarchical galaxy formation: disk instability vs. interactions. *A&A*, 569:A37. 41, 43, 47

Mernier, F., de Plaa, J., Kaastra, J. S., Zhang, Y.-Y., Akamatsu, H., Gu, L., Kosec, P., Mao, J., Pinto, C., Reiprich, T. H., Sanders, J. S., Simionescu, A., and Werner, N. (2017). Radial metal abundance profiles in the intra-cluster medium of cool-core galaxy clusters, groups, and ellipticals. *A&A*, 603:A80. 79

Mihos, J. C. and Hernquist, L. (1996). Gasdynamics and Starbursts in Major Mergers. *ApJ*, 464:641. 20

Molnár, D. C., Sargent, M. T., Elbaz, D., Papadopoulos, P. P., and Silk, J. (2017). Further

evidence for a quasar-driven jet impacting its neighbour galaxy: The saga of HE0450-2958 continues. *MNRAS*, 467:586–596. 11, 41

Monaco, P., Fontanot, F., and Taffoni, G. (2007). The MORGANA model for the rise of galaxies and active nuclei. *MNRAS*, 375:1189–1219. 25

Muanwong, O., Thomas, P. A., Kay, S. T., Pearce, F. R., and Couchman, H. M. P. (2001). The Effect of Radiative Cooling on Scaling Laws of X-Ray Groups and Clusters. *ApJ*, 552:L27–L30. 44

Muzzin, A., Marchesini, D., Stefanon, M., Franx, M., McCracken, H. J., Milvang-Jensen, B., Dunlop, J. S., Fynbo, J. P. U., Brammer, G., Labbé, I., and van Dokkum, P. G. (2013). The Evolution of the Stellar Mass Functions of Star-forming and Quiescent Galaxies to z = 4 from the COSMOS/UltraVISTA Survey. *ApJ*, 777:18. xiv, 23, 36, 52, 53

Navarro, J. F., Frenk, C. S., and White, S. D. M. (1996). The Structure of Cold Dark Matter Halos. *ApJ*, 462:563. 4

Nulsen, P. E. J. and Fabian, A. C. (2000). Fuelling quasars with hot gas. *MNRAS*, 311:346–356. 44

Oesch, P. A., Bouwens, R. J., Illingworth, G. D., Labbé, I., Trenti, M., Gonzalez, V., Carollo, C. M., Franx, M., van Dokkum, P. G., and Magee, D. (2012). Expanded Search for z ˜ 10 Galaxies from HUDF09, ERS, and CANDELS Data: Evidence for Accelerated Evolution at z ¿ 8? *ApJ*, 745:110. 1

Okamoto, T., Gao, L., and Theuns, T. (2008). Mass loss of galaxies due to an ultraviolet background. *MNRAS*, 390:920–928. 18, 30

Planck Collaboration, Ade, P. A. R., Aghanim, N., Armitage-Caplan, C., Arnaud, M., Ashdown, M., Atrio-Barandela, F., Aumont, J., Baccigalupi, C., Banday, A. J., and et al. (2014). Planck 2013 results. XVI. Cosmological parameters. *A&A*, 571:A16. xiv, 3, 29, 30, 35, 41, 65

Pratt, G. W., Arnaud, M., and Pointecouteau, E. (2006). Structure and scaling of the entropy in nearby galaxy clusters. *A&A*, 446:429–438. 7

Pratt, G. W., Croston, J. H., Arnaud, M., and Böhringer, H. (2009). Galaxy cluster X-ray luminosity scaling relations from a representative local sample (REXCESS). *A&A*, 498:361–378. xv, xvi, 73, 74, 76

Rupke, D. S. N. and Veilleux, S. (2011). Integral Field Spectroscopy of Massive, Kiloparsec-scale Outflows in the Infrared-luminous QSO Mrk 231. *ApJ*, 729:L27. 41

Sahlén, M., Viana, P. T. P., Liddle, A. R., Romer, A. K., Davidson, M., Hosmer, M., Lloyd-Davies, E., Sabirli, K., Collins, C. A., Freeman, P. E., Hilton, M., Hoyle, B., Kay, S. T., Mann, R. G., Mehrtens, N., Miller, C. J., Nichol, R. C., Stanford, S. A., and West, M. J. (2009). The XMM Cluster Survey: forecasting cosmological and cluster scaling-relation parameter constraints. *MNRAS*, 397:577–607. 64

Sanders, J. S., Fabian, A. C., Russell, H. R., and Walker, S. A. (2018). Hydrostatic Chandra X-ray analysis of SPT-selected galaxy clusters - I. Evolution of profiles and core properties. *MNRAS*, 474:1065–1098. 69, 83

Savorgnan, G. A. D., Graham, A. W., Marconi, A., and Sani, E. (2016). Supermassive Black Holes and Their Host Spheroids. II. The Red and Blue Sequence in the M_{BH}-$M_{*,sph}$ Diagram. *ApJ*, 817:21. xv, 50, 57

Schaye, J., Crain, R. A., Bower, R. G., Furlong, M., Schaller, M., Theuns, T., Dalla Vecchia, C., Frenk, C. S., McCarthy, I. G., Helly, J. C., Jenkins, A., Rosas-Guevara, Y. M., White, S. D. M., Baes, M., Booth, C. M., Camps, P., Navarro, J. F., Qu, Y., Rahmati, A., Sawala, T., Thomas, P. A., and Trayford, J. (2015). The EAGLE project: simulating the evolution and assembly of galaxies and their environments. *MNRAS*, 446:521–554. 11, 14, 40

Silk, J. and Mamon, G. A. (2012). The current status of galaxy formation. *Research in Astronomy and Astrophysics*, 12:917–946. xiii, 9

Somerville, R. S. (2001). Disks at High Redshift: Interactions, Mergers, and Starbursts. In Funes, J. G. and Corsini, E. M., editors, *Galaxy Disks and Disk Galaxies*, volume 230 of *Astronomical Society of the Pacific Conference Series*, pages 477–486. 20

Spergel, D. N. (2001). Extracting Cosmology from the Cosmic Microwave Background Radiation. In Bergström, L., Fransson, C., and Carlson, P., editors, *Particle Physics and the Universe*, pages 142–147. 15

Springel, V. (2005). The cosmological simulation code GADGET-2. *MNRAS*, 364:1105–1134. 15, 25, 29, 41, 65

Springel, V., White, S. D. M., Tormen, G., and Kauffmann, G. (2001). Populating a cluster of galaxies - I. Results at [formmu2]z=0. *MNRAS*, 328:726–750. 15, 16, 66

Srisawat, C., Knebe, A., Pearce, F. R., Schneider, A., Thomas, P. A., Behroozi, P., Dolag, K., Elahi, P. J., Han, J., Helly, J., Jing, Y., Jung, I., Lee, J., Mao, Y. Y., Onions, J., Rodriguez-Gomez, V., Tweed, D., and Yi, S. K. (2013). Sussing merger trees: The merger trees comparison project. *MNRAS*, 436:150. 24, 31, 33

Sun, M. (2012). Hot gas in galaxy groups: recent observations. *New Journal of Physics*, 14(4):045004. 40

Sun, M., Voit, G. M., Donahue, M., Jones, C., Forman, W., and Vikhlinin, A. (2009). Chandra Studies of the X-Ray Gas Properties of Galaxy Groups. *ApJ*, 693:1142–1172. xiv, xvi, 23, 40, 51, 52, 77

Thomas, P. (1988). Multiphase cooling flows - A Lagrangian approach. *MNRAS*, 235:315–341. 67, 69

Tomczak, A. R., Quadri, R. F., Tran, K.-V. H., Labbé, I., Straatman, C. M. S., Papovich, C., Glazebrook, K., Allen, R., Brammer, G. B., Kacprzak, G. G., Kawinwanichakij, L., Kelson, D. D., McCarthy, P. J., Mehrtens, N., Monson, A. J., Persson, S. E., Spitler, L. R., Tilvi, V., and van Dokkum, P. (2014). Galaxy Stellar Mass Functions from ZFOURGE/CANDELS: An Excess of Low-mass Galaxies since z = 2 and the Rapid Buildup of Quiescent Galaxies. *ApJ*, 783:85. xiv, 23, 36, 52, 53

Tonini, C., Mutch, S. J., Croton, D. J., and Wyithe, J. S. B. (2016). The growth of discs and bulges during hierarchical galaxy formation - I. Fast evolution versus secular processes. *MNRAS*, 459:4109–4129. 92

Toomre, A. (1964). On the gravitational stability of a disk of stars. *ApJ*, 139:1217–1238. 93

Tremonti, C. A., Moustakas, J., and Diamond-Stanic, A. M. (2007). The Discovery of 1000 km s^{-1} Outflows in Massive Poststarburst Galaxies at z=0.6. *ApJ*, 663:L77–L80. 41

Urry, M. (2003). The AGN Paradigm for Radio-Loud Objects. In Collin, S., Combes, F., and Shlosman, I., editors, *Active Galactic Nuclei: From Central Engine to Host Galaxy*, volume 290 of *Astronomical Society of the Pacific Conference Series*, page 3. 10

van de Voort, F., Schaye, J., Booth, C. M., Haas, M. R., and Dalla Vecchia, C. (2011). The rates and modes of gas accretion on to galaxies and their gaseous haloes. *MNRAS*, 414:2458–2478. 5

Vika, M., Driver, S. P., Graham, A. W., and Liske, J. (2009). The Millennium Galaxy Catalogue: the M_{bh}-$L_{spheroid}$ derived supermassive black hole mass function. *MNRAS*, 400:1451–1460. xv, 60

Vikhlinin, A., Burenin, R. A., Ebeling, H., Forman, W. R., Hornstrup, A., Jones, C., Kravtsov, A. V., Murray, S. S., Nagai, D., Quintana, H., and Voevodkin, A. (2009). Chandra Cluster Cosmology Project. II. Samples and X-Ray Data Reduction. *ApJ*, 692:1033–1059. xv, xvi, 64, 73, 74, 76

Vikhlinin, A., Kravtsov, A., Forman, W., Jones, C., Markevitch, M., Murray, S. S., and Van Speybroeck, L. (2006). Chandra Sample of Nearby Relaxed Galaxy Clusters: Mass, Gas Fraction, and Mass-Temperature Relation. *ApJ*, 640:691–709. xiv, xvi, 23, 40, 51, 52, 64, 77

Vogelsberger, M., Genel, S., Springel, V., Torrey, P., Sijacki, D., Xu, D., Snyder, G., Nelson, D., and Hernquist, L. (2014). Introducing the Illustris Project: simulating the coevolution of dark and visible matter in the Universe. *MNRAS*, 444:1518–1547. 14, 40

Vogelsberger, M., Marinacci, F., Torrey, P., Genel, S., Springel, V., Weinberger, R., Pakmor, R., Hernquist, L., Naiman, J., Pillepich, A., and Nelson, D. (2018). The uniformity and time-invariance of the intra-cluster metal distribution in galaxy clusters from the IllustrisTNG simulations. *MNRAS*, 474:2073–2093. 79

Voit, G. M., Balogh, M. L., Bower, R. G., Lacey, C. G., and Bryan, G. L. (2003). On the Origin of Intracluster Entropy. *ApJ*, 593:272–290. 30

Voit, G. M. and Bryan, G. L. (2001). Regulation of the X-ray luminosity of clusters of galaxies by cooling and supernova feedback. *Nature*, 414:425–427. 44

White, S. D. M. and Frenk, C. S. (1991). Galaxy formation through hierarchical clustering. *apj*, 379:52–79. 18, 25, 29, 40, 64, 66, 67, 68

White, S. D. M. and Rees, M. J. (1978). Core condensation in heavy halos - A two-stage theory for galaxy formation and clustering. *MNRAS*, 183:341–358. 4, 20, 40, 67

Yates, R. M., Henriques, B., Thomas, P. A., Kauffmann, G., Johansson, J., and White, S. D. M. (2013). Modelling element abundances in semi-analytic models of galaxy formation. *MNRAS*, 435:3500–3520. 21

Yates, R. M., Thomas, P. A., and Henriques, B. M. B. (2017). Iron in galaxy groups and clusters: confronting galaxy evolution models with a newly homogenized data set. *MNRAS*, 464:3169–3193. xvi, 21, 33, 36, 51, 79, 83, 84, 85, 88

Yuan, F. and Narayan, R. (2014). Hot Accretion Flows Around Black Holes. *ARA&A*, 52:529–588. 11

Zwaan, M. A., Meyer, M. J., Staveley-Smith, L., and Webster, R. L. (2005). The HIPASS catalogue: Ω_{HI} and environmental effects on the HI mass function of galaxies. *MNRAS*, 359:L30–L34. xiv, 54